

INFORMATION TO USERS

This manuscript has been reproduced from the microfilm master. UMI films the text directly from the original or copy submitted. Thus, some thesis and dissertation copies are in typewriter face, while others may be from any type of computer printer.

The quality of this reproduction is dependent upon the quality of the copy submitted. Broken or indistinct print, colored or poor quality illustrations and photographs, print bleedthrough, substandard margins, and improper alignment can adversely affect reproduction.

In the unlikely event that the author did not send UMI a complete manuscript and there are missing pages, these will be noted. Also, if unauthorized copyright material had to be removed, a note will indicate the deletion.

Oversize materials (e.g., maps, drawings, charts) are reproduced by sectioning the original, beginning at the upper left-hand corner and continuing from left to right in equal sections with small overlaps. Each original is also photographed in one exposure and is included in reduced form at the back of the book.

Photographs included in the original manuscript have been reproduced xerographically in this copy. Higher quality 6" x 9" black and white photographic prints are available for any photographs or illustrations appearing in this copy for an additional charge. Contact UMI directly to order.



University Microfilms International
A Bell & Howell Information Company
300 North Zeeb Road, Ann Arbor, MI 48106-1346 USA
313/761-4700 800/521-0600

Order Number 1355198

**A study of the photodissociation dynamics of dimethylzinc and
the implications for the growth of ZnSe films**

Elias, Joseph A., M.S.

Rice University, 1993

U·M·I

**300 N. Zeeb Rd.
Ann Arbor, MI 48106**

RICE UNIVERSITY

A STUDY OF THE PHOTODISSOCIATION DYNAMICS OF DIMETHYLZINC
AND THE IMPLICATIONS FOR THE GROWTH OF ZnSe FILMS

by

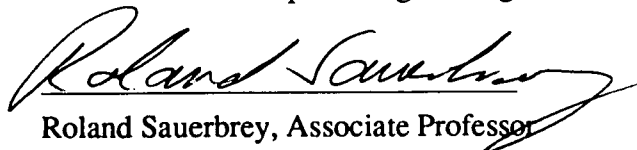
JOSEPH A. ELIAS

A THESIS SUBMITTED
IN PARTIAL FULFILLMENT OF THE
REQUIREMENTS FOR THE DEGREE
MASTER OF SCIENCE

APPROVED, THESIS COMMITTEE :



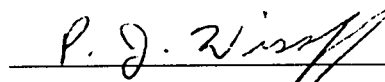
William L. Wilson, Jr., Professor, Chair
Electrical and Computer Engineering



Roland Sauerbrey, Associate Professor
Electrical and Computer Engineering



Robert Curl, Professor
Chemistry



P. Jeffrey Wisoff, Adjunct Professor
Electrical and Computer Engineering

Houston, Texas

May 1993

ABSTRACT

A STUDY OF THE PHOTODISSOCIATION DYNAMICS OF DIMETHYLZINC AND THE IMPLICATIONS FOR THE GROWTH OF ZnSe FILMS

by

JOSEPH A. ELIAS

The dynamics of the ArF photodissociation of DMZn (dimethylzinc) have been studied. The implications of the results for the growth of ZnSe thin films are discussed. Time-resolved absorption profiles of ground state Zn and methyl radicals have been acquired using a plasma emission source. Time-resolved fluorescence from excited CH radicals has also been studied. The results indicate that the Zn concentration remains constant after the dissociating ArF pulse, indicating the system is a good source for free Zn atoms. The CH₃ radicals that are created recombine to form ethane, and simulations of the kinetics indicate that the concentration of methyl radicals reaching the substrate is insignificant. There was no indication of monomethylzinc formation. The CH radical is likely to combine with H₂ to form CH₃ within several microseconds. Thus the major sources for carbon contamination in the growth process (CH₃, MMZn, CH) are unlikely to reach the substrate.

Acknowledgments

I would like to thank my committee members for their patience and willingness to lend advice on this project. Dr. Bill was understanding throughout the duration of the experiments, even when they were not going so hot, and that was encouraging. Drs. Roland Sauerbrey and Bob Curl were instrumental in helping decipher some of the data, as was Dr. Jeff Wisoff, who took time on the weekends to drive up to Rice. I owe a great deal of gratitude to my committee for helping me publish this thesis. I would also like to thank Dr. Frank Tittel, Dr. Skip Porter, and Advantest for providing the initial financial support which encouraged me to come to Rice.

Several of my colleagues helped initiate me to graduate school, both socially and professionally. Dr. Paul Gillespie took the time to teach me some of the basics about the project, and his willingness to listen was invaluable. Dr. Tim Rost was also there to lend a hand whenever necessary. Both Paul and Tim helped me adjust to Houston, and made bearable the initial few months of graduate school. Dr. Tracy Sharp, Dr. Harvey Phillips, and Paul LeBlanc were generous in letting me scrounge their labs for equipment. Kang Lee and Owen Kelly provided a good perspective on our department, graduate school, and life in general. I would also like to thank the numerous friends I have made through my work with the GSA.

My family has always been there for me, with love and understanding. Finally, I would like to thank Stacey Wallace, who was always there to listen to my ravings, and her support has made this thesis possible.

TABLE OF CONTENTS

Chapter 1	Introduction	1
Chapter 2	Background	
2.1	Theory	6
2.2	The Study of DM(Zn, Cd, Hg)	8
Chapter 3	Experimental Setup	
3.1	Overall System	20
3.2	VUV-VIS Plasma Probe Source	23
3.3	Geometry and Alignment of System	28
3.4	Timing and Data Acquisition	35
Chapter 4	Results	
4.1	Summary	38
4.2	Absorption Experiments	41
	Methyl Radical Concentration	46
	Atomic Zn Concentration	52
4.3	Fluorescence Experiments	59
4.4	Energy Dependence of Photoproducts	
	CH ₃ vs. ArF Energy	62
	CH* vs. ArF Energy	65
Chapter 5	Discussion	
5.1	Absorption and Fluorescence Results	73

5.2	Energy Dependence Results	80
Chapter 6	Conclusions and Recommendations	85
	References	88
	Appendix A - DMZn specifications	102
	Appendix B - Computer Programs	104

List of Figures

2-1	Pack's diagram for XY_2 molecules	7,9
2-2	Symmetry elements of DMZn	11
2-3	Absorption cross section from Chen and Osgood	13
2-4	Absorption cross section from Fujita	14
2-5	Yield of MMZn vs. Zn	17
2-6	Absorption cross section from Ibuki	18
3-1	Layout of experimental system	21
3-2	Vacuum flanges: uniform flow and PMT holder	22
3-3	Typical spectral features of plasma	25
3-4	Blackbody for $T = 14.5$ eV and $T = 3.1$ eV	27
3-5	Plasma intensity vs. pressure for different wavelengths	29
3-6	Repeatability of plasma is $\pm 5\%$	30
3-7	Blowup of ArF / plasma / spectrometer geometry	31
3-8	Alignment procedure for system	33
3-9	ArF beam profile measurements	34
3-10	Timing for the YAG, ArF, and SRS trigger signals	36
3-11	Plasma, YAG, and ArF signals in time	37
4-1	Absorption profiles of Zn and methyl radicals	39
4-2	Deep VUV CH ₃ absorptions	40
4-3	Summary of dissociation species	42
4-4	Absorption cross section of DMZn	45
4-5	Mass spectra of photoproducts	48
4-6	Decay of methyl absorbance signal over time	50
4-7	Curve of growth for determining Zn concentration	54

4-8	Zn concentration versus time	60
4-9	CH emission vs. wavelength	61
4-10	CH emission over time	63
4-11	Methyl absorbance vs. ArF energy	64
4-12	Three-level diagram	66
4-13	Simulations of saturation effects	68
4-14	LOG/LOG plot of CH* vs. ArF energy	70
5-1	Diffusion of Zn and CH ₃ to the substrate	75
5-2	Multi-photon paths for CH production	81

List of Tables

1-1	Absorption cross sections for several metalorganics	3
2-1	Observed optical properties of DMZn	15
4-1	Summary of some experimental data	44
4-2	Reaction rate constants	47
4-3	Broadening mechanisms and formulas	56
4-4	Summary of broadening calculations for Zn	57
4-5	Some of the system parameters	69
4-6	Energies of the dissociation reactions of DMZn	71

Chapter 1

Introduction

ZnSe is a direct, wide bandgap, II-VI semiconductor with promising electro-optic applications, as the active material in blue lasers ^{1,2} LED's ^{3,4}, and optical switches ⁵, and as the insulator in GaAs-based MISFET's ⁶. However, the ZnSe film quality grown by MOCVD is limited by number of defects introduced during the growth process ⁷. It has been shown that lower growth temperatures reduce the density of defects ^{8,9}. Motivated by this, our group has grown ZnSe films at reduced substrate temperatures ¹⁰ by using an ArF laser to photodissociate the source gases. More recently, this technique has been used to grow p-type ZnSe films ¹¹ by photodissociating NH₃ as a dopant source. While this laser-assisted MOCVD (LAMOCVD) method yields good quality ZnSe films, the fundamental chemistry of the dissociation process is not well understood. In the growth system, dimethylzinc (DMZn), diethylselenide (DESe), and ammonia (NH₃) are used as source gases for Zn, Se, and N (by way of NH₂) atoms, respectively. Depending on the UV source, the dissociation of these precursors has been shown by other groups to break into intermediate compounds such as MMZn ¹², and NH₂ ¹³, but the role of these intermediates in the growth process has not been studied. As a first step to addressing this question, this thesis concentrates on the 193 nm photodissociation of DMZn in a hydrogen atmosphere, and the implications of these observations on the growth of ZnSe films.

The use of DMZn and the related compounds dimethylcadmium (DMCd) and dimethylmercury (DMHg) in the growth of semiconductors is

well established in the growth of ZnSe ^{10,11,14,15}, HgCdTe ¹⁶, CdTe ¹⁷, and HgTe ¹⁸ as well as in the deposition of Cd films ¹⁹. These compounds are particularly useful for laser-assisted chemistry since they have large cross sections of absorption in the UV ²⁰⁻²² where ArF and KrF lasers operate, as shown in Table 1-1. In addition to its use in the growth of ZnSe films, DMZn has also been used in the photodeposition ZnO ²³. The photodissociation of these metalorganics have been the subject of numerous gas phase studies. Work on these compounds began in the 1930's ^{24,25} and continued in the 1950's ²⁶. More recent efforts ²⁷⁻³⁰ indicate the return of strong interest in these compounds.

Since the growth of ZnSe by MOCVD involves several molecules, there are many possibilities for the intermediate chemistry. Depending on the energy supplied to the system, DMZn {Zn(CH₃)₂} may dissociate to either (Zn + 2 CH₃) or (ZnCH₃ + CH₃), while the methyl radical produced, CH₃, can further dissociate to (C + 3H), (C + H + H₂), (CH + H₂), (CH₂ + H), etc. The intermediate radicals and/or atoms may also be found in excited states. The Zn atom may appear in the ground state, initially occupy an excited state, or become ionized. Depending on its atomic state, the Zn may react with other products in the gas phase to form compounds such as ZnH ^{31,32}, thus scavenging free Zn atoms from the growth region. Further complicating the picture is the possibility for recombination reactions of the dissociation products to form compounds such as C₂H₆ or CH₄. If radicals such as CH₃ arrive at the growth surface and bond, the resultant carbon contamination could have serious consequences for the electrical properties of the semiconductor ^{33,34}. Thus, the role these intermediates play in the

Table 1-1.

Absorption cross sections of II-VI metalorganic compounds (from Fujita ²¹)
(units are in $1 \times 10^{-17} \text{ cm}^2$)

	ArF (193 nm)	KrCl (222 nm)	KrF (248 nm)	XeCl (308 nm)	XeF (350 nm)
DMCd	0.9	3.0	0.4	0	0
DMTe	2.8	0.3	3.6	0.05	<0.03
DETe	4.8	1.2	3.6	0.05	<0.03
DMZn	1.8	0.9	0	0	0
DMS	0.6	0.17	<0.01	0	0
DES	1.1	0.8	<0.05	0	0
DMSe	1.1	0.9	0.15	0.02	0
DESe	1.9	1.3	0.2	0.03	0

DM dimethyl $(\text{CH}_3)_2$

DE diethyl $(\text{C}_2\text{H}_5)_2$

growth process needs to be explored in order to improve the overall control and quality of LAMOCVD ZnSe films.

In general, carbon contamination in semiconductors and metal films has been shown to be a problem. The role of carbon in ZnSe films has been explored by Giapis ³³, and it is regarded as a problem due to the fact that carbon is a shallow acceptor (0.026 eV) in GaAs. In the photodeposition of Al using the precursor trimethylaluminum (TMAI), Higashi and Rothberg ^{35,36} found that methyl radicals are incorporated into the films photodeposited by 193 nm and 248 nm radiation. Further work by Zhang and Stuke ³⁷ showed that the monomethylaluminum (MMAI) fragment is created in the 193 nm photolysis of TMAI and that the MMAI might be responsible for the transport of the methyl radical to the surface of photodeposited Al films. InP deposition from metalorganic sources shows qualitatively similar results ³⁸. Carbon contamination was shown to exist in InP films in which a focused ArF laser beam impinged on the substrate surface, while no C contamination was found when the beam was directed parallel to the surface of the substrate.

Several techniques are conventionally used to study the molecular photodissociation process. Mass spectrometry has been used to determine the photofragments of the dissociation process ³⁹. Quantitative results from this technique are dependent upon knowing the ionization efficiencies of the molecules and atoms. Qualitatively, the products detected in mass spectrometry studies have to be distinguished between neutral photoproducts that are ionized in the ion chamber and ions formed in the dissociation process. Mass spectrometry studies are limited in temporal resolution, in that most experiments conducted in growth cells detect only the by-products

of the dissociation process, after the radicals have recombined or reacted to form stable molecules. Laser induced fluorescence (LIF) studies have also been used to qualitatively identify photoproducts ⁴⁰. However, the detection of photoproducts is dependent upon the ranges of the sources used for the excitation. Since the strongest ground state Zn transition is in the deep UV (~2150Å) ⁴¹, tunable excitation sources which can excite the ground state are difficult to obtain. The methyl radicals can not be detected by LIF as they do not fluoresce ⁴². A non-invasive technique for *in situ* probing of photoproducts for growth monitoring is optical absorption, and this technique has been applied quantitatively in the present work to investigate the photodissociation of DMZn.

The photodissociation of molecules yields atoms and/or radicals, which have electronic transitions in the VUV-VIS wavelength range. Detection of these various photoproducts in absorption requires a broadband VUV-VIS light source, which can be provided by a synchrotron source. However, the prohibitive cost of synchrotron sources limits their use to only a handful of laboratories around the world. In this thesis, an inexpensive, broadband VUV-VIS light source is described and is used in absorption experiments to determine quantitative measurements of the photoproducts resulting from the photodissociation of DMZn by an ArF laser beam.

In summary, an understanding of the basic photochemical reactions is needed to determine what pathways are available for contaminants (mostly carbon) to reach the growth surface. The present work explores the issue of transport of atomic zinc to the GaAs substrate, as well as the role of carbon containing intermediates, and concludes with recommendations for improving the growth process.

Chapter 2

Theory

The molecule DMZn can be modeled as a general triatomic. This is due to the fact that the, as is true for DMCd and DMHg, the metal atom in DMZn has a tight inner shell (3_{spd} orbitals extend to 0.32\AA) and a much larger outer shell (4_s extends to 1.06\AA). The bond length of Zn-C is $r = 1.93\text{\AA}$, which implies only the $4s$ electrons play a role in the chemical bond²⁰. The linear states of DMZn can then be analyzed as essentially a H-Zn-H molecule. Walsh⁴³ has proposed that the ground state of such a metal dihydride is linear in its ground state, bent in its first excited state, and linear in the second excited state.

The potential energy diagram for a general polyatomic molecule XY_2 is shown in Figure 2-1, which is taken from the work by Pack⁴⁴. Figure 2-1(a) and (b) are contour maps representations of the molecule's ground state and excited state potential energy versus internuclear distance, where contours are of the potential energy. The excited potential surface is binding with respect to dissociation of the molecule into $X+Y+Y$, but is repulsive with respect to dissociation into $XY+Y$. As the bond distance r_1 increases at constant r_2 , the molecule separates into $Y+XY$, and as r_2 increases at constant r_1 , it separates into $YX+Y$. The coordinate s in Figure 2-1(a) is the symmetric stretch coordinate of XY_2 , and "a" is the anti-symmetric stretch coordinate. As defined by Pack, in Figure 2-1(b), the coordinate z is the "reaction coordinate" and measures the distance along the dashed line from the barrier top, and "x" describes the vibrational motion perpendicular to z .

Figure 2-1a.

Pack's diagram for the ground state of the XY_2 molecule, where "s" and "a" are the symmetric and anti-symmetric stretch coordinates, respectively.

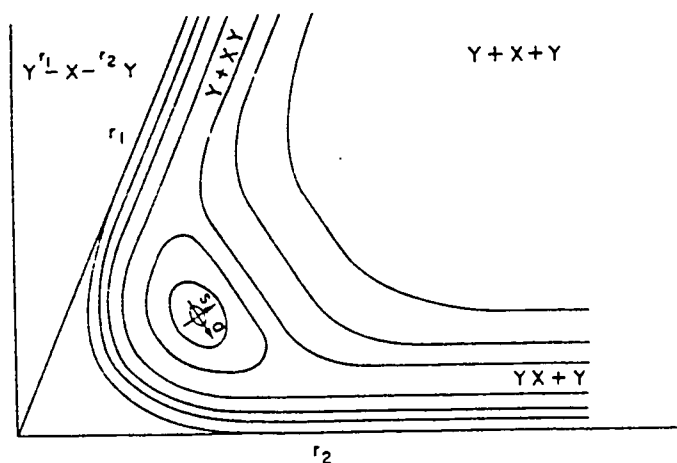
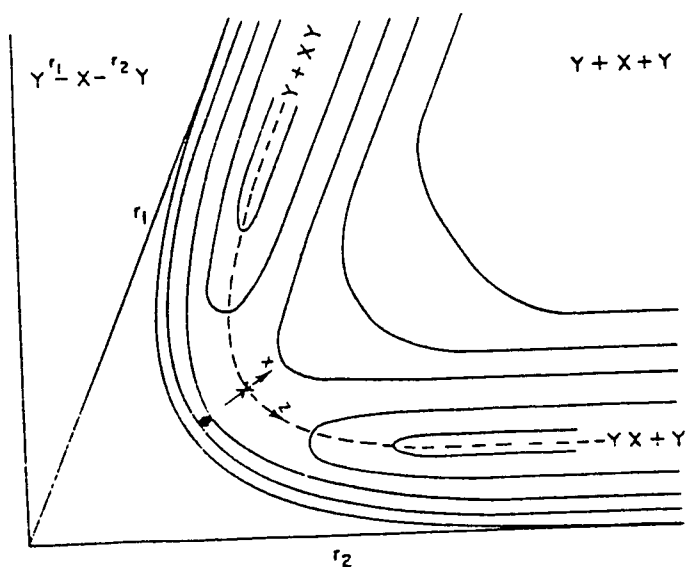


Figure 2-1b.

Pack's diagram for the excited state of the XY_2 molecule, where "x" and "z" are the reaction coordinates near the barrier top.



Asymptotically, x is the XY vibration coordinate, and " z " is the distance from Y to the center of mass of XY.

By constraining the dimensions $a=0$ and $z=0$, the potential energy along the "symmetric-stretch" x coordinate is obtained as shown in Figure 2-1(c), which is essentially the diagram one would obtain with a diatomic molecule. The allowed vibrational modes of the symmetric stretch of XY_2 are indicated by horizontal lines, and the wavefunction for one vibrational state is shown. The overlap of the ground state wavefunctions with the excited state wavefunctions is small for the lower vibrational states, reaches a maximum at $v=5$ and $v=6$, then gets smaller in the higher vibrational states. This gives rise to a continuum absorption with some vibrational structure.

For the case of asymmetric vibrational motion, Figure 2-1(d) shows the potential energy of XY_2 along the reaction coordinate z - axis with the symmetric stretch coordinates $s=0$ and $x=0$. This plot shows a potential well for the ground state and a potential barrier for the excited state. As Pack has shown, the allowed transitions from the ground state can have a very small energy overlap with excited state. This narrow band of energies also gives rise to a structured continuum, and is one explanation of the observed absorption spectra for the molecule DMZn.

The Study of DMX (X=Zn, Cd, Hg)

The absorption spectra of group 12 metal dialkyls was first studied by Thompson and Linnet²⁵ in 1935. Work has progressed from that initial experiment, which identified the upper states as repulsive due to two broad "diffuse" bands in DM(Zn, Cd, Hg) and DEZn, to the more recent works of Chen and Osgood²⁰, which have labeled those two states and postulated that

Figure 2-1c.

Pack's diagram for the cut along x (with $z=0$) from Figure 2-1(a) and (b), where the wavefunction with the peak overlap is shown.

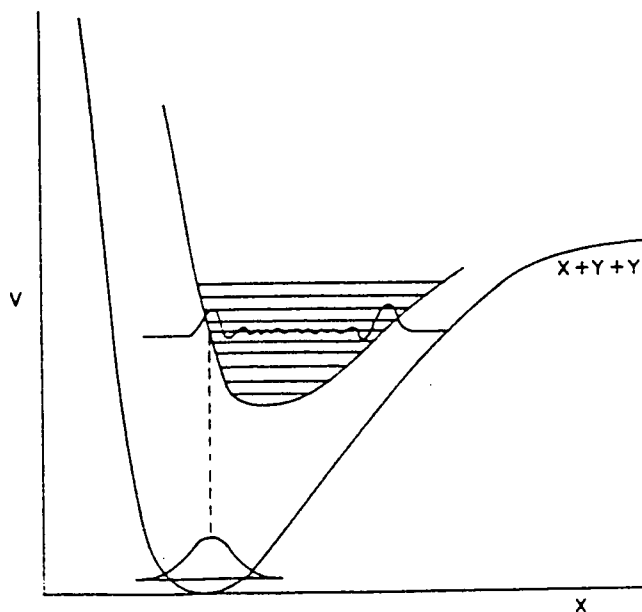
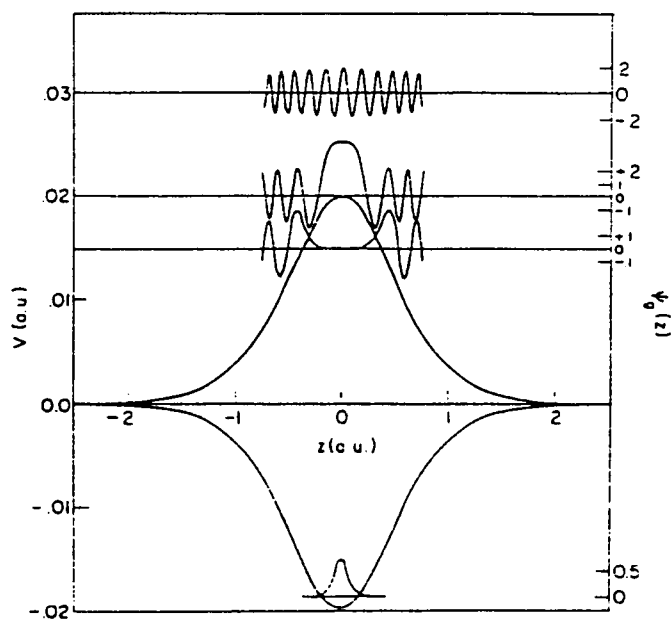


Figure 2-1d.

Pack's diagram for the cut along z (with $s=0$ and $x=0$), with several wavefunctions shown.



these upper states might be bound but dissociative. Theoretical work has also been done by Baake ⁴⁵ to determine the molecular constants and geometries of the molecules. More recent work by Jackson ²⁸, Robles ⁴⁰, and others have been interested in the formation of MMZn as a stable product of the photodissociation process. The work discussed in this thesis builds on these studies to try to determine what intermediate molecules are to be expected from the 193 nm photodissociation of DMZn and what chemical reactions take place with these intermediate radicals.

As a background for studying any molecule and its photodissociation, it is useful to have information on its ground state and excited states. In the ground state, DM(Zn, Cd, Hg) has a quasi-linear M-C-M skeleton, with methyl groups that are free to rotate ⁴⁵. This type of molecule belongs to the D_{3h} group, which is shown in Figure 2-2 and contains ⁴⁶:

one 3-fold rotation axis C_3^z

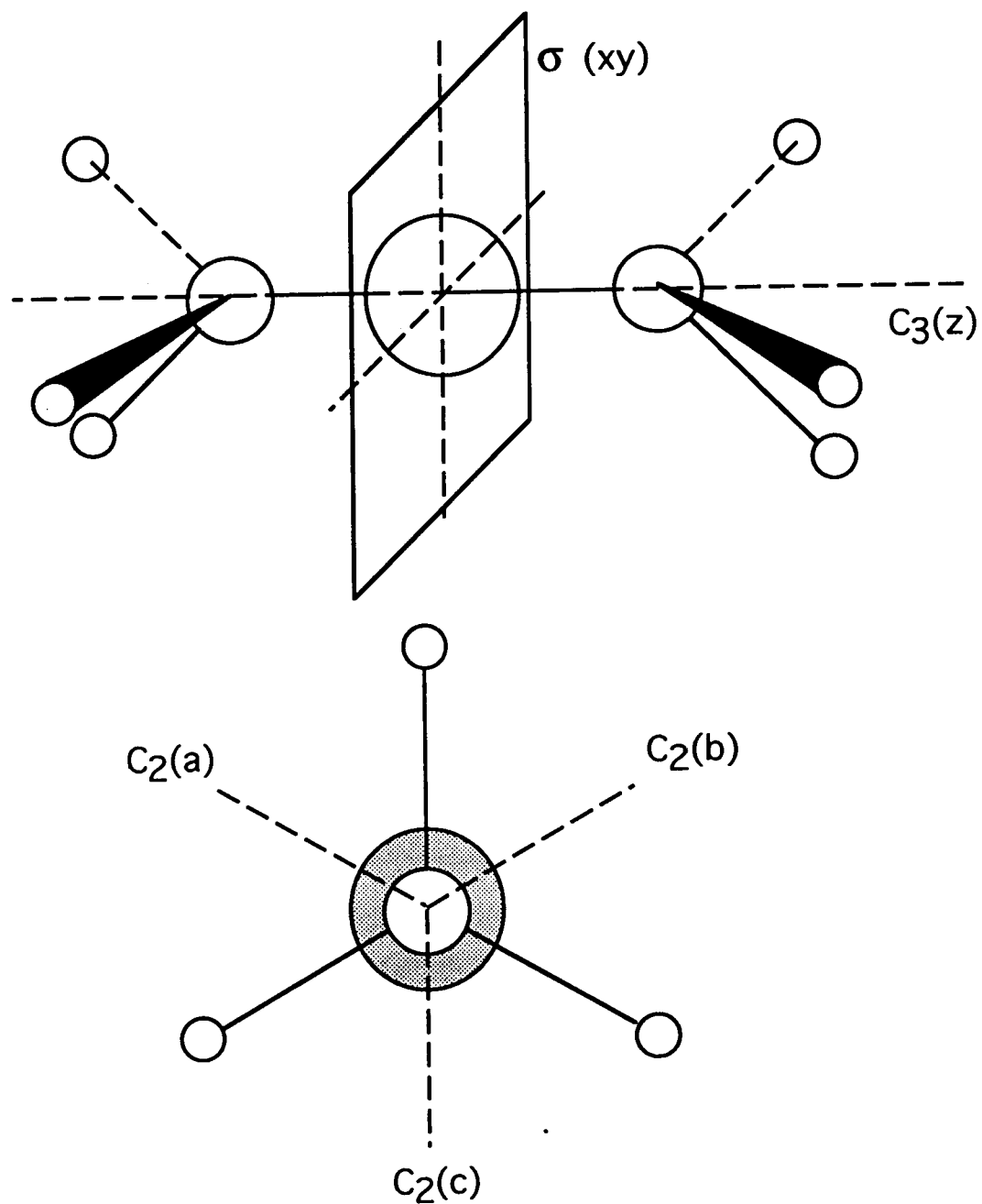
three 2-fold rotation axes (C_2^a , C_2^b , C_2^c) perpendicular to C_3^z

one reflection plane (σ_{xy}) perpendicular to C_3^z

three mirror planes through the z-axis

Since the M-C bond is longer than the C-H bond in methane, the bond angle in the methyl groups have been shown to be less than the 109° for a regular tetrahedron ²⁰.

Several groups have proposed molecular models for DMZn photodissociation. In 1984, Chen and Osgood ²⁰ proposed the geometry of the excited states as bent for the first state and linear for the second state. This conclusion is based on the UV absorption spectrum of DM(Zn, Cd, Hg)

Figure 2-2.Symmetry elements of DMZn (D_{3h})(3 reflection planes for the CH_3 are not shown)

and assumptions made about the electrons and the bonding. All three compounds show similar absorption spectra, with vibrationally structured continua between 2700Å and 1700Å. This type of structured continua has been previously described as "diffused bands", which implies predissociation by potential surface crossing. However, Pack ⁴⁴ has proposed that this type of structured continua can also be due to excitation to an upper electronic state that is "simply dissociative", which is the view taken in Chen and Osgood in their work.

In addition to Chen, Fujita has studied the absorption cross section of DMZn. The results of the two groups are similar and are shown in Figures 2-3 and 2-4. In Table 2-1, the data of Chen and Osgood from the UV absorption spectrum of DMZn are given. The fragments produced in the photodissociation process can also be identified by analysis of the photoabsorption spectrum. The $B \leftarrow X$ transition of DMZn has enough energy to break one Zn-C bond, resulting in a methyl radical and a MMZn radical. Since the B state has a non-bonding orbital ²⁰, breaking this bond should leave the MMZn in an excited state, as the Zn would be in its first excited state (3P_1). In both the excited state transitions, the methyl groups that are ejected go from a tetrahedral arrangement to a planar arrangement, thus one should detect the umbrella mode to be excited in the photodissociation process.

The MMZn radical has been studied by several groups ^{27,28,40}. The yield of MMZn versus free Zn atoms has been studied by Jackson ²⁸. The absorption of a single 248 nm photon produces vibrationally hot MMZn, which spontaneously dissociates into Zn atoms in $t < 40$ ns. However, when a He buffer gas is added, the MMZn fragment is stabilized and becomes the

Figure 2-3.

Absorption spectrum from Chen and Osgood ²⁰

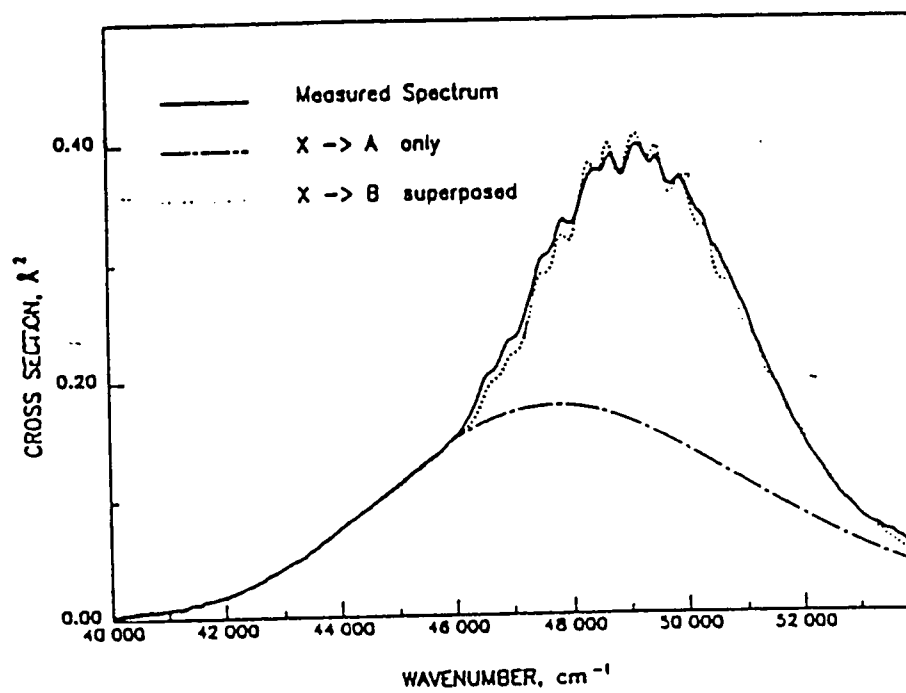


Figure 2-4.

Absorption spectrum from Fujita ²¹

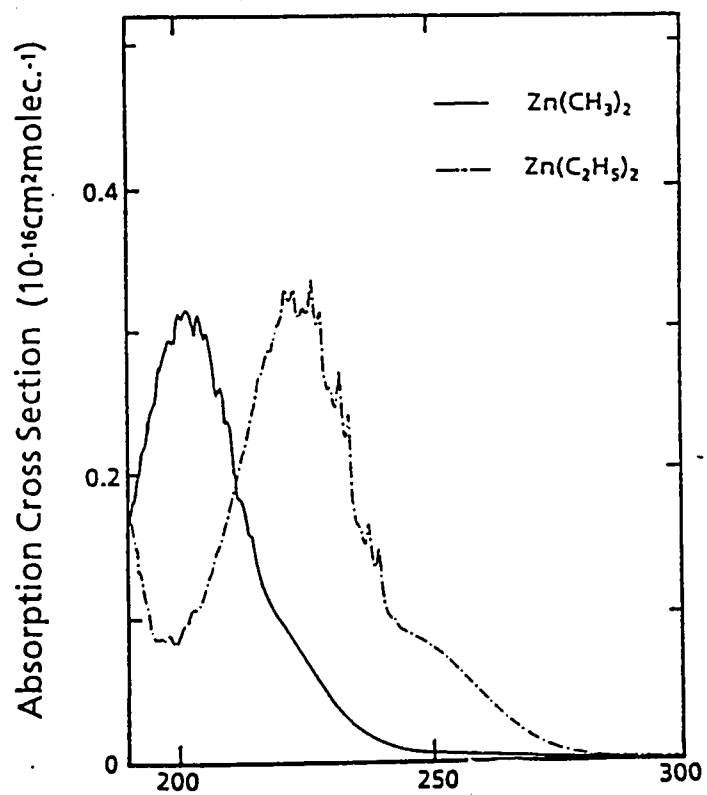


Table 2-1.Observed spectral properties of DMZn (data is from Chen ²⁰)

Umbrella mode of CH ₃	840 cm ⁻¹ ~ 39 Å
Zn-C-H bond angle	104.7 °
Zn-C stretch of MMZn	330 cm ⁻¹ ~ 15 Å
Antisymmetric C-H stretch	~ 3300 cm ⁻¹ ~ 152 Å
Oscillator Strength	
(X → A)	0.475
(X → B)	0.302
Center of first vibrational peak	
(X → A)	44,700 cm ⁻¹ = 2237 Å
(X → B)	46,550 cm ⁻¹ = 2148 Å

dominant product at high pressures (see Figure 2-5). It has also been shown by Jackson that use of Ar as a buffer gas improves the yield of MMZn at a given pressure. This implies that at the pressures used in the LAMOCVD chamber (typically 100 torr), *if* a MMZn species is being formed, it could be a major factor in the overall growth process.

A different view of the DMZn molecule and its absorption spectrum has been proposed by Bancroft ⁴⁷. Instead of assuming only the outer most orbitals contribute to the bonding, all the valence electrons can assumed to be active. With this in mind, the valence shell of the $M(CH_3)_2$ molecules can be labeled as:

$$(2e')^4 (2e'')^4 (3a_1')^2 (2a_1'')^2$$

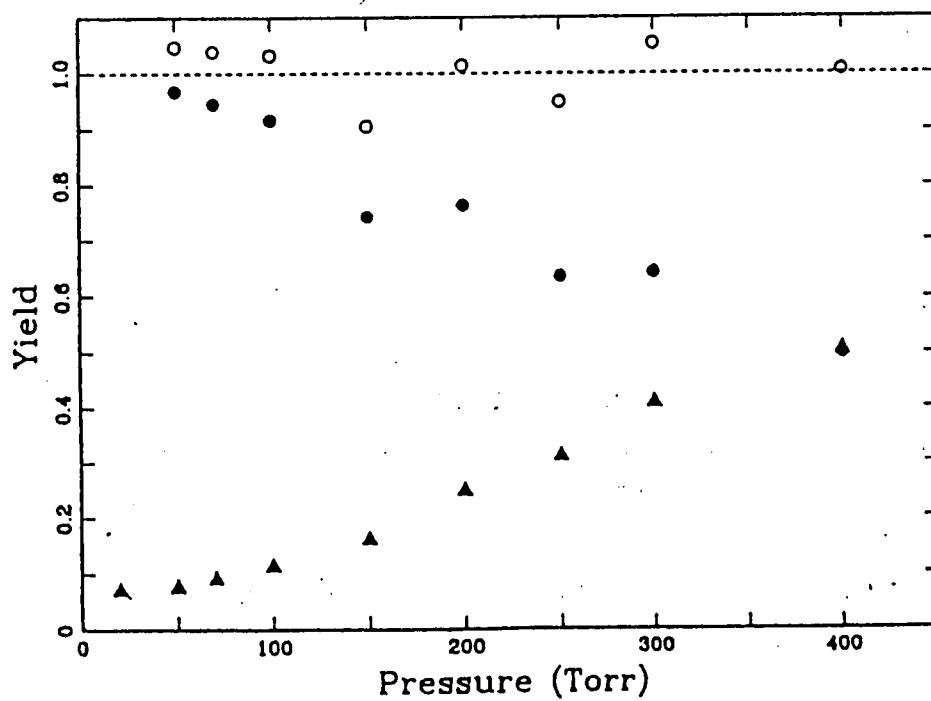
where the outer orbitals $2a_1$ and $3a_1$ have mostly metal-carbon bonding character, and the $2e$ orbitals form the C-H bonds. Ibuki ²² has used this orbital structure as a basis for interpreting the absorption spectra shown in Figure 2-6. The absorption transitions are proposed as Rydberg transitions which have the following designation :

<u>Absorption Peak</u>	<u>Rydberg Designation</u>
(~2020Å)	$4p \leftarrow 2a_1''$
(~1520Å)	$4p \leftarrow 3a_1'$
(~1180Å)	$3p \leftarrow 2e'; 3p \leftarrow 2e''$

Although the two basic interpretations of the DMZn photodissociation vary (active vs. non-active outer electrons), the anticipated photofragments

Figure 2-5.

Yield of MMZn versus Zn in the 248 nm photodissociation of DMZn²⁸

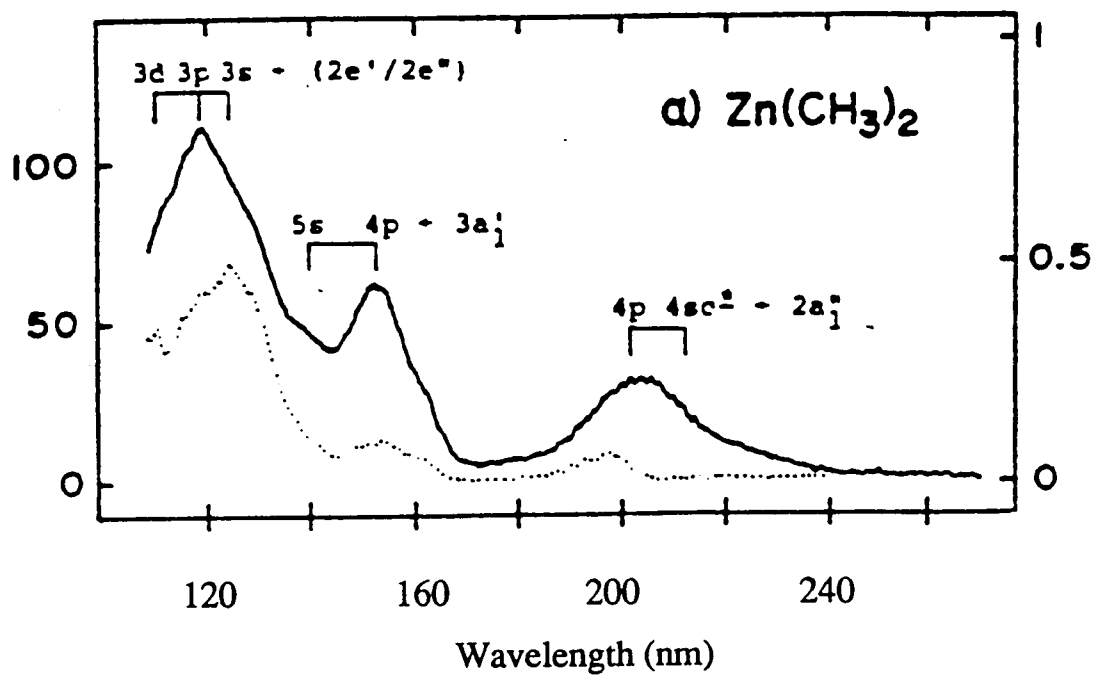


Yield of CH₃Zn (▲) and Zn (●) obtained upon photodissociation of (CH₃)₂Zn vs He buffer gas pressure. Data are normalized to an average total yield of 1.0 (○), represented by the dotted line.

Figure 2-6.

Absorption spectrum from Ibuki ²²

(y-axis units are in megabarns ; $1 \text{ Mbarn} = 1 \times 10^{-22} \text{ m}^2 = 1 \times 10^{-18} \text{ cm}^2$)



(excited CH_3 radicals, MMZn radical) can be determined by both analysis. Interpretation of the UV absorption spectra can also account for the energy that is distributed throughout the system by determining which vibrational modes of the molecule are being excited. The absorption spectra mentioned in this chapter are used for comparison to the results of this thesis. The interpretations of the absorption spectra by the above groups are used as a basis in this thesis for postulating the formation of other photofragments. The state of the Zn atom after the dissociation process is complete has not been determined by any group, however, and this is one of the results which will be discussed.

Chapter 3

Overall System

In order to study the growth process of ZnSe on GaAs substrates, a special reaction cell was constructed. As shown in Figure 3-1, an ArF laser (Questek, Model 2220, operating at 5 Hz, 100 mJ/pulse) is focused into a stainless steel absorption cell, which contains DMZn in a hydrogen ambient atmosphere. This is similar to the geometry which is used in the actual LAMOCVD growth cell, where the ArF beam profile is focused approximately 0.5 cm above the surface of the GaAs substrate ¹¹. The DMZn (Texas Alkyls, 99.9995%; see Appendix A) is obtained from a bubbler immersed in a constant temperature bath. Extra dry hydrogen is passed through a palladium diffuser and is used as the carrier gas. A control system interacting with mass flow controllers and pressure controllers allows for separate adjustment of the flow rate, metal organic partial pressures, and the total system pressure. Hydrogen is passed over the windows of the absorption cell to prevent unwanted metal deposition. The purge flow rate is maintained around 50 times the metal organic flow rate. In order to create a uniform flow of DMZn into the absorption cell, a specially designed flange distributes the gas across the dissociation region, as shown in Figure 3-2a.

The flow rates and the pressures can be used to calculate the number of molecules in the absorption cell, by the relations:

$$(3.1) \quad \frac{Q_{\text{DMZn}}}{P_{\text{DMZn}}} = \frac{Q_{\text{H}_2}}{P_{\text{H}_2}}$$

Figure 3-1.
Experimental layout showing lasers, cells, timing, and data acquisition

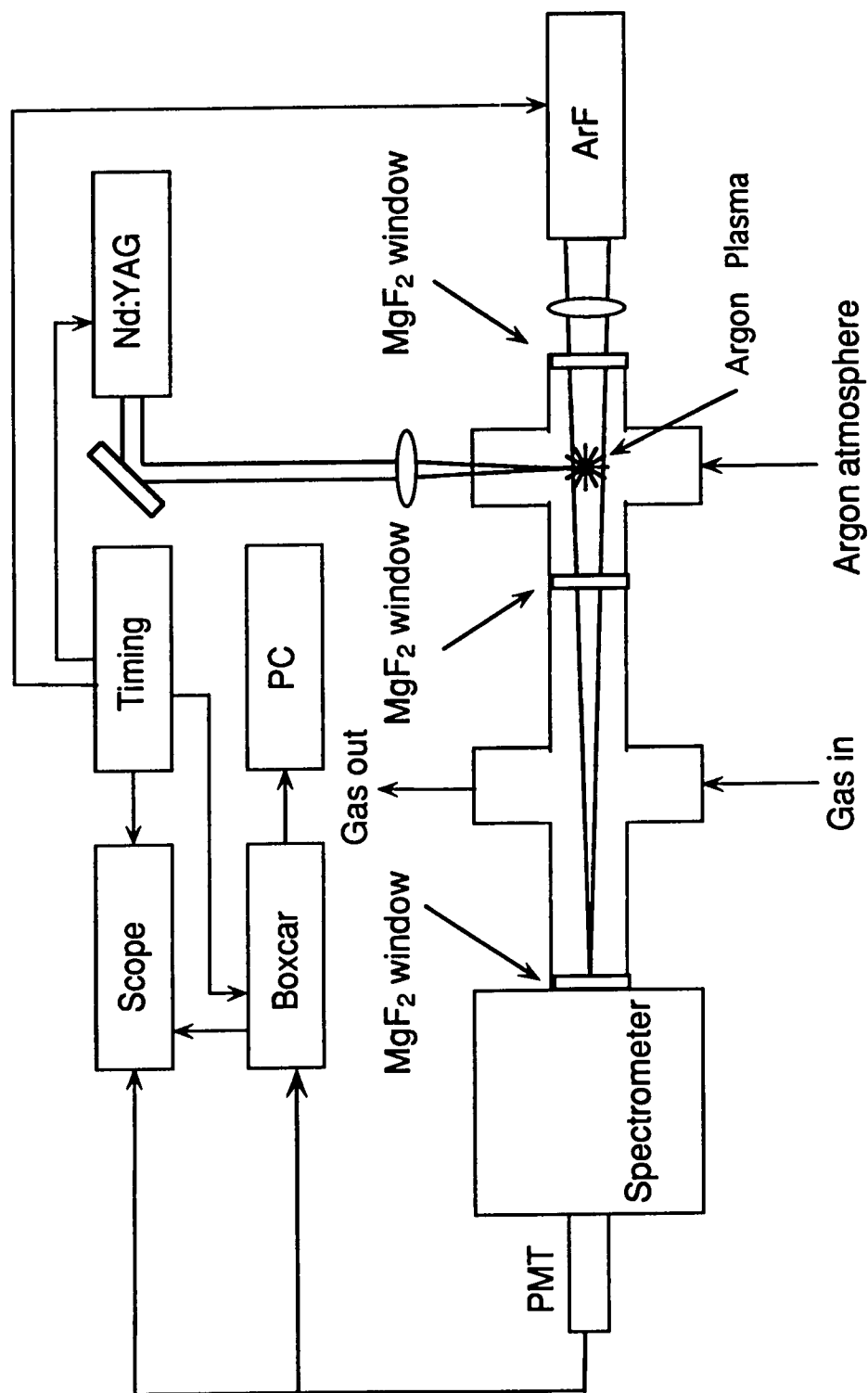


Figure 3-2a.

Vacuum flange designed for uniform gas flow

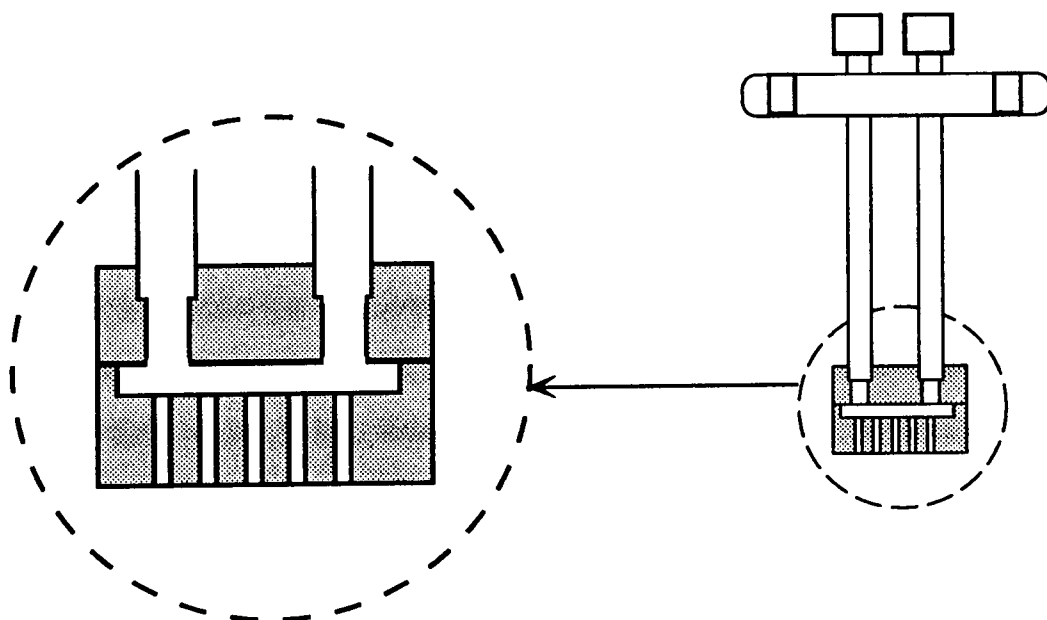
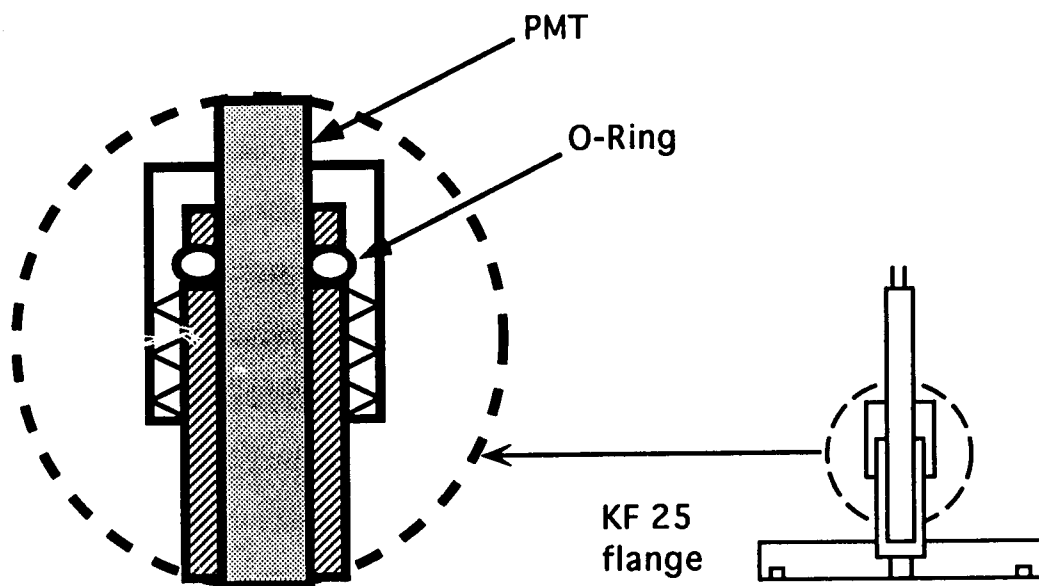


Figure 3-2b.

Vacuum flange designed to mount PMT on spectrometer



$$(3.2) \quad \frac{P_{\text{DMZn}}}{P_{\text{total}}} = \frac{Q_{\text{DMZn}}}{Q_{\text{total}}}$$

A computer program is given in Appendix B which calculates the density of molecules for the absorption cell.

VUV-VIS Plasma Probe Source

In order to determine the species created in the ArF dissociation of DMZn, an absorption probe experiment was designed using a novel plasma light source ⁴⁸. The plasma is created by focusing an Nd:YAG laser (Spectra Physics, Quanta Ray Model DCR-3, operating at 5 Hz, 0.8 J/pulse) into a stainless steel plasma cell containing an argon atmosphere at several hundred torr of pressure. This plasma emits a temporally short, broadband continuum of radiation due mainly to free-free transitions (bremsstrahlung) in the Ar ⁴⁹. Most rare gases plasmas have similar emissions, but Ar is used because its first resonance absorption is ~1060 Å, which is below the cutoff of the windows, and it is inexpensive. The plasma emission is used to back-light the absorption cell, allowing absorption studies of the products that are formed due to the photoabsorption of the ArF laser photons. The DMZn molecule has a large cross section for absorption around 193 nm ²⁰, and is readily dissociated by the ArF laser photons. By varying the timing between the ArF laser pulse and the Nd:YAG laser pulse (and thus the plasma emission), the temporal dependence of the absorption profile is acquired. The plasma emission is also detected from a side window at the plasma cell by a UV-VIS photodiode (Hamamatsu R1193U-02). This is used to normalize the PMT signal detected at the spectrometer in order to account for shot-to-shot variation in the plasma intensity. The spectrometer is kept

in vacuo during the experiments, and the PMT is sealed by way of an Ultratorr vacuum flange, as shown in Figure 3-2b.

For some of the experiments, a quadrupole mass analyzer (Micromass PC, VG Quadrupoles) was used to detect the by-products of the photodissociation process. The gas was sampled by a 1/4" stainless steel tube inserted into the center of the ArF laser beam in the absorption cell. The quadrupole analyzer head was located over a meter away from the absorption cell, therefore any radicals that are formed due to the dissociation process have recombined by the time the gas reaches the analyzer.

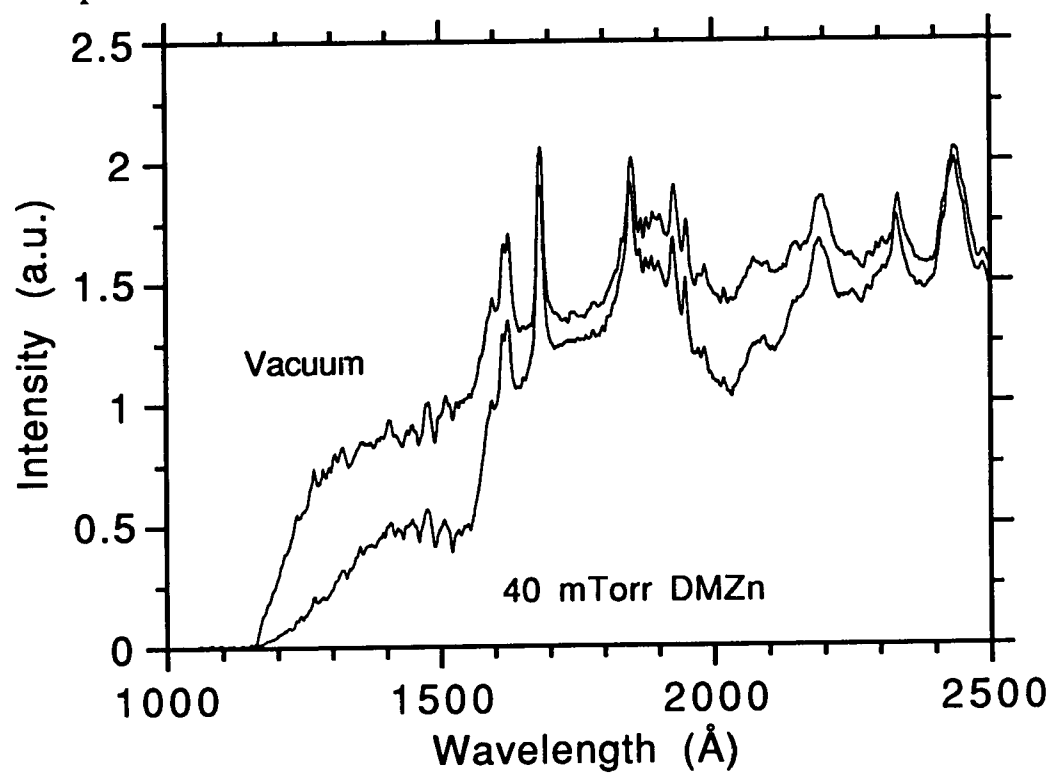
The plasma cell is separated from the absorption cell by a MgF₂ window which transmits wavelengths longer than $\lambda \sim 1150 \text{ \AA}$. Typical spectral features of the plasma emission from 1000 to 2500 \AA are shown in Figure 3-3, with and without DMZn in the absorption cell. The spectra have not been corrected for window, spectrometer, or PMT efficiencies. The spectrum is a mixture of continuum (free-free transitions) and line (bound-free) emission ⁴⁹, mostly from Ar II and Ar III. The temporally short (~ 200 ns) plasma emission allows for good time resolution of the absorption profiles. Similar plasma sources have been used to perform spectroscopy and excitation of alkali halide and rare gas alkali molecules ^{50,51}.

In order to determine whether the plasma itself is causing any further photodissociation processes, it is useful to estimate the number of photons that are incident upon the DMZn within the wavelength range of its absorption cross section. Using an "energy-balance" equation, the electron temperature of the plasma can be estimated ⁵²:

$$(3.3) \quad T_p = 2.9 \times 10^4 (I \lambda^2)^{2/3}$$

Figure 3-3.

Plasma spectrum with and without DMZn in the absorption cell



where T_p is in electron volts, I is the intensity of the excitation laser in W/cm^2 , and λ is the excitation laser wavelength in meters. An IR lens with $f = 25$ cm was used to focus the Nd:YAG laser beam (pulse width = 5 ns), and this would give a typical spot size of several hundred microns. Using an order of magnitude estimate of $I = 1 \times 10^9 - 1 \times 10^{10} \text{ W}/\text{cm}^2$ for the focused Nd:YAG laser beam yields a temperature of $T_p = 3.1 - 14.5$ eV. Assuming the plasma acts as a blackbody, the peak wavelength is given by the relation⁴⁹ :

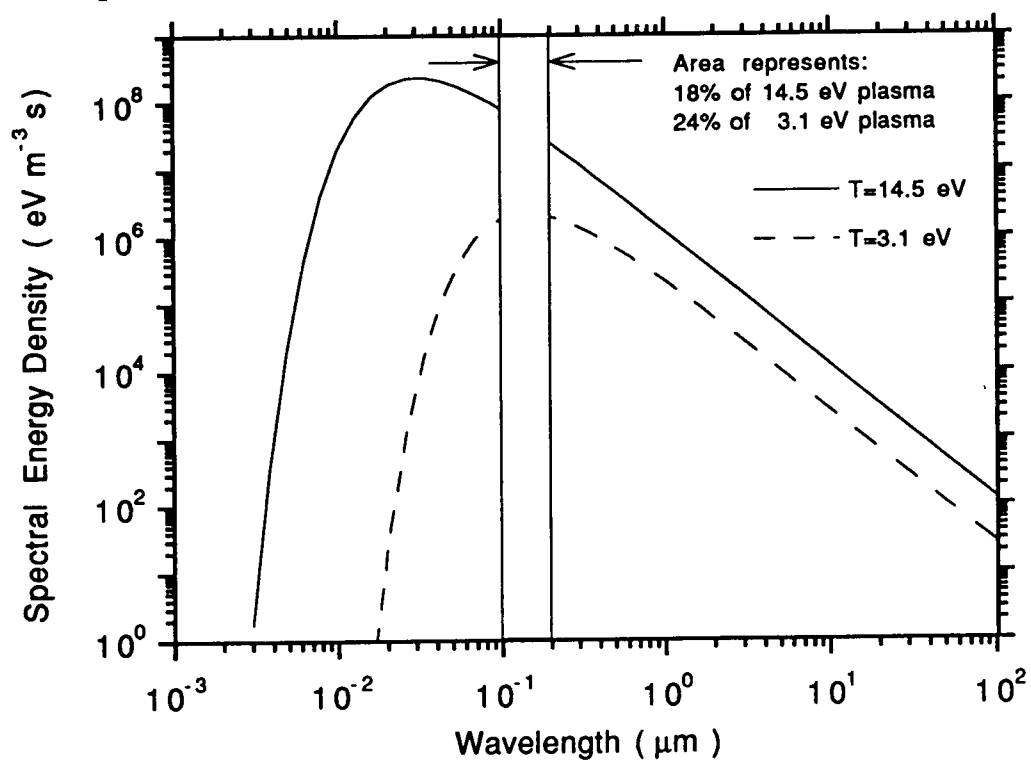
$$(3.4) \quad T\lambda_{\text{max}} = 2898 [\text{K}] [\mu\text{m}]$$

which gives $\lambda_{\text{max}} = 170 \text{ \AA} - 800 \text{ \AA}$, as shown in Figure 3-4. For the two curves, the percentage of radiation contained within the wavelengths of interest ($0.1 \mu\text{m} < \lambda < 0.2 \mu\text{m}$) is shown. The frequency interval of interest indicated in the figure represents the range of wavelengths from the cutoff of the windows to the tail of the cross section of absorption for DMZn (see Figure 2-6).

Since the percentage of the energy contained in this frequency interval is significant, it is necessary to determine the approximate number of photons in this interval. The energy emitted by the 14.5 eV plasma between $0.1 \mu\text{m} < \lambda < 0.2 \mu\text{m}$ is $\sim 2 \times 10^{17} \text{ eV cm}^{-3}$, and is $\sim 2 \times 10^{15} \text{ eV cm}^{-3}$ for the 3.1 eV plasma. For an average photon energy within the absorption cross section ($8.3 \text{ eV} = 1500 \text{ \AA}$), this means that the Ar plasma emits approximately $2 \times 10^{14} < \text{photons} / \text{cm}^{-3} < 2 \times 10^{16}$ from the focal point of the laser. The photons from the plasma act essentially as a point source and are distributed uniformly in a spherical pattern, so by the time the photons reach

Figure 3-4.

Plasma represented as a blackbody spectrum at different temperatures



the absorption region in the cell, they are distributed over an area of $1.2 \times 10^4 \text{ cm}^2$. This implies that the photon density of the plasma is approximately $2 \times 10^{10} < \text{photons} / \text{cm}^3 < 2 \times 10^{12}$. This is four orders of magnitude less than the density of the DMZn, so it is assumed that the argon plasma does not cause any significant number of photodissociation reactions.

The plasma emission varies with both Argon pressure and Nd:YAG laser intensity, and the optimal ranges were determined. Figure 3-5(a) shows the variation of the plasma emission with pressure, and as the pressure increases, the line emission becomes less distinct, and the broadband emission increases slightly. Figure 3-5(b) shows the ratio of two adjacent emission peaks at different wavelength regions. Again the intensity of the line emission decreases with increasing pressure, and the effect is greater at the shorter wavelength region. This decrease in the intensity with increasing pressure is contrary to the effect noticed by others⁵³, although that work used a KrF laser as the excitation source. This effect may be due to self-absorption, however, this observation was not further explored, and the lower Ar pressures were used throughout the experiments. The plasma emission was determined to have optimal output at higher laser intensities, and all the experiments were performed with an Nd:YAG output of $\sim 850 \text{ mJ}$. Typical repeatability of the spectral output is within $\pm 5\%$, as is shown in Figure 3-6, with better repeatability at longer wavelengths where the emission signal is stronger.

Geometry and Alignment of System

The ArF dissociating beam and the plasma are centered on the optical axis of the spectrometer, as shown in Figure 3-7. The ArF laser beam is focused with a 1m focal length CaF_2 lens and is directed slightly off-axis

Figure 3-5a.

Plasma emission for two Ar pressures

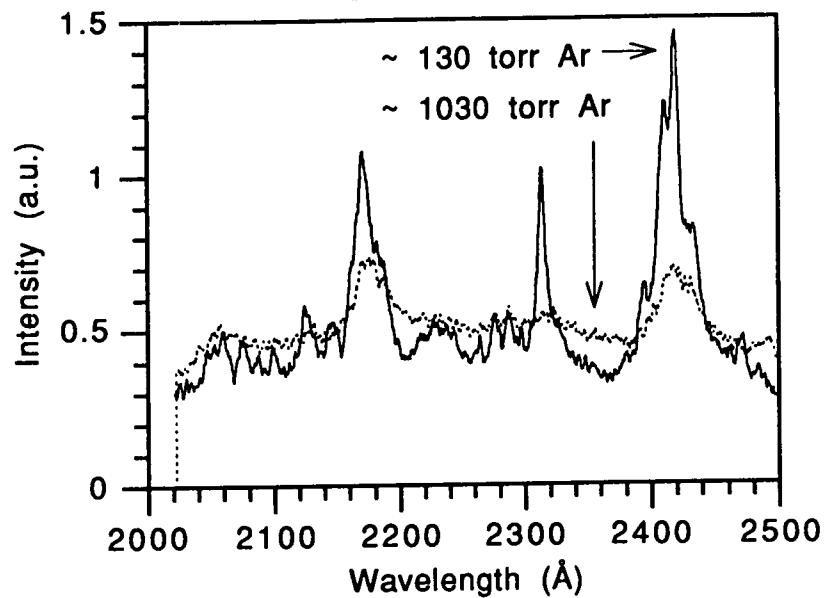


Figure 3-5b.

Ratio of adjacent line emission peaks at two different wavelength regimes

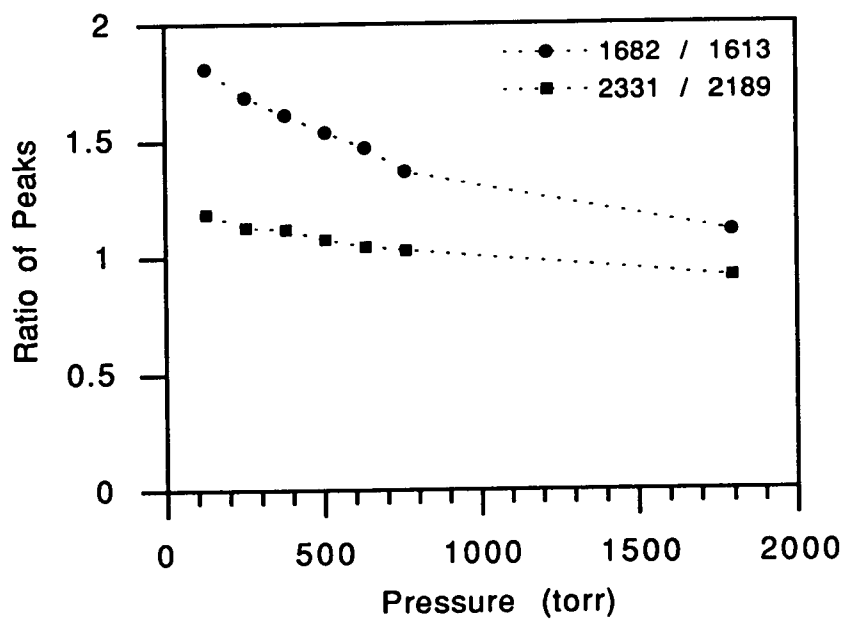


Figure 3-6a.

Plasma spectrum for two consecutive scans

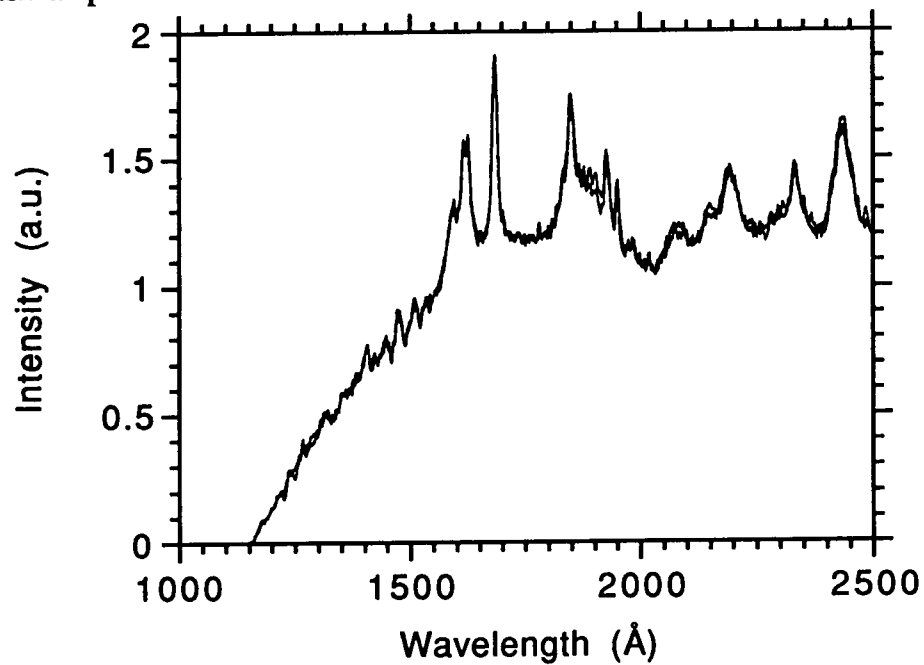


Figure 3-6b.

Variation between spectra

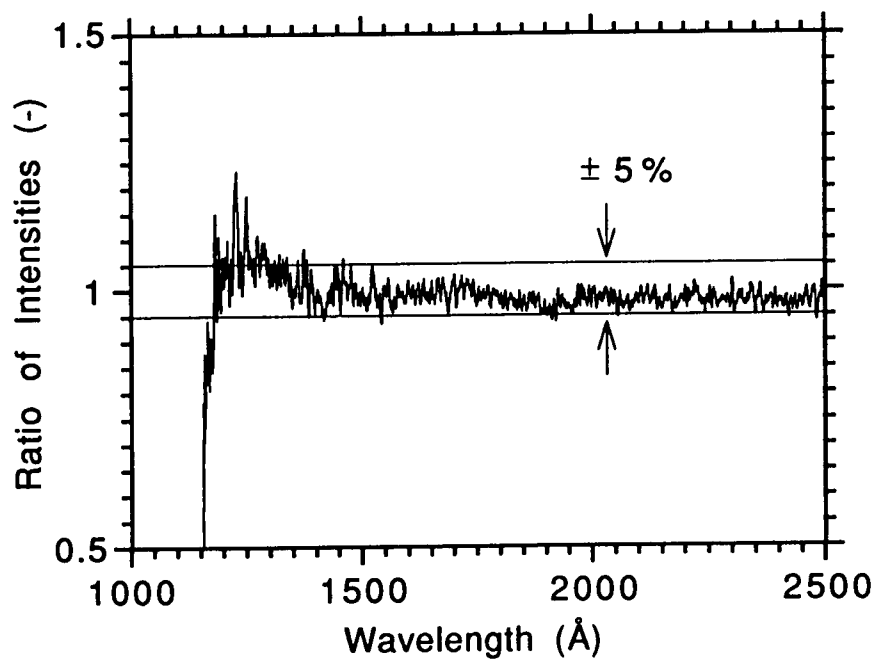
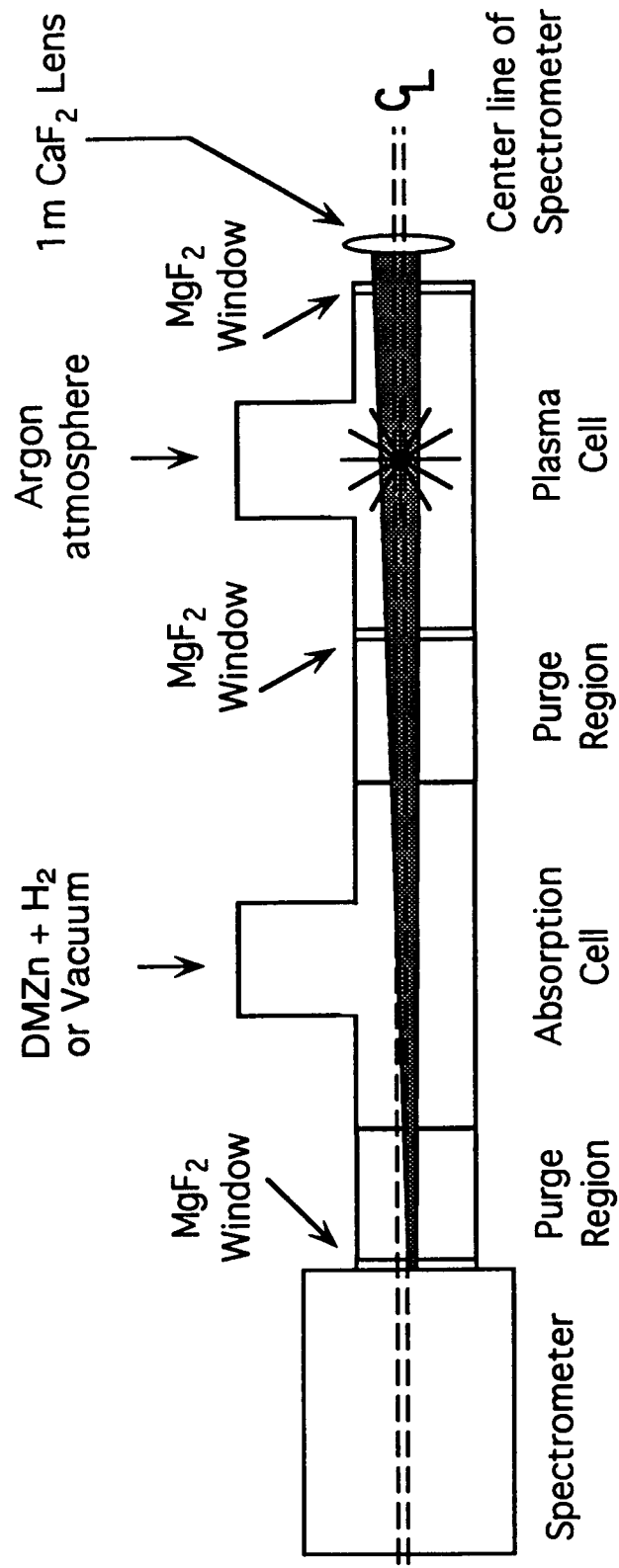


Figure 3-7.
Side view of experimental setup showing details of the ArF alignment
with the spectrometer and plasma emission



onto a beam block so as to prevent most of the 193 nm radiation from entering the spectrometer. Some radiation from the ArF was detected at the PMT, however, and this limited the temporal resolution of the system. This alignment allows for maximum spatial overlap of the dissociating beam and the plasma emission. The system was aligned using a HeNe laser beam by directing it backwards through the spectrometer slits, the reflecting mirror, the zeroth order of the grating, and through the absorption cell as indicated in Figure 3-8. The defining apertures, in order, are the horizontal and vertical spectrometer slits, a stainless steel beam block, and a purge baffle. Using this system the PMT and plasma emission can accurately be aligned within 5 mm.

The ArF beam profile has a rectangular cross section and the area was measured as shown in Figure 3-9. A razor blade was scanned across the beam at the center of the absorption cell and the output energy was detected. An energy versus position graph was acquired, and by differentiating this graph it was found that the beam profile measures $\sim 3 \text{ mm} \times 9.5 \text{ mm}$ (0.285 cm^2) at the center of the dissociation region in the absorption cell.

The ArF beam is attenuated by several factors once it reaches the center of the absorption cell: attenuation of the MgF_2 windows ($\sim 8\%$ each), a slight Zn film on the windows, and the broadband absorption of the DMZn molecule. All three of these attenuations can reduce the energy of the ArF by 30% once it reaches the end of the absorption region in the cell. Taking these factors into account means that the maximum average energy density of the beam is $\sim 250 \text{ mJ/cm}^2$ (12 MW/cm^2) at the center of the cell.

Figure 3-8.
Alignment procedure for experiment and close-up of apertures
(Not drawn to scale)

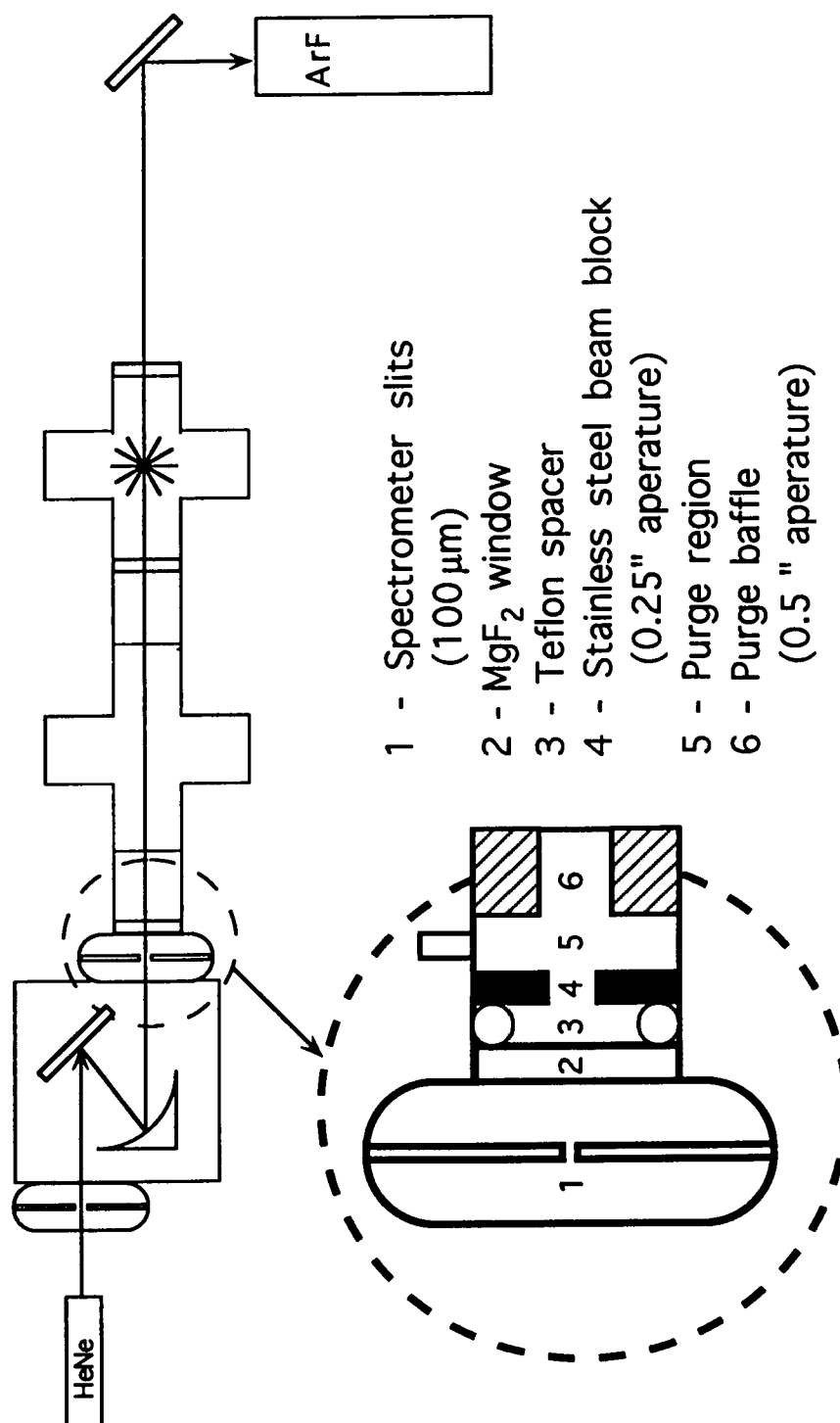


Figure 3-9a.

ArF horizontal beam profile at the center of the absorption cell

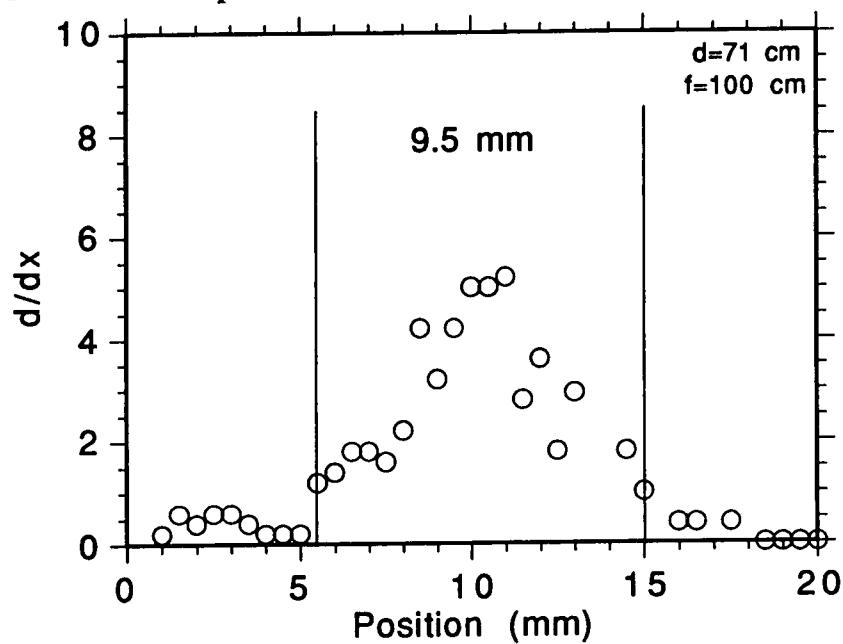
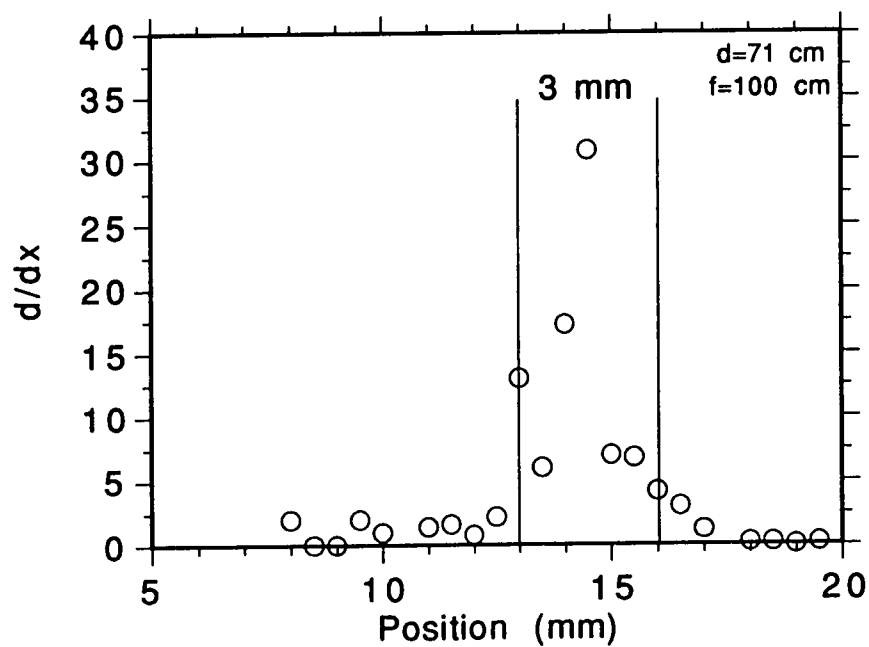


Figure 3-9b.

ArF vertical beam profile at the center of the absorption cell



Timing and Data Acquisition

The timing between the dissociating beam and the plasma probe is controlled by a digital pulse generator (Stanford Research Systems Model DG-535). The detection system consists of a 0.25m vacuum spectrometer (Acton Research Model VM502), to which a solar blind PMT (Hamamatsu R1080) is attached. A typical slit width is 100 μm , yielding a wavelength resolution of $\sim 4\text{\AA}$. The signal from the PMT is processed by a boxcar integrator (SRS 245, 250) and the data is recorded with a microcomputer. The details of the timing triggers for the Nd:YAG laser, the ArF laser, and the SRS boxcar are shown in Figure 3-10. The temporal relation of the plasma emission, the ArF pulse, and the boxcar gate is shown in Figure 3-11. The timing resolution of the system is limited by the jitter of the ArF laser discharge, which is ± 25 ns. Due to the flow of undissociated DMZn back into the optical column, the maximum delay time from the dissociating laser for probing photoproducts is ~ 2 ms.

This system was used to acquire information on the photodissociation of DMZn by a 193 nm laser. However, the setup is readily capable of switching to the other source gases (NH_3 and DESe). As will be discussed in the next chapter, the results of this thesis are comparable to those mentioned in Chapter 2, which were done mainly with synchrotron sources. The versatility and inexpensive nature of the setup lends itself well as a valuable tool for studying the growth process.

Figure 3-10.
Timing and triggers for the Nd:YAG laser, ArF laser, and SRS boxcar

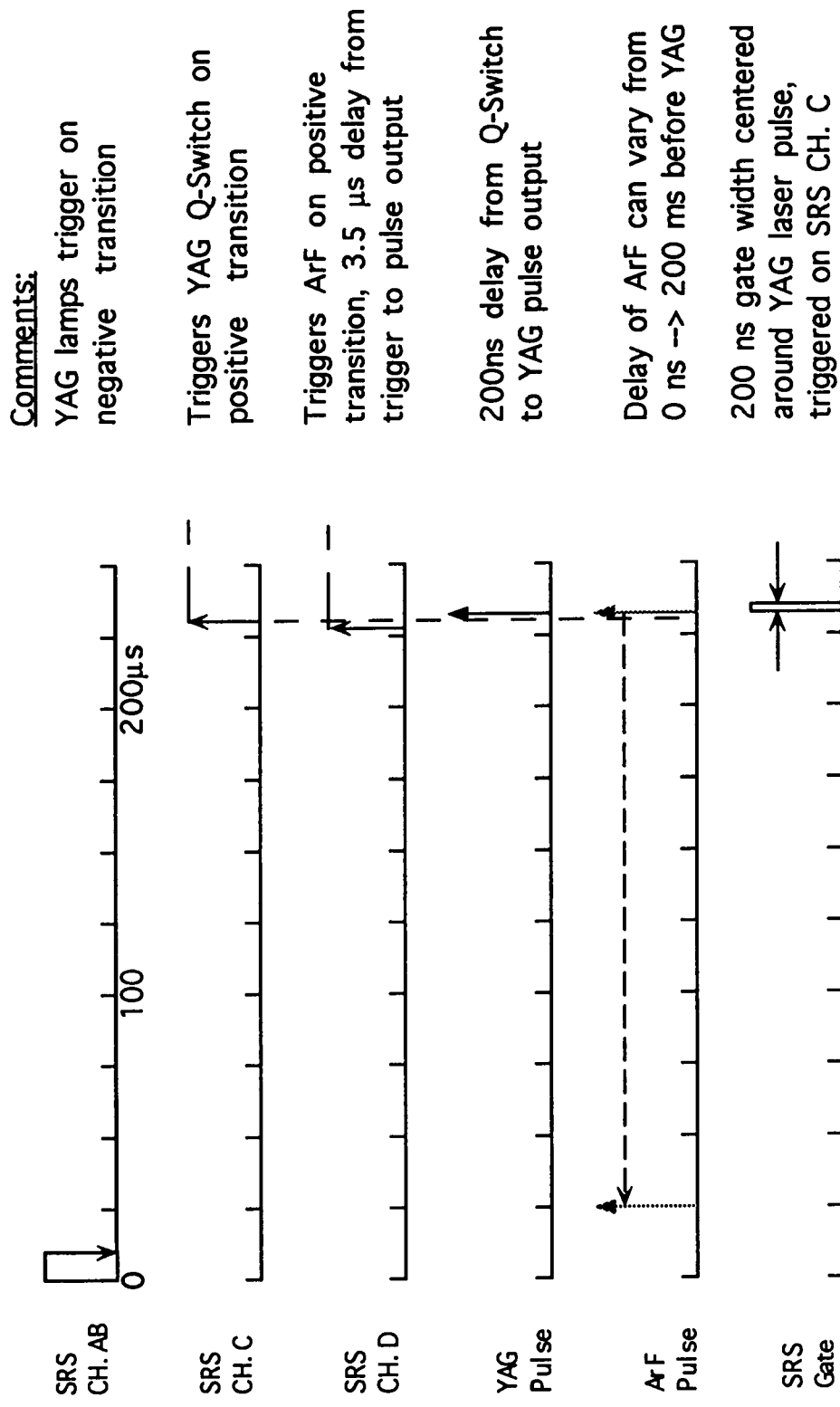
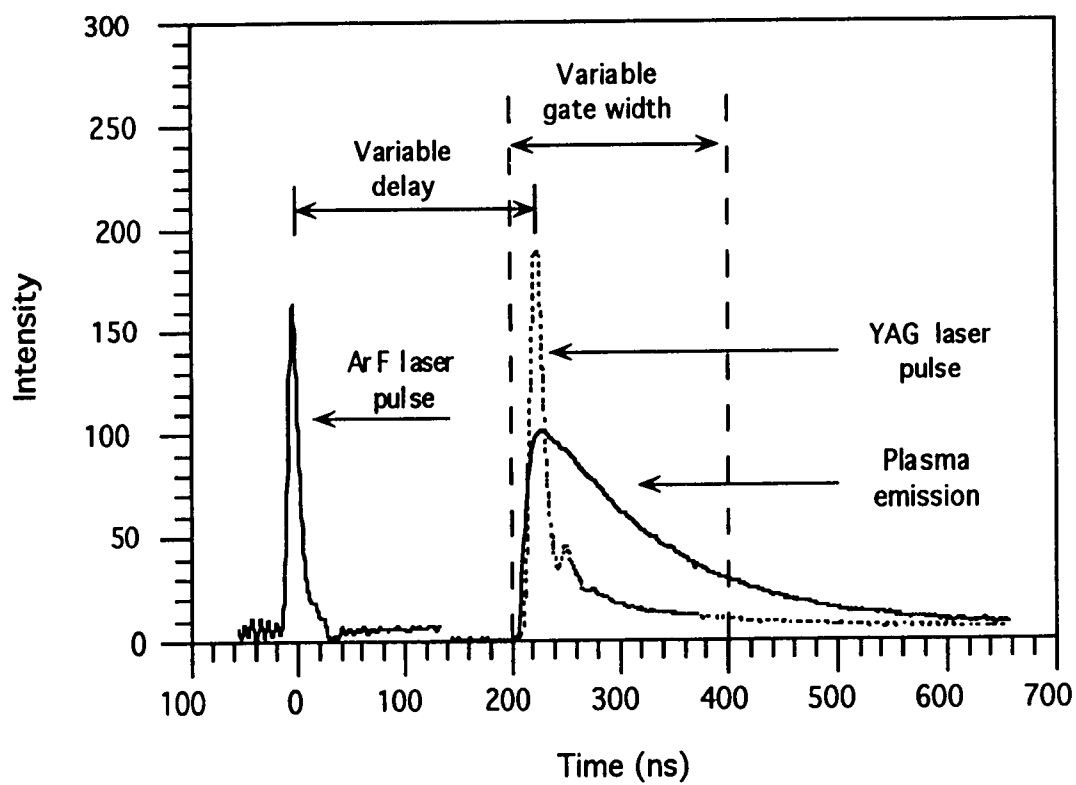


Figure 3-11.

Temporal relations between the ArF laser pulse, the Nd:YAG laser pulse, the plasma emission, and the data acquisition boxcar integrator gate.



Chapter 4

Summary of Experiments

The experiments on the photodissociation of DMZn were performed in several phases, and will be discussed separately. The first phase was absorption experiments that probed the photoproducts; the second phase studied the visible emission noticed during the ArF dissociation laser pulse; and the third phase explored the dependence of the first two phases on the ArF energy density. A summary of the experiments is given below.

The only photoproducts observed in absorption were ground state Zn and ground state methyl radicals, as is seen in Figure 4-1. The transitions shown are the $(4^1P_1) \leftarrow (4^1S_0)$ transition at 2139Å for Zn, and the $(B^2A_1) \leftarrow (X^2A_1)$ transition at 2160Å for CH₃. Curve A is the plasma spectrum seen with the absorption cell evacuated, Curve B is an empirical fit to the baseline of the absorption curve, and Curve C is the detected plasma spectrum with DMZn in the absorption cell. Curve C is separated into three regions: (1) the ArF laser on, but with the output shutter closed, (2) the ArF laser on, with the output shutter open, and (3) the ArF laser on, and the output shutter closed. This was done so as to eliminate the effect of any electrical noise in the data due to the firing of the ArF thyatron, and to observe the variation in the spectra due to the broadband DMZn absorption due to only the photodissociation process.

Two other transitions of CH₃ besides the one at 2160Å were detected in absorption as shown in Figure 4-2, the $(C^2E \leftarrow X^2A_1)$ transition of CH₃ at 1503Å, as well as an absorption at 1385Å, which may be due to the $\delta_2 \leftarrow X$ and $\gamma_2 \leftarrow X$ transitions of CH₃^{42,54}. Similar to Figure 4-1, Curve D is the

Figure 4-1.

Plasma spectra showing absorption profiles of Zn and CH₃

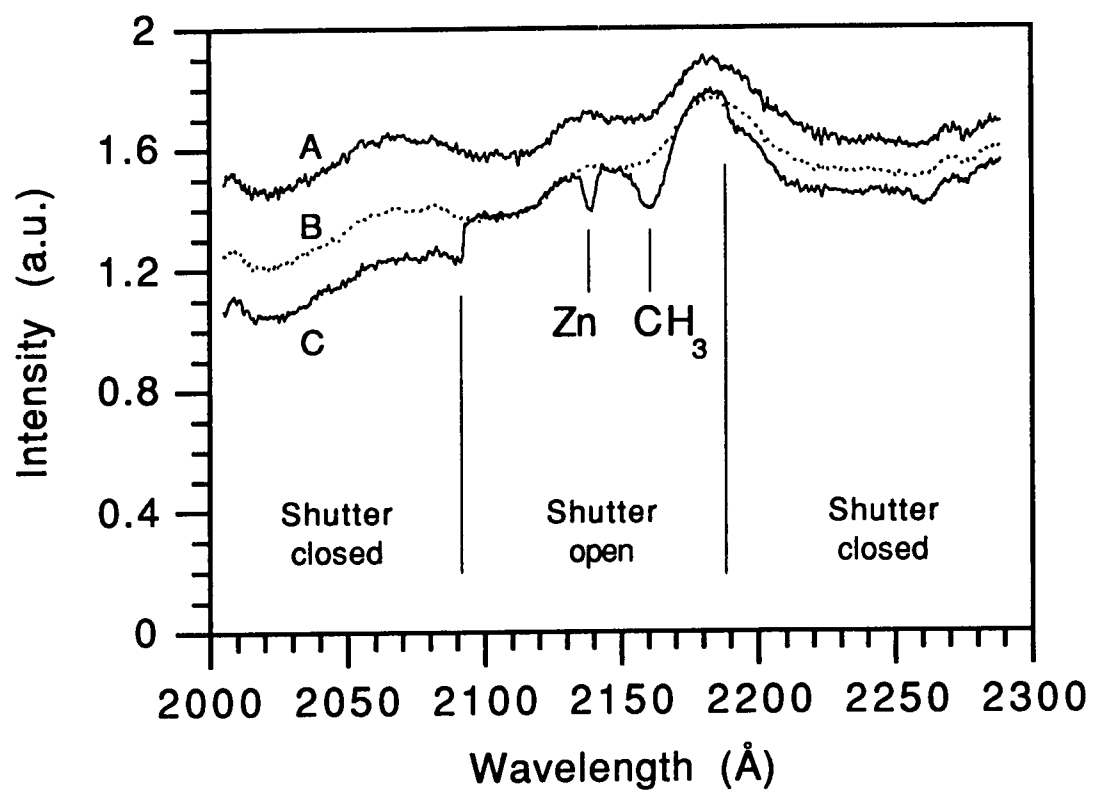
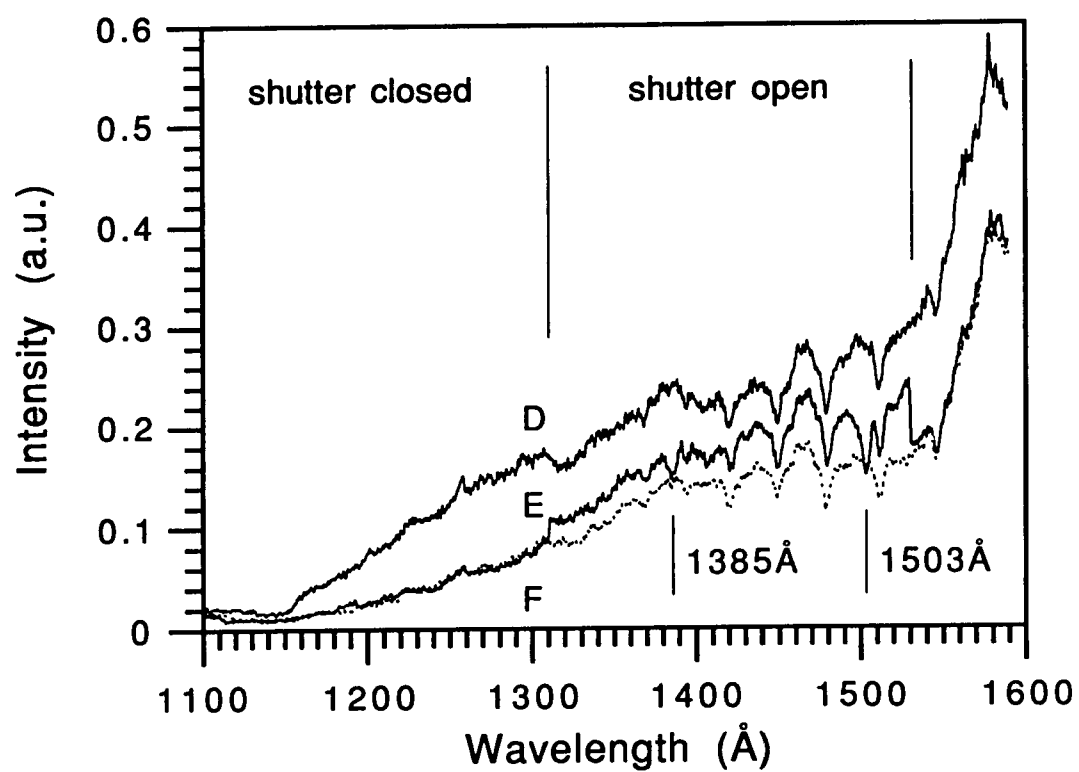
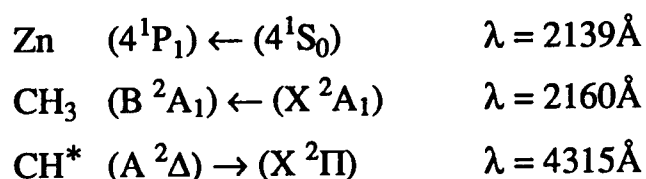


Figure 4-2.

Absorption profiles of VUV CH_3 bands at 1385Å and 1503Å



plasma spectrum with vacuum in the cell. Curve E is the plasma spectrum with DMZn in the cell with the ArF laser on and the shutter cycled opened and closed, and Curve F is the plasma emission with DMZn in the cell and the ArF laser shutter closed. Due to the relatively low signal levels of the plasma at the shorter wavelengths, the absorption transition of CH₃ at 2160Å provided the best signal to noise ratio of the three methyl absorptions and it was used to determine the methyl radical concentration. Visible emission from excited state CH radicals were also observed. A summary of the species detected and of the relevant time scales is shown in Figure 4-3, where the transitions are:



The results from the absorption experiments are discussed below, and the results from the fluorescence experiments and the energy dependence experiments are discussed in later in the chapter.

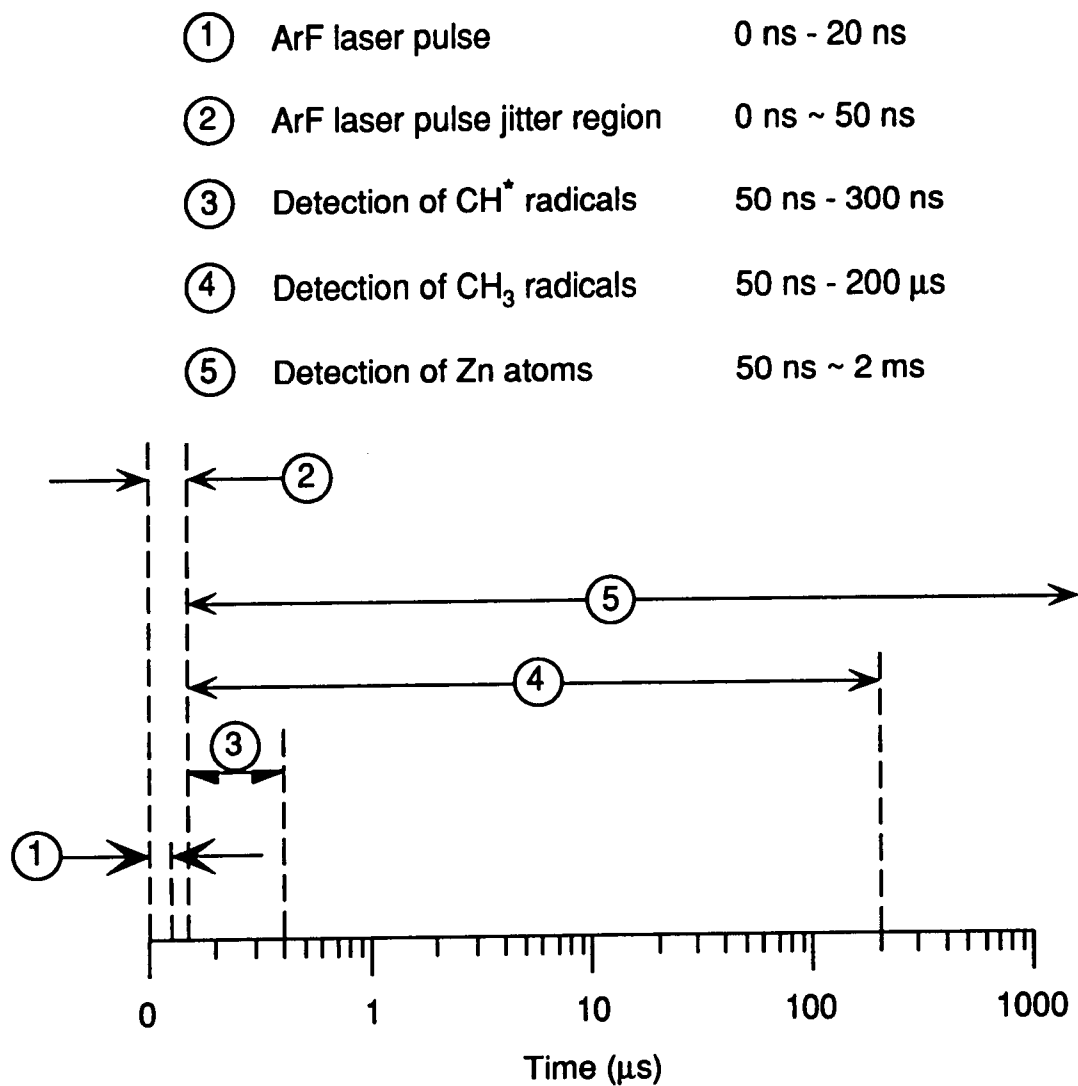
Absorption Experiments

Because of the hydrogen window purge, the actual length of the absorption region in the cell had to be determined. The DMZn absorption cross section is determined using Beer's Law:

$$(4.1) \quad \sigma(\lambda) = \frac{1}{NL} \ln \frac{I_0}{I}$$

Figure 4-3.

Summary of the detected photodissociation species and their lifetimes



where N is the density of absorbing species per cm^3 , L is the absorption length in cm, I_0 is the detected intensity of the plasma with vacuum in the cell, and I is the intensity with DMZn in the cell. The effective absorption length is determined by measuring the DMZn absorption cross section with no purge gas flowing, using the known length of the cell. An absorption measurement is then taken with the purge gas flowing, and it is compared to the measured DMZn absorption cross section. By this method, it is found that the average absorption path length in the cell is approximately $L = 8$ cm with the hydrogen purge. This length varies ± 1 cm from experiment to experiment (see Table 4-1).

The cross section of absorption for DMZn has been reported by several groups (see Figures 2-3,4,6) ²⁰⁻²². As shown in Figure 4-4(a), the cross section obtained in this work is in good agreement with the results of the other groups. The absorption feature centered around 2020\AA has a peak cross section of approximately 0.3\AA^2 , close to the value obtained by Fujita ²¹ and Ibuki ²² whereas the maximum obtained by Chen and Osgood ²⁰ at this wavelength is 0.4\AA^2 . Comparing our results to Ibuki, the deeper UV feature centered at $\sim 1550\text{\AA}$ is in good agreement with a maximum of $\sim 0.7\text{\AA}^2$. However, the feature at $\sim 1200\text{\AA}$ yields a maximum of $\sim 1.6\text{\AA}^2$, compared to a maximum of $\sim 1.1\text{\AA}^2$ for Ibuki. Figure 4-4(b) is a high resolution scan of the absorption cross section, where the vertical lines indicate superposed vibrational progressions of Zn-C stretching and CH_3 deformation first identified by Chen and Osgood (see Figure 2-3). Similar to the observations of Ibuki, the Zn-C stretching mode is also evident in the deeper wavelength region from $\sim 1520\text{\AA}$ to $\sim 1180\text{\AA}$.

Table 4-1.

Summary of data for several typical experiments

			Zinc Absorption			Methyl Absorption			
			Equivalent Width Method*			Fit to Decay Curve Method			
	N_{DMZn} (cm-3)	Length (cm)	Eq.W. (Å)	N_{Zn} (cm-3)	% Abs. (-)	A_0 (-)	K (us-1)	N_{CH_3} (cm-3)	% Abs. (-)
I	1.3 e15	6.4	0.56	3.5 e15	270	0.0694	1.649	1.3 e15	50
II	1.3 e15	7.4	0.47	1.8 e15	138	--	--	--	--
III	1.3 e15	9.0	0.53	2.5 e15	192	0.1311	0.856	1.3 e15	50
IV	1.3 e15	(5.5)	0.60	4.6 e15	353	0.0840	0.806	7.7 e14	30
V	4.0 e15	9.3	1.96	9.8 e15	245	--	--	--	--

I : Zn equivalent width averaged from 1-200 us

II : Zn equivalent width averaged over 9 runs with varying energy

III : Zn equivalent width averaged from 1-200 us ; CH₃ profile taken with $t_0=2$ us

IV : Vacuum and DMZn spectra do not match well for calculating length

V : Zn equivalent width averaged over 4 runs with varying energy ; 100 torr H₂ $f = 1.3$ for Zn (4P \leftarrow 4S) $\Gamma_{total} = 151$ MHz (@ 25 torr H₂) $\Delta = 13.5$ s⁻¹ (Doppler width) $\Gamma_{total} = 250$ MHz (@ 100 torr H₂)

* note: calculations based on curve of growth with $\alpha = 0.1$; actual concentration of Zn calculated by this method is less due to the fact that the ratio of Lorentzian to Gaussian linewidths is $\alpha = 0.14$ (@ 25 torr H₂) and $\alpha = 0.23$ (@ 100 torr H₂)

Figure 4-4a.

Absorption cross section of DMZn (compare to Figures 2-3,4,6)

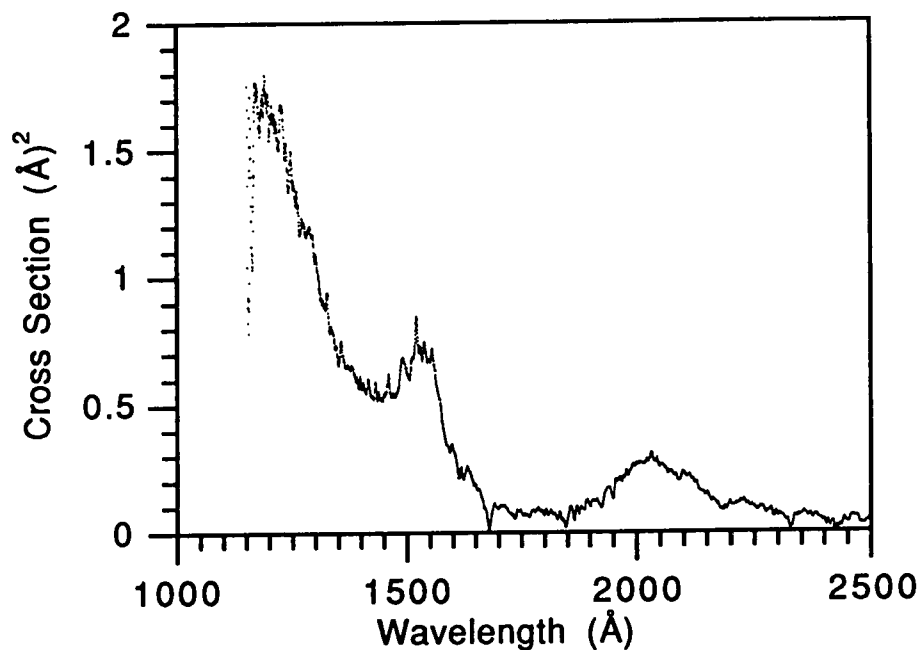
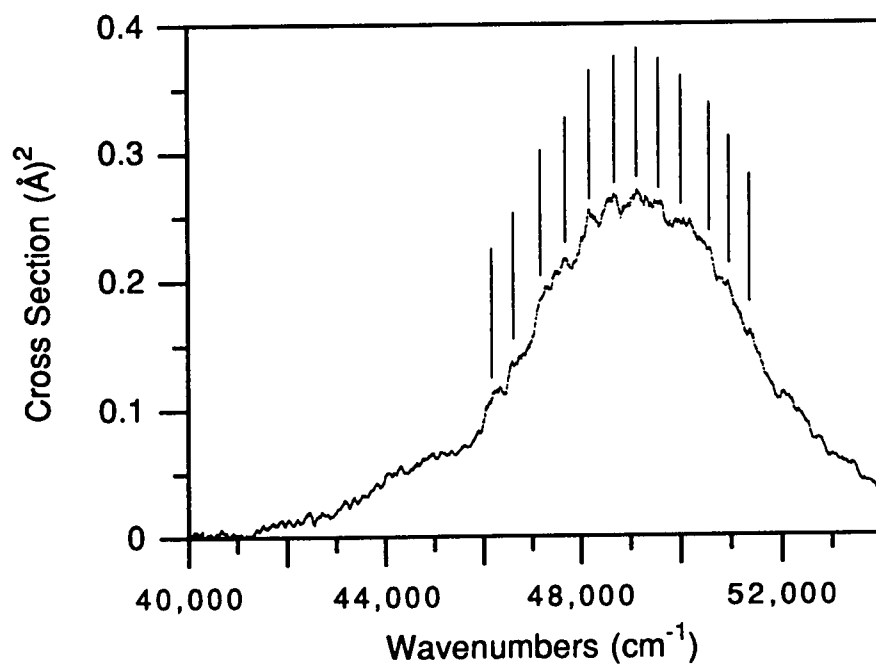


Figure 4-4b.

High resolution scan of DMZn cross section (compare to Figure 2-3)



In order to calculate the concentrations of absorbers (either Zn or CH_3) from the absorption profiles, it is necessary to estimate the depth of the absorptions. An empirical estimate of the baseline of the absorption curve is determined to compensate for the broadband absorption due to the DMZn molecule. This method is used because as the ArF dissociates the DMZn in its optical path, the broadband molecular absorption due to the DMZn decreases, thus the signal to the spectrometer increases. As more DMZn dissociates (by increasing the ArF energy), the detected spectrum more closely resembles the vacuum spectrum. From this fit as shown in Curve B of Figure 4-1, the observed concentration of both Zn atoms and CH_3 radicals can be calculated.

A summary of the experimental data for both the Zn atoms and methyl radicals is given in Table 4-1. This data is used to find the concentrations of the species as described below.

Methyl Radical Concentration

To determine the density of CH_3 absorbers in the optical column, it is necessary to observe the decay of the methyl radical absorption in time and use gas kinetics to determine the initial concentration of radicals. The dominant reaction is taken to be the recombination reaction $\text{CH}_3 + \text{CH}_3 + \text{M} \rightarrow \text{C}_2\text{H}_6 + \text{M}$, based on the reaction rate constants listed in Table 4-2. The reaction to form ethane is kinetically favorable over the formation of methane.

Mass spectra studies support this conclusion, as shown in Figure 4-5. Figure 4-5(a) shows that when the laser is on, the concentration of mass 28 (C_2H_4) increases by over an order of magnitude and the concentration of mass 27 (C_2H_3) also increases. However, the concentrations of mass 16

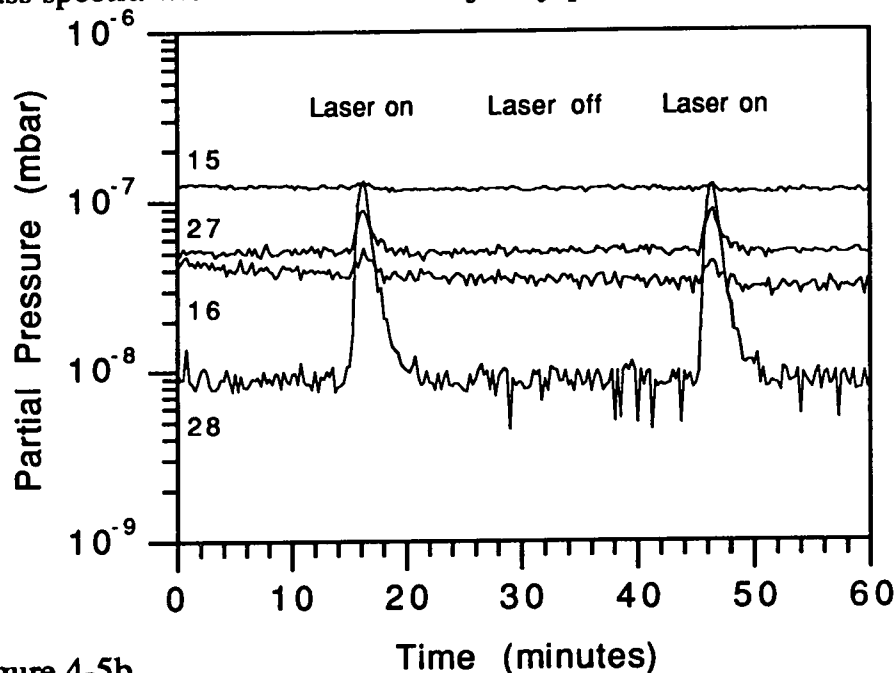
Table 4-2.Reaction rate constants for several important reactions (from Tsang ⁵⁷)

Reaction				k (300K)	k (673K)
				$\frac{\text{cm}^3}{\text{molecule second}}$	
I	$\text{CH}_3 + \text{H}_2$	\rightarrow	$\text{CH}_4 + \text{H}$	$1.2 \text{ e-}20$	$4.7 \text{ e-}16$
II	$\text{CH}_3 + \text{H}$	\rightarrow	CH_4	$2.0 \text{ e-}10$	$1.5 \text{ e-}10$
III	$\text{CH}_3 + \text{CH}_3$	\rightarrow	C_2H_6	$4.4 \text{ e-}11$	$2.6 \text{ e-}11$
IV	C_2H_6	\rightarrow	$\text{CH}_3 + \text{CH}_3$	$5.2 \text{ e-}49^*$	$7.2 \text{ e-}13^*$

*units for unimolecular reaction rate coefficient: $\frac{\text{cm}^6}{\text{molecules}^2 \text{ sec}^2}$

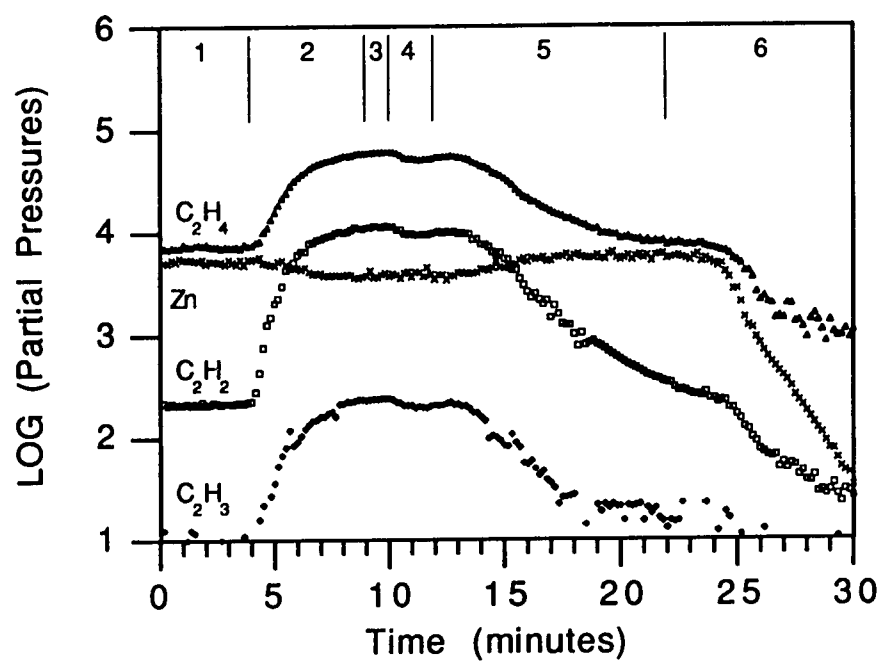
Figure 4-5a.

Mass spectra with ethane as the major by-product of the photodissociation

**Figure 4-5b.**

Mass spectra showing several hydrocarbons in relation to Zn concentration

1-DMZn only; 2-ArF on; 3-ArF off; 4- ArF on; 5-ArF off; 6-DMZn flow off



(CH₄) and mass 15 (CH₃) do not increase or only increase slightly. This implies that ethane (C₂H₆ - mass 30) is most likely the dominant by-product in the reaction cell, as it is then cracked into masses 27 and 28 in the quadrupole analyzer head. *If* methane (CH₄ - mass 16) were the major by-product, one would expect a large increase in the concentration of both masses 16 and 15, which does not occur. It has also been shown by other groups ^{55,56} using residual gas analysis that ethane is the major product of the recombination of methyl radicals in the photolysis of DMCd.

Figure 4-5(b) gives an indication of the diffusion time of the products to the analyzer head. Region 1 shows the background constituents of the cracking of DMZn; region 2 is when the ArF laser beam is turned on; during region 3 the laser is temporarily turned off; the laser is on again during region 4; the laser is off during region 5; and during region 6, the DMZn gas flow is shut off and only H₂ flows through the cell. When the ArF laser is on, the partial pressure of Zn decreases due to the fact that fewer complete DMZn molecules reach the analyzer head, thus the molecule's contribution to the Zn concentration goes down. While the quadrupole is a good qualitative tool, the time delay due to diffusion limits its time-resolved diagnostic capabilities.

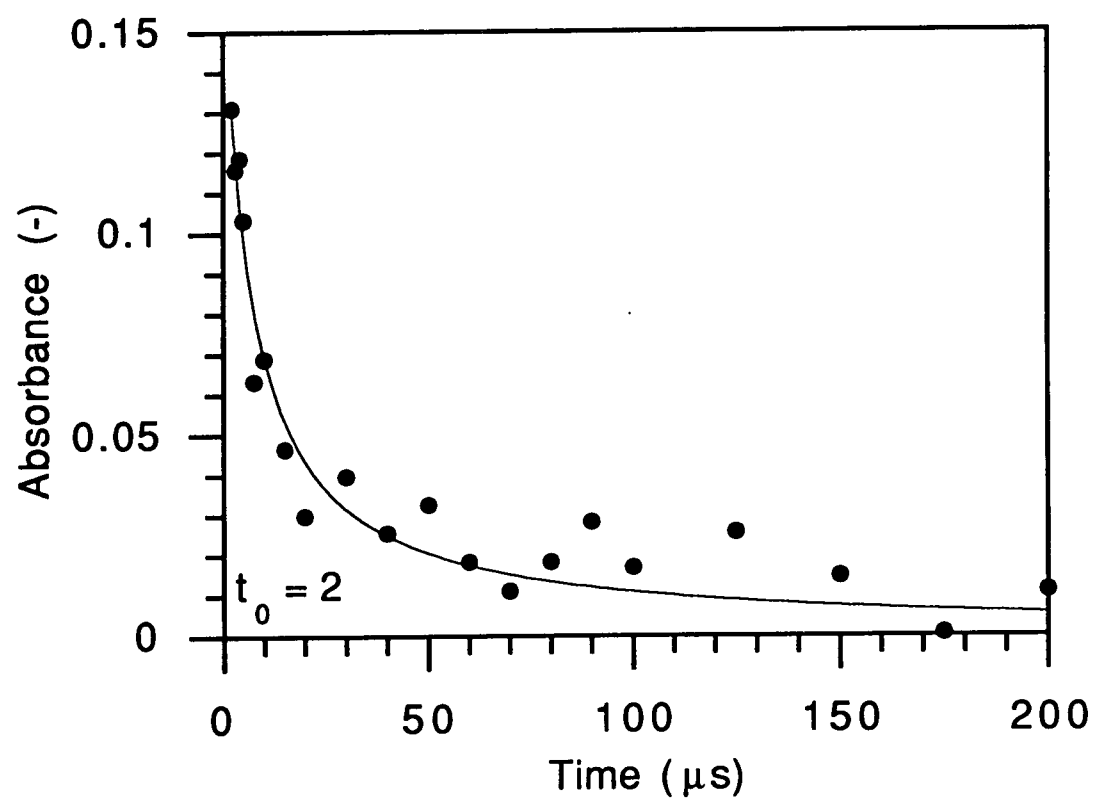
The decay of the methyl radical absorbance signal at 2160Å versus time is shown in Figure 4-6. In order to determine the number of absorbing radicals N, the kinetic equations for a second-order reaction are used ⁵⁸:

$$(4.2) \quad \frac{dN}{dt} = -2k N^2$$

Rearranging and integrating:

Figure 4-6.

Methyl radical decay in time



$$(4.3) \quad N = \frac{N_0}{N_0 2k t + 1}$$

From Beer's Law, the absorbance (A):

$$(4.4) \quad A = \ln \frac{I_0}{I} = N \sigma L$$

Combining (4.3) and (4.4):

$$(4.5) \quad A = N \sigma L = \frac{A_0}{A_0 K t + 1}$$

where:

$$K = \frac{2k}{\sigma L} \quad \text{and} \quad A_0 = N_0 \sigma L$$

Equation (4.5) is then used to fit the CH₃ absorbance signal decay. From the curve fit, the constant K is determined. To determine N₀, the term (σ L) is found from the relations in Equation (4.5):

$$\sigma L = \frac{2k}{K} \quad \text{and} \quad N_0 = \frac{A_0}{\sigma L}$$

where *k* is the known rate constant of the recombination rate for methyl radicals to form ethane, and A₀ is the initial absorbance. Similar to the results of Callear⁵⁹ and Bass⁵⁶, the methyl radical absorption does not peak until several microseconds after the dissociation. This is due to the fact that ~ 85% of the methyl radical initially appear in an excited state⁵⁹, which are then collisionally relaxed to the ground state. As is discussed later, some of

the increase in CH_3 absorbance may also be due to the reaction: $\text{CH} + \text{H}_2 \rightarrow \text{CH}_3$. For the present work, a typical initial time is $t = 2 \mu\text{s}$.

For a typical set of data, the initial number of CH_3 molecules is obtained by the following calculations. Referring to tabulated rates on the production of ethane from the recombination of methyl radicals ⁵⁷, $k = 4.4 \times 10^{-11} \text{ molecules}^{-1} \text{ cm}^3 \text{ sec}^{-1}$ at room temperature. For the data shown in Figure 4-6 and its curve fit, the constant K is found to be $K = 0.856 \mu\text{s}^{-1}$. The rate constant k and curve fit constant K are then substituted back into Equation (4.5). This gives $(\sigma L) = 1.03 \times 10^{-16} \text{ cm}^3$, which yields $N_0 = 1.28 \times 10^{15} \text{ cm}^{-3}$. This compares with the known initial concentration of DMZn, $N_{\text{DMZn}} = 1.30 \times 10^{15} \text{ cm}^{-3}$, calculated from flow rates and pressures of the gas delivery system (see Chapter 3 and Appendix B). This result implies that approximately half of the methyl radicals from the complete dissociation of DMZn ($\text{DMZn} \rightarrow 2\text{CH}_3 + \text{Zn}$) are being seen in absorption at 2160\AA . This is consistent with the observed spectra, as the broadband attenuation of the DMZn molecule is still present as is seen in Curve C of Figure 4-1, indicating approximately half of the DMZn is dissociated.

Atomic Zn Concentration

To extract the number of absorbing Zn atoms, the equivalent width of the Zn resonant absorption line is analyzed. Following Corney ⁶⁰ and Thorne ⁶¹, the number of absorbing atoms in a column of gas at high densities that is optically thick can be found by :

$$(4.6) \quad N = \frac{(W_\omega)^2 \epsilon_0 m c}{\pi e^2 f_{ik} L \Gamma}$$

where:

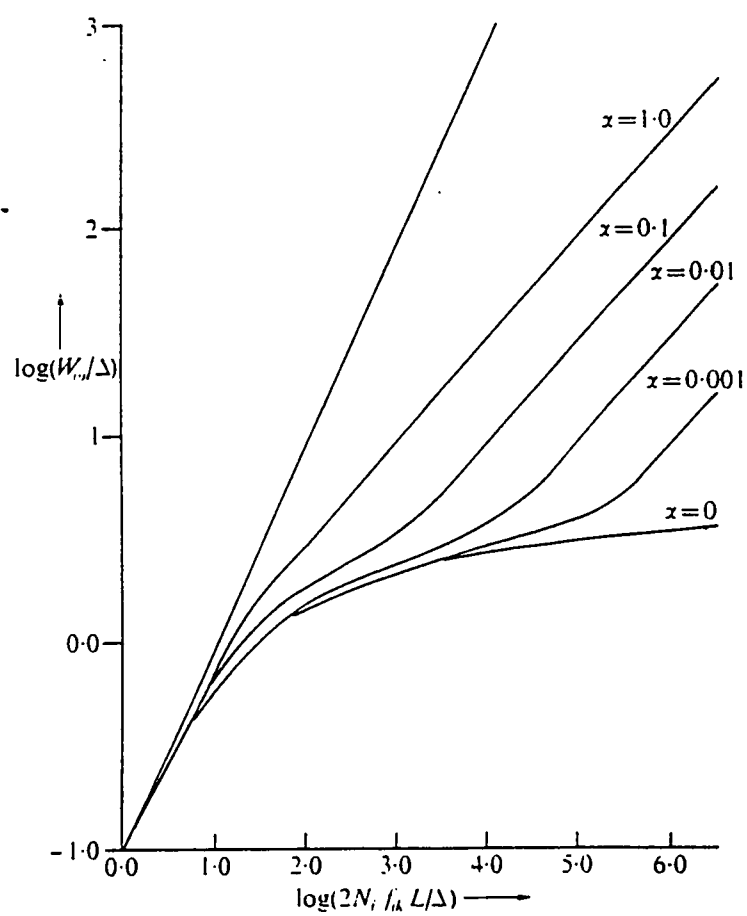
L	absorption length (m)	ϵ_0	permittivity of free space
f_{ik}	absorption oscillator strength	e	charge of an electron
Γ	Lorentzian linewidth (s^{-1})	m	mass of an electron
W_ω	equivalent width (s^{-1})	c	speed of light

However, when the gas is not in a high pressure regime, the line shape is described by a combination of Gaussian (Doppler broadened) and Lorentzian (pressure broadened) linewidths. In this case, in order to determine the density of absorbers, a "curve of growth" is used as shown in Figure 4-7. The plot is of $\log (W_\omega / \Delta)$ vs. $\log (2 N_i f_{ik} L / \Delta)$, where N is in cm^{-3} and L is in cm, for various ratios of the Lorentzian to Gaussian linewidth parameters. The ratio term α is defined as $\alpha = 2 (\Gamma) / \Delta$, where Γ is the Lorentzian half-width and Δ is the Gaussian half-width. Thus knowing the equivalent width, the oscillator strength, the absorption length, and the linewidth parameters, one can extract the number of absorbers.

The parameters needed for the curve of growth calculations are determined as follows. The equivalent width is found for each experiment from the absorption profile. The area under Curve C in Figure 4-1 is subtracted from the area under Curve B, and this difference in area is divided by the average plasma intensity over the width of the transition. The oscillator strength for this transition is $gf = 1.3^{62}$. The length of the absorbing column is determined from the cross section calculations, and averages $L = 8$ cm. For determining the linewidth, several types of broadening mechanisms are calculated, including resonant self-broadening (also called Holtzmark broadening), pressure broadening, and Doppler

Figure 4-7.

Curve of growth for several values of α (from Corney ⁶⁰)



broadening, as summarized in Table 4-3 and Table 4-4. The total Lorentzian linewidth is a combination of natural and hydrogen pressure broadening ($\Gamma = 118 \text{ MHz} + 33 \text{ MHz}$). Several points should be noted about these broadening formulas and the resulting numbers. For broadening widths with units of s^{-1} , this means that the unit of measure is angular frequency and should be compared to similar units when converting from frequency to wavenumbers. Depending on the definition of the lineshape function, the width can be expressed in either wavenumbers, radians per second, or angstroms, although most authors use radians per second. For the resonant self-broadening calculation, Hindmarsh⁶³ has indicated that the factor $\{(2 j_i + 1) / (2 j_k + 1)\}^{1/2}$ should be included, whereas Corney⁶⁰ has excluded this term. The broadening due to resonant self-broadening was calculated using the average observed concentration of Zn. The pressure broadened widths for Zn and CH_3 use an order of magnitude estimate of $1 \times 10^{15} \text{ cm}^{-3}$ for both species. The broadening due to hydrogen uses $8 \times 10^{17} \text{ cm}^{-3}$ as a typical concentration.

For a typical absorption experiment, it is found that the equivalent width is $W_\lambda = 0.5 \text{ \AA}$. This is converted to s^{-1} by the relationship:

$$(4.7) \quad W_\omega = \frac{2 \pi c}{\lambda^2} W_\lambda = \frac{2 \pi c}{(2139 \text{ \AA})^2} (0.5 \text{ \AA}) = 2.06 \times 10^{12} \text{ s}^{-1}$$

Thus the y-axis term $\log (W_\omega / \Delta) = \log (2.06 \times 10^{12} / 1.35 \times 10^{10}) = 2.18$.

The ratio term α is found to be:

$$(4.8) \quad \alpha = \frac{2 \Gamma}{\Delta} = \frac{2 (151 \text{ MHz})}{2.15 \text{ GHz}} = 0.14$$

Table 4-2. Broadening Mechanisms

Type of Broadening	Line Shape	Formula	Units	Reference
Natural	Lorentzian	$\Delta\nu = \frac{A_{ki}}{2\pi}$	s ⁻¹	⁶⁰ p.235
Pressure	Lorentzian			
(a) Resonant Self Broadening		$\Delta\nu = \sqrt{\frac{2j_i + 1}{2j_k + 1}} \frac{N e^2 f_{ik}}{\epsilon_0 m \omega_{ik}}$	s ⁻¹	⁶⁰ p.244, 267 ⁶³ p.195
(b) Foreign Gas Broadening		$\Delta\nu = \frac{1}{2\pi \cdot \tau}$ $\frac{1}{\tau} = \sum N(A) \sigma(A, B) \bar{v}(A, B)$ $\sigma(A, B) = \frac{\pi}{4} (d_A + d_B)^2$ $\bar{v}(A, B) = \left[\frac{8kT}{\pi \cdot \mu} \left(\frac{1}{M_A} + \frac{1}{M_B} \right) \right]^{1/2}$	Hz	⁶⁴ p.99
Doppler	Gaussian	$\Delta\nu = \frac{0.716 \cdot c}{\lambda(\mu\text{m})} \sqrt{\frac{T(K)}{M(\text{amu})}}$	Hz	⁶⁴ p.104

where: A_{ik} - Einstein coefficient for spontaneous emission ; f_{ik} - absorption oscillator strength ; ω_{ik} - angular frequency; j_i (j_k) - angular momentum quantum number of lower (upper) state ; A - resonant gas ; B - foreign gas ; $\sigma(A, B)$ - collisional cross section ; $d_{A, B}$ - diameter of molecule ; μ - reduced mass ; $M_{A, B}$ - mass (kg) ; \bar{v} - average velocity of molecules ; $N(A)$ - density of A ; s⁻¹ is angular frequency (radians per second) and Hz is cycles per second

Table 4-4. Summary of Broadening Calculations for the Zn line at 2160Å

Type of Broadening	MHz	cm ⁻¹	Å
Natural Broadening	118	0.004	2 e -4
Resonant Self Broadening	5.3	2 e -4	8 e -6
Foreign Gas (25 torr H ₂) Broadening	32.7	0.001	5 e -5
Foreign Gas (100 torr H ₂) Broadening	132	0.004	2 e -4
Foreign Gas (CH ₃) Broadening	0.017	6 e -7	3 e -8
Foreign Gas (DMZn) Broadening	0.034	1 e -6	5 e -8
Doppler Broadening	2,149	0.072	0.003

This implies that: $\log \left\{ \frac{2 N_i f_{ik} L}{\Delta} \right\} \cong 6.4$

$$(4.9) \quad N_i = \frac{10^{6.4} \Delta}{2 f_{ik} L} = \frac{(2.5 \times 10^6)(1.35 \times 10^{10})}{2(1.3)(8)} = 1.6 \times 10^{15} \text{ cm}^{-3}$$

This compares with the initial concentration of DMZn, $N = 1.3 \times 10^{15} \text{ cm}^{-3}$. This calculation agrees within a factor of two for the number of methyl radical absorbers calculated earlier in the chapter.

As a check for the equivalent width calculations, another method can be used to determine the concentration of Zn atoms ⁶⁵. Taking the spectrometer resolution into account, the number of absorbers in an optically thick column can be expressed as :

$$(4.10) \quad N = \left\{ \frac{a}{2 \alpha} \right\}^2 \frac{1}{\sigma L} \quad \alpha = \frac{\gamma}{2 \Delta \nu}$$

where a is the fraction of absorbance, σ is the cross section for absorption, $\Delta \nu$ is the resolution of the spectrometer, and γ is the Lorentzian linewidth. Taking some typical numbers :

$$\Delta \nu = 4 \text{ \AA} = 2.6 \times 10^{12} \text{ Hz} \quad a = 0.09 \text{ (see Figure 4-1)}$$

$$\alpha = \frac{\gamma}{2 \Delta \nu} = \frac{151 \text{ MHz}}{2 (2.6 \times 10^{12} \text{ Hz})} = 2.9 \times 10^{-5} \quad \sigma = 1.5 \times 10^{-10} \text{ cm}^2$$

The number of absorber is:

$$N = \left\{ \frac{0.09}{2 (2.9 \times 10^{-5})} \right\}^2 \frac{1}{(1.5 \times 10^{-10})(8)} = 2.0 \times 10^{15} \text{ cm}^{-3}$$

This number agrees well with the equivalent width method for determining the concentration of Zn. There is a slight variation from experiment to experiment in the amount of Zn detected, and this may depend on the alignment of the dissociating beam and the plasma probe source.

The concentration of Zn does not change from 100 ns to 2 ms after the dissociating pulse as shown in Figure 4-8. This is an indication that the Zn atoms are not reacting with any of the free radicals to form an intermediate compound over this time period. Due to the fact the Zn concentration does not change, this also shows that *if* any intermediate compound is formed that consumes Zn (such as ZnH, which is discussed later), its lifetime with respect to the formation of free Zn atoms must be longer than several milliseconds.

Fluorescence Experiments

The photodissociation of DMZn by 193 nm radiation also produces a blue fluorescence centered around 4315 Å. In order to determine the source of the observed emission, a slightly different experimental arrangement was employed. The solar blind PMT was replaced by a UV-VIS tube (either Hamamatsu PMT 6199 or R943-02) which has a wide spectral response. In order to obtain good signal to noise ratios, the slits on the spectrometer were opened from 250 to 750 μm, depending on the experimental conditions and the type of PMT.

The blue emission, shown in Figure 4-9, is due to the CH ($A^2\Delta \rightarrow X^2\Pi$) transition ⁶⁶. The resolution of the data in the figure is 6 Å and the

Figure 4-8.

Observed Zn concentration vs. time

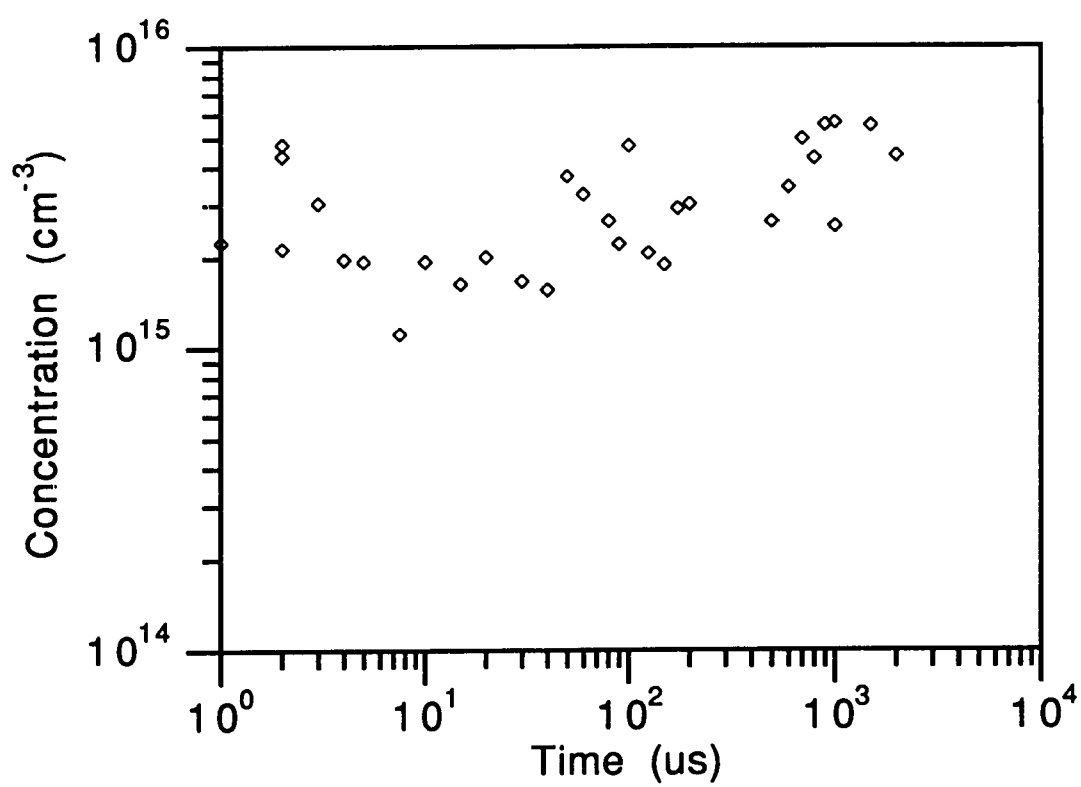
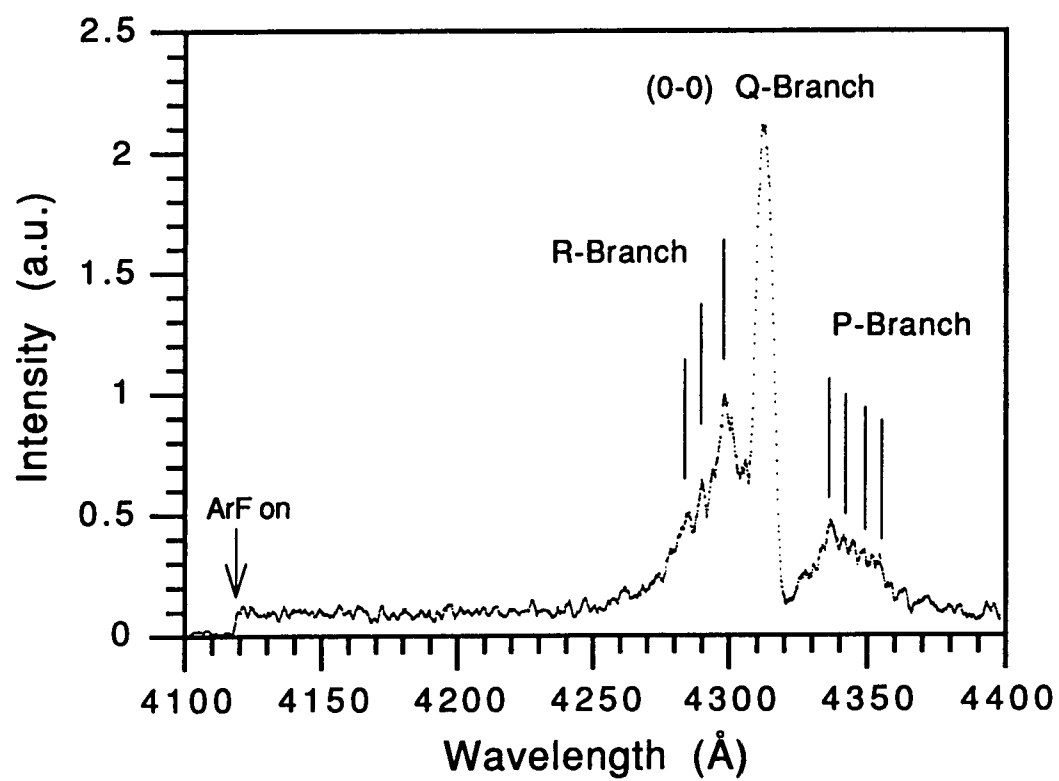


Figure 4-9.

Emission from excited CH radicals



features of the P, Q, and R branches of the transition are evident. A plot of the decay of CH* emission versus time is shown in Figure 4-10. Using an exponential curve fit, the upper state lifetime of the A state is estimated to be $\tau = 81 \text{ ns}$. This compares with published radiative lifetimes ⁶⁷ of $\tau \sim 540 \text{ ns}$, as an average of several of the vibrational bands of CH*, and $t = 580 \text{ ns}$ ⁶⁸. Thus the upper state decay of CH* in our system is assumed to be mainly non-radiative collisional de-excitation of excited CH radicals with H₂ molecules.

Energy Dependence of the Absorption and Fluorescence Photoproducts

CH₃ vs. ArF Energy

The effect of ArF energy fluence on the absorption and fluorescence signals was measured. The plot of CH₃ absorbance versus ArF energy is shown in Figure 4-11. The plot indicates that the absorbance of CH₃ follows an exponential curve that is dependent on the fluence. The curve fit is dependent on the fluence (F) and cross section (σ) :

$$(4.11) \quad g(F) = K(1 - e^{-\sigma F})$$

If the saturation point is defined as the 1/e part of the curve, the saturation energy density is $\sim 75 \text{ mJ/cm}^2$. This compares to the calculated saturation energy density of :

$$(4.12) \quad E_{\text{SAT}} = \frac{h\nu}{\sigma} = 68 \text{ mJ / cm}^2$$

where $\sigma (193 \text{ nm}) \cong 0.15 \times 10^{-16} \text{ cm}^2$.

Figure 4-10.

Decay of Q-branch emission from excited CH radicals

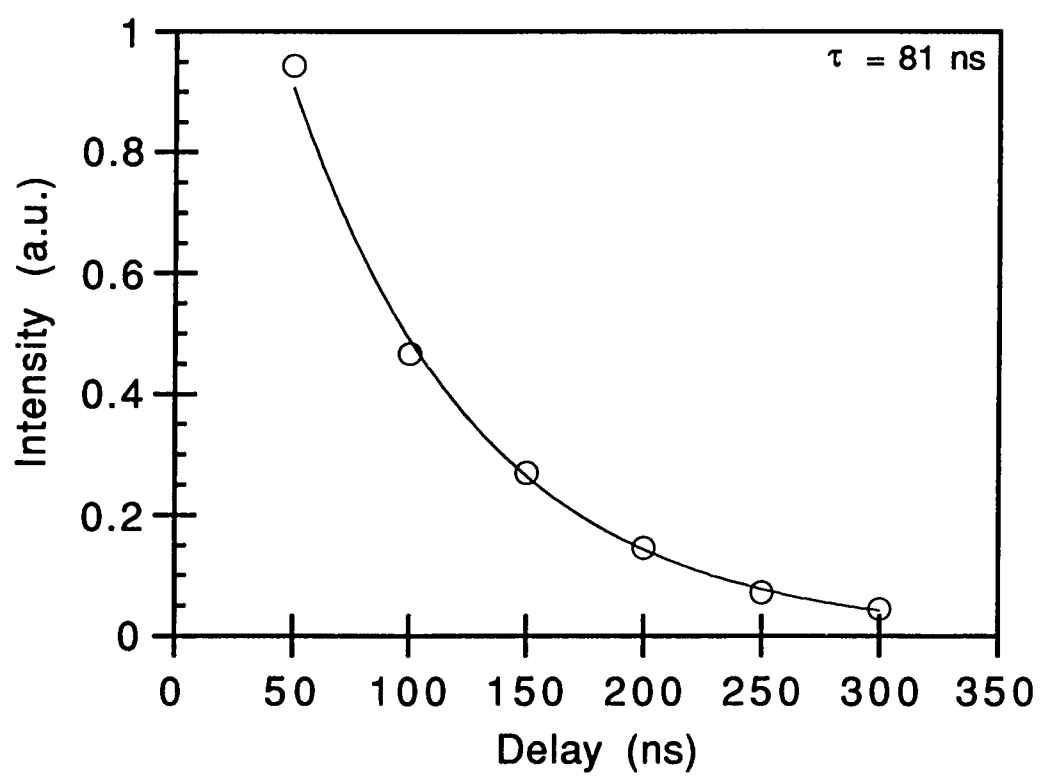
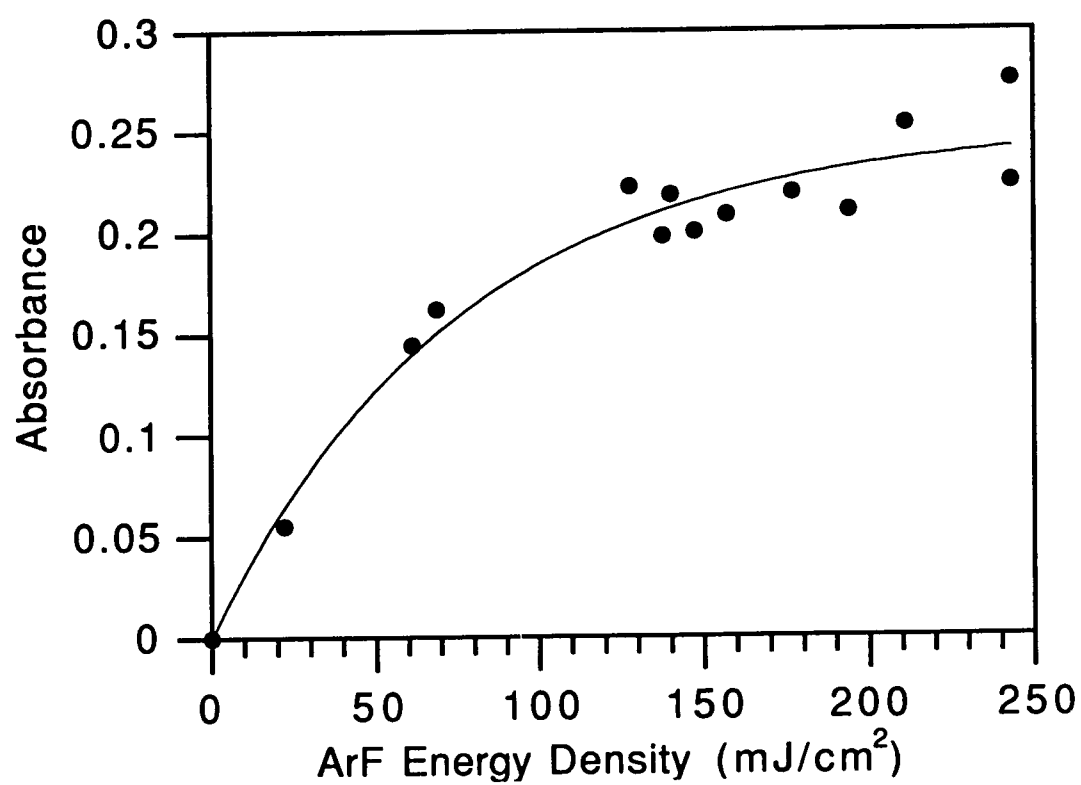


Figure 4-11.

Methyl radical absorbance vs. ArF energy density, and curve fit to data



CH* vs. ArF Energy

In a high energy density system, absorptions of multiple photons can occur. When the excitation intensity is below the saturation point of a system, a plot of the log of the emission intensity as a function of the log of the excitation intensity should have a slope of an integer value : $\log(I_{\text{emission}}) = n \log \{(h\nu) / t\}$, as has been shown in the dissociation of DMCD at 193 nm⁶⁹. However, when the excitation intensity is in the saturation regime of the system, the slope is no longer an integer, but depends on the rates of population and depopulation of the levels involved, the energy fluence, the absorption cross sections of the intermediates, and lifetimes of their states⁷⁰.

The generation of CH* can be modeled as a simple three level system, where the lowest level is DMZn, the intermediate level is an intermediate species such as excited CH₃ and/or excited CH₂ (which will be discussed in Chapter 5), and the top level is the detected excited-state CH radical. Given a general three-level system shown schematically in Figure 4-12, the rates of change of the populations are:

$$(4.13) \quad \frac{dN_1}{dt} = -\sigma_{12}N_1 \frac{I_v}{h\nu}$$

$$(4.14) \quad \frac{dN_2}{dt} = \sigma_{12}N_1 \frac{I_v}{h\nu} - \sigma_{23}N_2 \frac{I_v}{h\nu} - \frac{N_2}{\tau_2}$$

$$(4.15) \quad \frac{dN_3}{dt} = \sigma_{23}N_2 \frac{I_v}{h\nu} - \frac{N_3}{\tau_3}$$

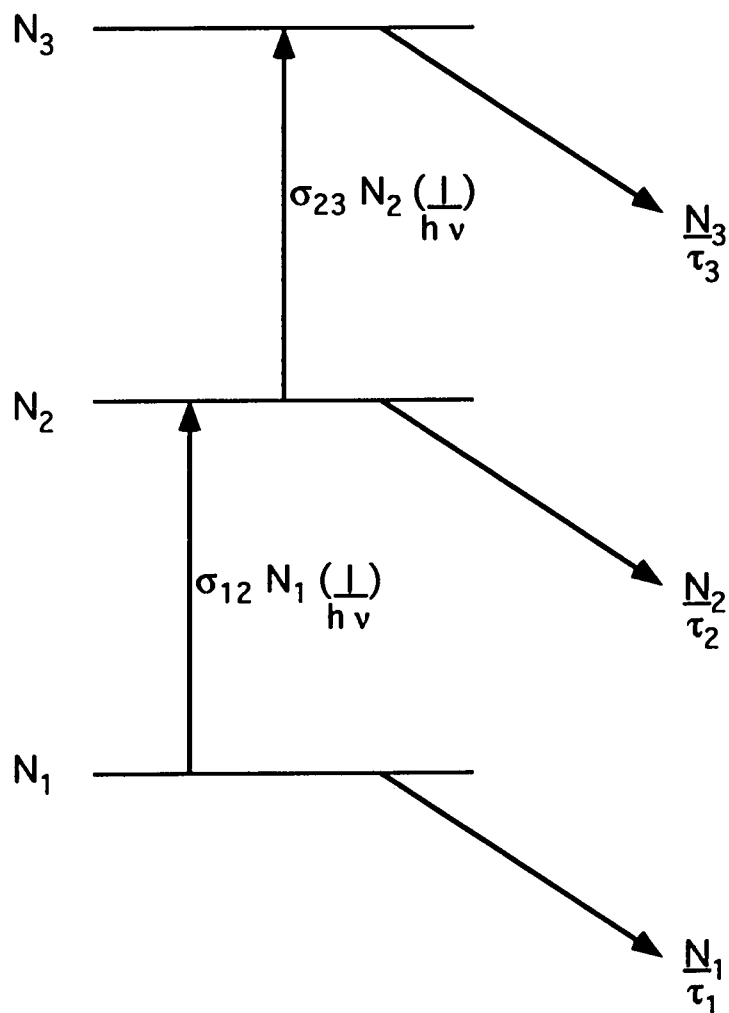
Figure 4-12.

Schematic of a 3-level molecular system, with :

Level 1 - ground state DMZn

Level 2 - excited CH₃ or excited CH₂

Level 3 - excited CH



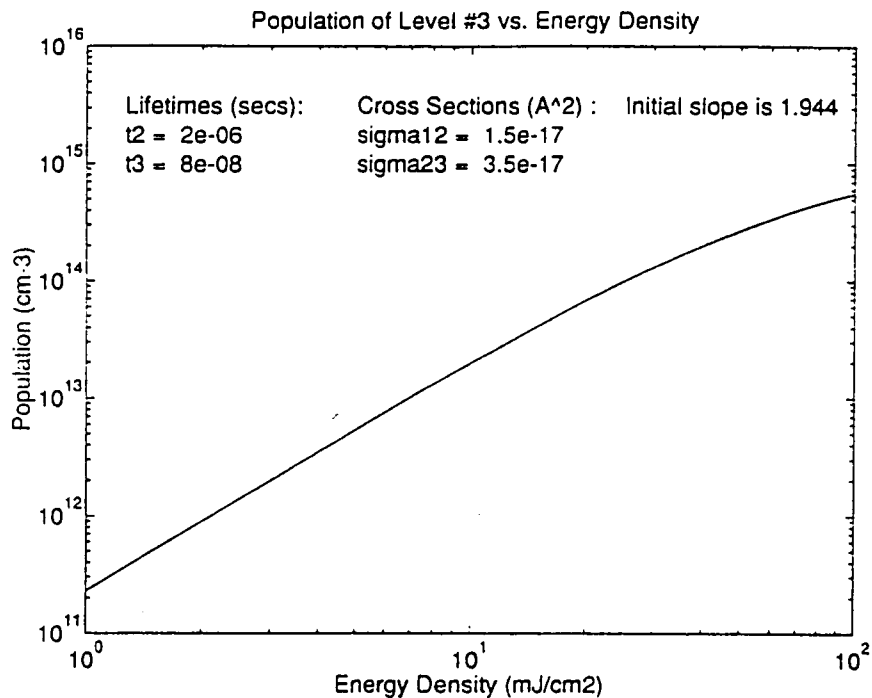
The decay in population from the upper states does not add to the lower states, since in this type of molecular system, the decay of an intermediate CH_2^* (level N_2) does not increase the population of the DMZn (level N_1).

One can determine the functional dependence of the emission intensity on photon flux by numerically integrating the Equations (4.13)-(4.15), and graphing the $\log(N_3/\tau_3)$ vs. $\log(\text{photon flux})$, where N_3/τ_3 represents the detected intensity at the photomultiplier tube. The same qualitative result is obtained by plotting $\log(N_3)$ vs. $\log(\text{energy density})$. The code for numerically integrating the above set of equations is given in Appendix B, and examples of the results are given in Figure 4-13. In a three level system that is not saturated, one would expect the log/log of the emission from the upper state to show a slope of two. Figure 4-13(a) shows the three level system with the parameters listed in Table 4-5, while Figure 4-13(b) shows the system with much shorter lifetimes. The initial slopes of the two plots are close to $n=2$, and saturate at higher energy densities when the slope of the line approaches zero. Shorter lifetimes have the effect of shifting the saturation level to higher energy densities, which occurs in the range of 10 - 100 mJ/cm².

In Figure 4-14, the log/log plot of I_{emission} vs. ArF energy density for the CH^* state has a slope of $n=1.5$. There are at least four processes needed to create CH as shown in Table 4-6, and the population of the upper CH state (and thus the intensity of the emission) may be competing with the collisional or radiative depopulation of one of the intermediate steps. As shown in Figures 4-12 and 4-13, a high fluence of the excitation source also effects the upper state by depopulating one of the lower levels. The system which produces CH^* is likely in saturation at the energy densities shown in

Figure 4-13a.

Three level system using parameters listed in Table 4-5

Figure 4-13b.

Three level system using relatively short lifetimes

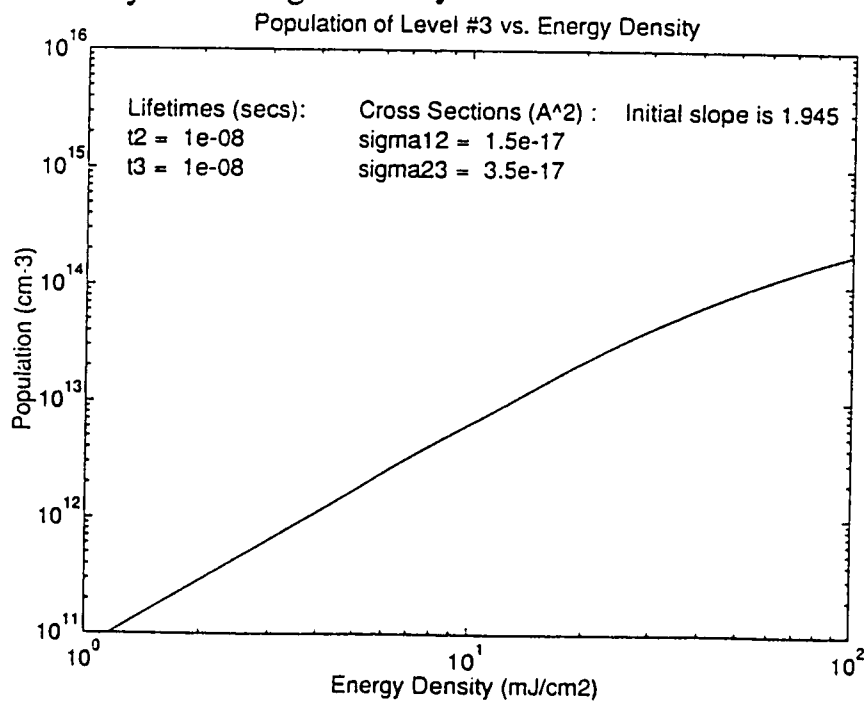


Table 4-5.**Some system parameters**

System Level	σ (\AA^2)	τ (μsec)	References
N ₁ - DMZn	0.15	--	this work
N ₂ - CH ₃ [†]	(0.3-0.4) [#]	~2	Bass, Parkes, this work
N ₂ - CH ₂ [*]	?	?	none
N ₃ - CH [*]	--	~0.08	this work

[†]vibrationally excited methyl radicals are assumed in this time regime

^{*}electronically excited state

[#]vibrationally cold CH₃ peak cross section

note: to the author's knowledge, neither the CH₃[†] nor CH₂^{*} cross sections have been measured.

Figure 4-14.

log/log plot of CH vs. energy density

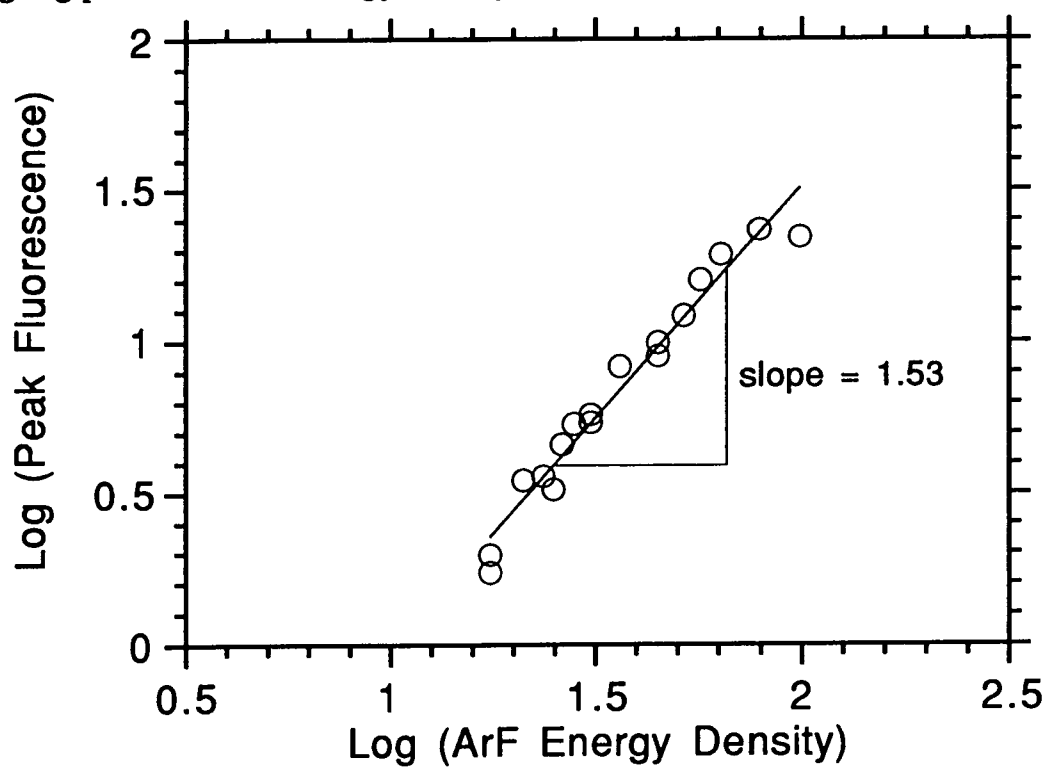


Table 4-6.**Energies for various photodissociation reactions of DMZn**

	<u>Dissociation Reaction</u>			<u>Energy</u>	<u>Reference</u>
I	Zn (CH ₃) ₂	→	Zn (CH ₃) + CH ₃	2.76 eV	Jackson ⁷¹
II	Zn (CH ₃)	→	Zn + CH ₃	1.06 eV	"
III	CH ₃	→	H + CH ₂	4.9 eV	Herzberg ⁴²
IV	CH ₂	→	H + CH	4.3 eV	"
V	CH (A ² Δ)	→	CH (X ² Π)	<u>2.87 eV</u>	Barnes ⁶⁶
	total required energy			15.89 eV	
	hv (193 nm)			6.42 eV	

the figure. Similarly, the log/log plots of the of Zn and methyl radical concentrations vs. ArF energy have slopes ranging from $n=0.3$ to $n=0.6$. If one assumes that the process to make Zn and methyl radicals is a one-photon process, this indicates that both the one-photon and multiple-photon processes are influenced by saturation effects.

Chapter 5

Absorption and Fluorescence Results

The diffusion of the observed photoproducts (Zn, CH₃, and CH) to the growth surface is important in determining how this photo-assisted growth process effects the quality of the ZnSe films. It is therefore useful to calculate the diffusion rate of the species to determine their concentrations once they reach the growth surface. The diffusion equation (referred to as Meyer's formula) is ⁷²:

$$(5.1) \quad \frac{dN_1}{dt} = D_{12} \frac{\partial^2 N_1}{\partial z^2}$$

where D_{12} is the diffusion coefficient given by:

$$(5.2) \quad D_{12} = \frac{N_1 \lambda_2 v_2 + N_2 \lambda_1 v_1}{3(N_1 + N_2)}$$

The mean free paths and thermal velocities of the species are:

$$(5.3) \quad \lambda_1 = \frac{1}{\sqrt{2} \pi N_1 d_1^2 + \sqrt{1 + \frac{m_1}{m_2}} \pi N_2 d_{12}^2}$$

$$(5.4) \quad v_{th} = \sqrt{\frac{3 k T}{M}} = 157.9 \sqrt{\frac{T \text{ (Kelvin)}}{M \text{ (amu)}}} \quad \frac{m}{s}$$

For example, using $d_1 = 3.8\text{\AA}$ for CH_3 ⁵⁶, $d_2 = 0.74\text{\AA}$ for H_2 ⁷³, $N_1 = 3 \times 10^{16} \text{ cm}^{-3}$ (1 torr) of methyl radicals, and $N_2 = 3 \times 10^{18} \text{ cm}^{-3}$ (100 torr) of hydrogen, the mean free path of the CH_3 is $\lambda = 0.70 \mu\text{m}$, and that of H_2 is $\lambda = 12.8 \mu\text{m}$, while the thermal velocities of the methyl radical at room temperature and a typical growth temperature are:

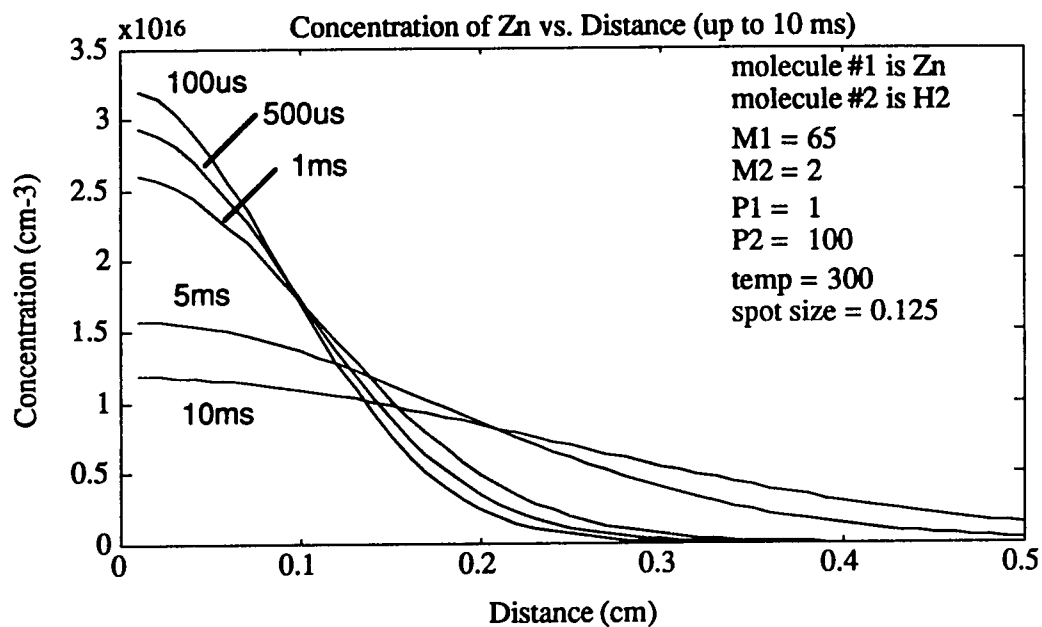
$$v_{\text{th}} = 706.2 \frac{\text{m}}{\text{s}} \text{ (300 K)} \quad \text{and} \quad v_{\text{th}} = 1058.9 \frac{\text{m}}{\text{s}} \text{ (673 K)}$$

The diffusion equation lends insight into the temporal relation of the photoproducts, and can be iteratively solved at discrete points in time, for which the code is given in Appendix B. The results of the simulations on the diffusion of various species are shown in Figure 5-1. The plots are of Zn and CH_3 concentrations as a function of distance from the center of the ArF laser beam. It has been shown by Chen ⁷⁴ that in the photodeposition of metal films using these types of metalorganics, the concentration of metal atoms is significant only within 1.5 radii of the beam. The same is true in this experimental system, as absorption profiles were not detected (and thus were not in significant concentrations) if the probe beam was aligned outside the ArF beam by more than several millimeters. The initial concentration profile of the photoproducts can be modeled as a Gaussian distribution (as the profile of the ArF beam can be modeled as a Gaussian), and it will remain Gaussian at all points in time throughout the diffusion.

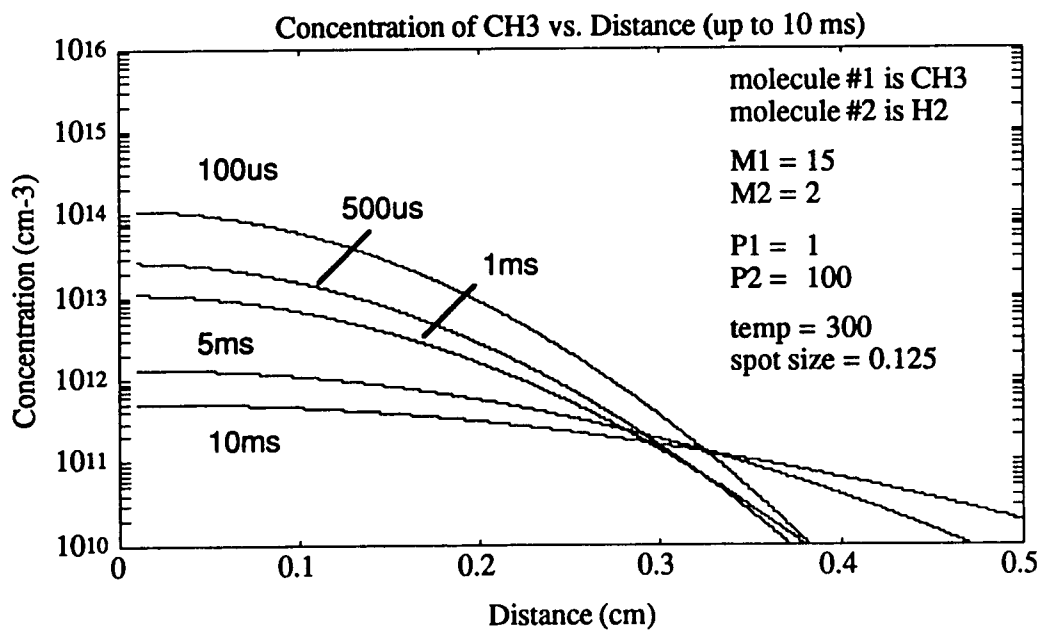
In order to determine the concentrations at any time, only the initial concentration of Zn and CH_3 is needed (along with known quantities such as mass and size of the species). The initial concentrations of the Zn and the CH_3 are known, as stated in the previous chapter. In addition, the Zn is

Figure 5-1a.

Diffusion of Zn to the growth surface

**Figure 5-1b.**

Diffusion of methyl radicals to the growth surface



known to remain unreactive, while the CH_3 decays as a second-order recombination function. Taking this into account, the model indicates that at typical growth temperatures and pressures, significant ($> 1 \times 10^{16} \text{ cm}^{-3}$) Zn concentrations will reach the growth surface (50 mm or 0.5 cm from the center of the laser) after several milliseconds. The methyl concentration, however, will be below $1 \times 10^{11} \text{ cm}^{-3}$ once it reaches the substrate surface. This is because the total Zn concentration remains constant, while the CH_3 radical concentration will decay due to recombination. It is likely that once its sticking coefficient (which is typically much smaller than unity ⁷⁴) and surface diffusion time is taken into account, the methyl radical will not be incorporated into the film in concentrations that will harm the electrical properties of the ZnSe films.

The data also implies the formation of ethane from the recombination of methyl radicals, which has important implications on the incorporation of C in the films. Ethane does not absorb 193 nm radiation ⁷⁵, thus one would not expect the ethane that has been formed by the recombination of methyl radicals to be dissociated by the next ArF pulse in time. The formation of ethane from methyl radicals has important consequences for ZnSe MOCVD growth. Fujita ^{76,77} attributed higher growth rates of ZnSe to the elimination of the alkyl groups from the precursor gases. The same group has also proposed that UV-induced oxidation-reduction mechanisms on the surface of the substrate lead to the elimination of alkyls from the substrate surface, thus lowering the carbon contamination in the films. This is in qualitative agreement with Giapis ³³ who showed with SIMS analysis that carbon incorporation in ZnSe films were lowered by changing the Se precursor from MAsSe to DESe. They proposed that a fundamental process that occurs on

the substrate is the formation of $\text{CH}_3\text{-Se}$ bonds or CH_3 radicals and Se atoms near the substrate surface. The presence or either of these two groups contributes to the incorporation of carbon in the films, as detected by SIMS and correlated to their PL (photoluminescence) spectra. The PL from the films grown by our LAMOCVD method show there is no I_c peak located at 2.7920 eV, thus is one indication that C contamination is not present in significant concentrations in the films.

The observed Zn concentration is within a factor of two of the total DMZn concentration. Although Zn may be formed in another state, no other transitions of Zn are detected, either from its ground state or its ionic state. There is a possibility that some Zn is being formed in the 4^3P_1 metastable state, but the yield to that state has been shown to be small by Yu ⁷⁸. In the present work, there are no indications of the formation of intermediate compounds such as MMZn or ZnH. Others have explored the MMZn radical by absorption ²⁷ and LIF ²⁸. For DMZn photodissociation, it has been established that the emission at $\lambda = 4128\text{\AA}$ and $\lambda = 4176\text{\AA}$ (noticeably absent in Figure 4-9) is due to the $A \rightarrow X$ band of MMZn. There was no detected emission in the present experiments from these transitions or any of the other known transitions bands of MMZn ²⁷, $\lambda = 2671\text{\AA}$ and $\lambda = 2739\text{\AA}$. A set of experiments was also carried out to look for the monomethyl fragment in absorption at these wavelengths and no signal was found. The photosensitized reaction to form ZnH { $\text{Zn}(4^3\text{P}_1) + \text{H}_2 \rightarrow \text{ZnH}$ } has also been explored ^{79,80}. No signal was detected in this work in the regions identified for ZnH emission ^{80,81}, and has been mentioned by several groups ^{22,82} as to why atomic Zn was not detected in their experiments. The lifetime of ZnH has been shown to be approximately 10 μs ⁸⁰. Any ZnH that is

formed would decay to ground state Zn and hydrogen, and a change in the Zn concentration would be observed on a 10 μ s time scale. As discussed previously, no significant change in the Zn concentration was observed over several milliseconds, so it is unlikely that any photosensitized reaction to form ZnH consumes an appreciable number of Zn atoms. Therefore, it can be inferred that all of the Zn is being formed in a ground state, and that *if* there is the formation of another state of Zn, it does not have an appreciable effect on the growth process.

The results of the fluorescence experiments also show that CH* is being produced, but its concentration has not been determined. The reactivity of CH is substantial due to the fact that it has two dangling bonds. Once the CH* decays to its ground state within 300 ns, it would presumably react very quickly. Braun⁸³ showed that CH radicals react very efficiently with H₂ in the reaction: $\text{CH} + \text{H}_2 \rightarrow \text{CH}_3$, which has a first-order dependence in H₂ concentration at high pressures :

$$(5.5) \quad \frac{-d[\text{CH}]}{dt} = k[\text{CH}][\text{H}_2]$$

The CH concentration at the initial (i) and final (f) times can then be expressed as:

$$(5.6) \quad \frac{[\text{CH}]_f}{[\text{CH}]_i} = e^{-\{k[\text{H}_2](t_f - t_i)\}}$$

The rate of reaction was found to be $k = 1.03 \times 10^{-12} \text{ molecules}^{-1} \text{ cm}^3 \text{ sec}^{-1}$. For typical H₂ concentrations used in the growth of ZnSe films ($\sim 3 \times 10^{18}$

cm⁻³), the CH concentration would decay to ~ 4% of its original concentration after 1 μ s.

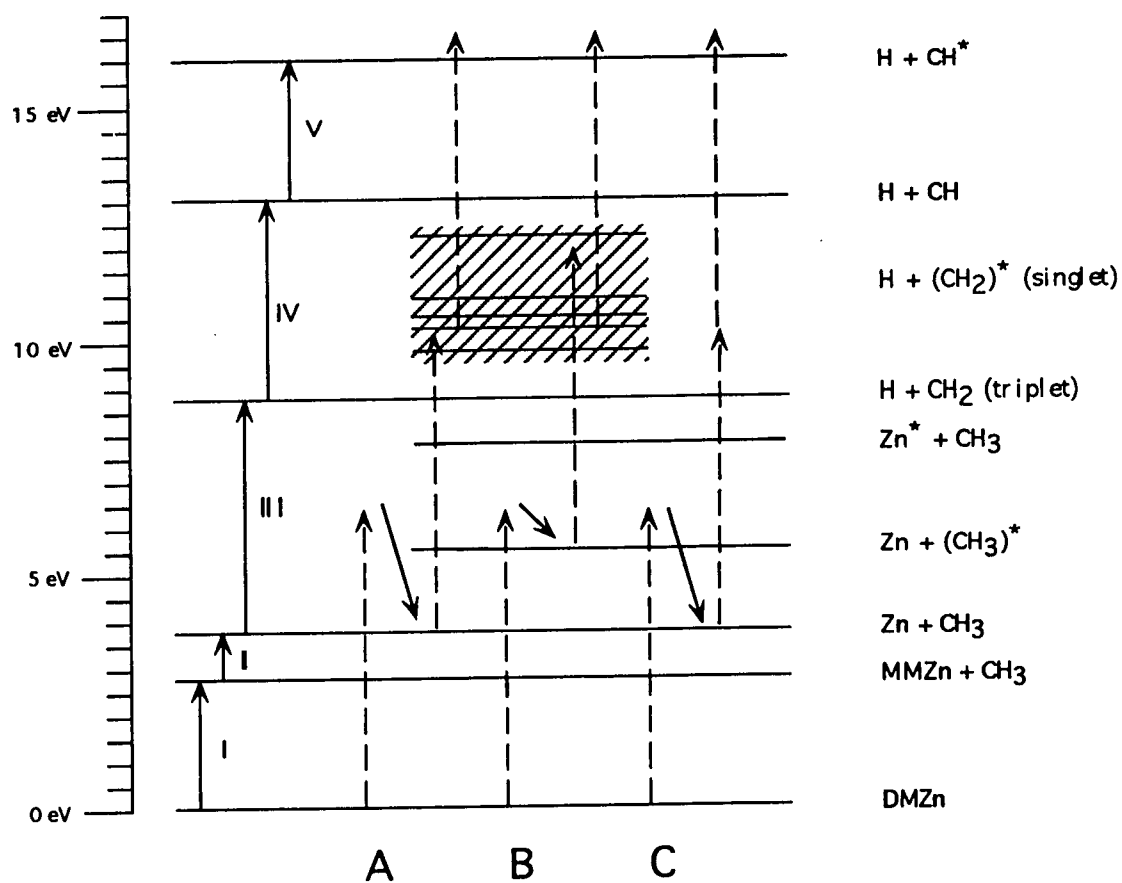
The initial concentration of the CH radical can be estimated by an energy argument. Continetti ⁸⁴ showed that CH₃ dissociation into CH₂ and H in the 193 nm irradiation of CH₃I takes place with laser fluences greater than 10 MW / cm². The quantum efficiency of this channel was estimated as 3%. In the present experimental work, the maximum energy density is ~12 MW/cm². The bond strength of the C-I bond in CH₃I is 2.38 eV, and is weaker than the first Zn-C bond (2.76 eV) in DMZn, (see Table 4-6). While the dissociation of CH₃I would presumably take place with one photon and leave ~4 eV to be distributed into the photoproducts (to create CH), the dissociation of DMZn would leave only ~2.6 eV. Thus it can be argued that the efficiency of the CH₃ dissociation channel in the dissociation of DMZn will be on the order of, if not less than, 3%. Thus $\sim 4 \times 10^{13}$ cm⁻³ can be made as an initial concentration of the CH radical. This radical reacts with other radicals and/or atoms (most likely H₂) and its concentration is reduced significantly in a time frame short (~1 μ s) compared to the diffusion time of the other species (Zn, CH₃), and thus has little effect on the ZnSe films.

The absorption experiments have identified the kinetics and concentrations of methyl radicals and Zn. The fluorescence of CH radicals is indicative of a high energy density system, but it does not seem likely to be a channel for C incorporation. The absence of MMZn and ZnH transitions, along with the constant concentration of Zn atoms over time, indicates that these two radicals are not a major concern for the growth system.

Energy Dependence Results

In order to create Zn, CH₃, and CH*, 15.97 eV must be input into the system, as shown in Table 4-6. The possible processes are summarized in Figure 5-2, and are discussed below. The solid arrows indicate the known dissociation energies, while the dashed arrows represent the absorption of an ArF laser photon (6.42 eV). The hashed area represents the many-line spectrum of the singlet methylene radical, which contains several broad bands. There are three possible reaction pathways shown in the figure for the dissociation process. The first possibility, labeled A, is the stepwise absorption of three photons, with the intermediates being Zn, CH₃, (CH₂)*, and CH*. The second possible reaction pathway, (B) is similar to the first except that excited (as opposed to ground state) methyl radicals are among the intermediates. The last pathway (C), involves the creation of Zn + CH₃, and then the simultaneous absorption of two photons, thus bypassing the creation of the (CH₂)* intermediate.

An ArF photon contains 6.42 eV of energy, and if the dissociation process proceeds one photon at a time, the first photon would be needed to create Zn atoms and CH₃ radicals. That leaves an excess of ~2.59 eV from the first photon that would need to be distributed into the photoproducts. Since we observe the formation of ground state Zn immediately (within 100 ns of the ArF pulse) and we do not detect MMZn, this implies that any intermediate state of the dissociation (such as MMZn) is short-lived (on the order of the ArF pulse), as was argued in the last chapter in the three-level model of the CH* emission. Thus, the possibilities for the excess energy from the first photon are: (1) ionizing Zn, (2) creating excited state Zn,

Figure 5-2.**Possible multiphoton paths for DMZn photodissociation**

and/or (3) going into the CH_3 radicals as a combination of rotational, vibrational, and translational energy.

In order to ionize Zn, 9.39 eV (1320\AA ; $75,735\text{ cm}^{-1}$) is required. Since the photoionization cross section for Zn is appreciable only from $1150\text{\AA} < \lambda < 1320\text{\AA}$ ⁸⁵, the only way Zn can ionize is to have resonance absorption of the ArF photon. The lowest energetic levels of Zn II are at 6.12 eV (2026\AA ; $49,354\text{ cm}^{-1}$) and/or 6.01 eV (2063\AA ; $48,481\text{ cm}^{-1}$). We did not observe any transitions in this region. If the excess energy of the first photon went into exciting Zn, the lowest energy level is the 4p ($^3\text{P}_1$) state at 4.00 eV ($32,311\text{ cm}^{-1}$). The excess energy of $\sim 2.59\text{ eV}$ ($20,890\text{ cm}^{-1}$) is not enough to excite Zn to a higher energy level, as is shown schematically in Figure 5-2.

This implies the energy must go into the CH_3 radical. The amount of energy acquired by the methyl radicals upon photodissociation from DMCd and DMZn has been explored by several groups ⁸⁶⁻⁸⁹. It is found that the ν_2 (out-of-plane bend) mode at 606.4 cm^{-1} (0.75 eV) and ν_3 (anti-symmetric stretch) mode at 3162 cm^{-1} (0.39 eV) are populated. The translational energy of the CH_3 radicals is found to be only a fraction (0.56 eV) of the excess energy in the 193 nm dissociation of DMCd ⁸⁹. This accounts for $\sim 1.70\text{ eV}$ of the $\sim 2.59\text{ eV}$ remaining from the first ArF photon. This means that $\sim 0.89\text{ eV}$ of energy needs to go into another mode, or might go into further translational energy of the methyl radical. The ν_1 (symmetric stretch) at $\sim 3000\text{ cm}^{-1}$ (0.38 eV) of the CH_3 radical has been observed in ArF photodissociation of CH_3I ⁸⁴, so this may account for some of the excess energy, although it has not been detected so far in the studies on DMZn.

The amount of energy required to make CH^* from CH_3 radicals is 12.07 eV. Parkes ⁹⁰ studied the absorption cross section for methyl radicals and found the absorption continuum extends to 210 nm, and it may continue to shorter wavelengths. A process that could take place involves the simultaneous absorption of two photons by the CH_3 radical. For two ArF photons (12.84 eV), there is enough energy to create CH^* from CH_3 , with 0.77 eV in excess. However, the ionization energy of CH_3 is 9.84 eV, so the simultaneous absorption of two photons would favor ionization of CH_3 rather than dissociation. The issue of absorption of 193 nm radiation by methyl radicals is discussed by Ye ⁹¹, and they propose that CH_3 dissociates into CH_2^* , which then absorbs another ArF photon to make CH^* . If one ArF photon creates CH_2 from ground state CH_3 , this leaves ~1.52 eV of energy to be distributed into the photoproducts, which may excite one of the various CH_2 bands ⁵⁴. The dissociation of methyl radicals would seem to favor creation of an excited state methylene radical $(\text{CH}_2)^*$, which then would absorb another ArF photon to create CH^* , leaving excess energy for vibrational-rotational-translational modes to be excited. As analyzed by the three-level model in the last chapter, the creation of excited CH radicals would seem to favor an intermediate species that have a lifetime shorter than or comparable to that of the ArF pulse.

There is a possibility of other species that remain undetected. In reference to the contamination of ZnSe films from highly excited species, one interesting process would be the formation of C atoms from the further photodissociation of CH. However, the dissociation energy for this is process is around 3.5 eV ⁸¹, so the formation of C is unlikely unless another ArF photon is absorbed by CH. Also, it has been shown that C-H scission is

selective, and is broken by radiation of wavelengths $140 \text{ nm} \leq \lambda \leq 170 \text{ nm}$ ⁹². In other high energy density systems, however, C has been detected. In the 193 nm dissociation of $\text{P}(\text{CH}_3)_3$, C emission was weak, but was detected at 248 nm³⁸. However, the C-P bond in $\text{P}(\text{CH}_3)_3$ is much weaker than the C-Zn bond in DMZn. This is evidenced by the detection of P emission at 253 nm³⁸, as excess energy from the ArF laser also goes into exciting the P atom. Therefore, while it has been observed in other high energy density systems, it can be argued that C formation in the focused 193 nm dissociation of DMZn is not likely to take place with significant concentrations.

In this chapter, the photodissociation of DMZn has been argued to be a three-photon process, with the detected photoproducts being Zn, CH_3 , and CH^* . There is an assumption of intermediate, short-lived molecules such as CH_3Zn and $(\text{CH}_2)^*$. Zn is transported to the surface in its ground state, and there is no detectable ZnH or MMZn formation. The CH_3 radicals are likely to be greatly reduced in concentration once they reach the growth surface, therefore are not a serious concern for contamination.

Chapter 6

Conclusions

The work summarized in this thesis demonstrated a tabletop, UV-VUV absorption experiment which is versatile and inexpensive. Although this system is constructed separate from the growth chamber, the system could be easily integrated into an *in-situ* growth monitoring technique. Hebner⁹³ proposed a similar *in-situ* monitoring system for the broadband absorption profile of the metalorganics. However, the system we have demonstrated in this work can detect concentrations of the photoproducts, thus allowing direct monitoring of deposition concentrations during growth.

We have detected both Zn atoms and CH₃ radicals in absorption and quantified their concentrations. The excited radical CH* was also detected, but it was argued that it is present in small quantities. The input energy of the system can be accounted for with a three photon process, meaning that the CH* is most likely the only excited long-lived radical being formed. The Zn is formed in its ground state and remains unreactive for at least several milliseconds. The calculated concentration of Zn is within a factor of two of the original DMZn concentration. As the detected Zn concentration does not change, any intermediate compounds that would scavenge Zn are assumed to be negligible. The methyl radicals combine to form ethane and are transported away from the dissociation region. This means that the methyl radicals are being removed from the growth area, and are thus not being incorporated into the ZnSe films. Thus the immediate removal of methyl radicals from the DMZn molecule is beneficial, as the radicals are allowed to recombine in a time frame short enough so that once they reach the growth

surface, they are likely to be of little consequence to the films. The CH radicals relax to their ground state within 300 ns and are assumed to react with H₂ to form CH₃. The formation of methyl radicals from CH is dependent on an excess of H₂. Growth systems that use inert gases (such as He) to transport the metalorganics would expect ethylene as a major byproduct of the reaction of CH + CH (see Braun ⁸³). Due to the expected low efficiency of the process to make CH* and its reactive efficiency with hydrogen, it is assumed that these radicals do not affect the films. Thus the use of a high energy density system (focused ArF) in the dissociation of DMZn does not seem to be detrimental to the growth process.

Recommendations

Although the work is performed at room temperature, it would be interesting to explore the effect of higher temperatures on the photodissociation process. The results at growth temperatures can be inferred from the relative ratios of the reaction rates. As is seen in Table 4-1, the ratio of the rates at room temperature of $k(\text{III} / \text{I}) = 4 \times 10^9$, whereas at growth temperature $k(\text{III} / \text{I}) = 6 \times 10^4$. This implies that Reaction III would still dominate the chemistry even at elevated temperatures.

Other groups have performed extensive work with LIF (laser induced fluorescence) to identify photoproducts, and this current system can be re-configured to accommodate this technique. The results of LIF would be more qualitative than quantitative, so it is not clear whether spending the extra time and effort to use this technique would be of great benefit.

The gas dynamics of the reactor need further study. The time frame of the diffusion times to the surface and the flow velocity of the metalorganics should be optimized to reduce the methyl radical concentrations (from

undissociated DMZn) even further. The growth chamber is also equipped to allow integration of a mass spectrometer, and this should lend further insight into some of the chemistry of the growth process, although the results of these studies can be ambiguous.

The other source gases, NH_3 and DESe, need to be studied to determine how they react when photodissociated, as separate gases and as a complete system of $\text{DMZn} + \text{DESe} + \text{NH}_3 + \text{H}_2$. It is believed the ammonia breaks into NH_2 and is transported to the surface, but with this system, the high energy densities may be causing further dissociations. The incorporation of the Nd:YAG laser in the growth process would provide an interesting study as to whether the creation of a plasma within the growth cell helps the formation of free N atoms (as the p-type dopant).

As is evident, the fundamental chemistry of this growth process needs to be studied in much greater detail in order to grasp the important processes that are affecting the ZnSe films. Techniques such as the one developed in this thesis should be of substantial help in modeling the growth system so as to unravel some of the mysteries behind the growth of ZnSe by LAMOCVD.

References

- ¹ H. Jeon, J. Ding, A.V. Nurmikko, W. Xie, D.C. Grillo, M. Kobayshi, R.L. Gunshor, G.C. Hua, and N. Otsuka, "Blue and Green Diode Lasers in ZnSe-based Quantum Wells," *Appl.Phys.Lett.* **60**, 2045 (1992).
- ² M.A. Haase, J. Qiu, J.M. DePuydt, and H. Cheng, "Blue-Green Laser Diodes," *Appl.Phys.Lett.* **59**, 1272 (1991).
- ³ T.V. Butkhuzi, A.N. Georgobiani, B.T. Eltazarov, T.G. Khulordava, and M.B. Kotljarevsky, "Blue Light Emitting Diodes on the Base of ZnSe Single Crystals," *J.Crys.Growth* **117**, 1055 (1992).
- ⁴ J. Ren, K.A. Bowers, B. Sneed, F.E. Reed, J.W. Cook, and J.F. Schetzina, "Blue (ZnSe) and Green (ZnSeTe) Light Emitting Diodes," *J.Crys.Growth* **111**, 829 (1991).
- ⁵ J.Y. Bigot, A. Daunois, R. Leonelli, M. Sence, J.G.H. Mathew, S.D. Smith, and A.C. Walker, "Nanosecond Switching of Bistable ZnSe Interference Filters at Room Temperature," *Appl.Phys.Lett.* **49**, 844 (1986).
- ⁶ G.D. Studtmann, R.L. Gunshor, L.A. Kolodziejski, M.R. Melloch, J.A. Cooper, R.F. Pierret, D.P. Munich, C. Choi, and N. Otsuka, "Pseudomorphic ZnSe/n-GaAs Doped-Channel Field-Effect Transistors by Interrupted MBE," *Appl.Phys.Lett.* **54**, 1249 (1988).

- ⁷ L. Wei, Y.K. Cho, and C. Dosho, "Defects in Metalorganic Chemical Vapor Deposition Epitaxy-Grown ZnSe Films on GaAs Investigated by Monoenergetic Positrons," *Jap.J.Appl.Phys. I* **30**, 2442 (1991).
- ⁸ S. Fujita, Y. Matsuda, and A. Sasaki, "Growth Temperature Dependence of Crystallographic and Luminescent Properties of ZnS(x)Se(1-x) by Low-Pressure MOVPE," *J.Crys.Growth* **68**, 231 (1984).
- ⁹ B. Cockayne, P.J. Wright, M.S. Skolnick, A.D. Pitt, J.O. Williams, and T.L. Ng, "The Growth by MOCVD Using New Group VI Sources and Assessment by HRTEM and CL of Zn-Based II-VI Single Crystal Layers," *J.Crys.Growth* **72**, 17 (1985).
- ¹⁰ G.B. Shinn, P.M. Gillespie, W.L. Wilson, and W.M. Duncan, "Laser-Assisted Metalorganic Chemical Vapor Deposition of Zinc Selenide," *Appl.Phys.Lett.* **54**, 2440 (1989).
- ¹¹ P.M. Gillespie, Photoluminescence of Nitrogen-Doped Zinc Selenide by Photo-Assisted MOCVD. (Ph.D., Rice University, 1992)
- ¹² R.L. Jackson, "Spectroscopy of the MMZn Radical. Vibrational Frequencies and Electronic Configurations of the X, A, and C States," *Chem.Phys.Lett.* **174**, 53 (1990).
- ¹³ H. Okabe, Photochemistry of Small Molecules. (New York: Wiley and Sons, 1978), p. 269

- ¹⁴ H. Ando, H. Inuzuka, M. Konagai, and K. Takahashi, "Photoenhanced Metalorganic Chemical Vapor Deposition of ZnSe films using Diethylzinc and Dimethylselenide," *J.Appl.Phys.* **58**, 802 (1985).
- ¹⁵ Sz. Fujita, A. Tanabe, T. Sakamoto, M. Isemura, and Sg. Fujita, "Investigations of Photo-Association Mechanism for Growth Rate Enhancement in Photo-Assisted OMVPE of ZnSe and ZnS," *J.Crys.Growth* **93**, 259 (1988).
- ¹⁶ B.J. Morris, "Photochemical Organometallic Vapor Phase Epitaxy of Mercury Cadmium Telluride," *Appl.Phys.Lett.* **48**, 867 (1986).
- ¹⁷ D.W. Kisker and R.D. Feldman, "Photon Assisted OMVPE Growth of CdTe," *J.Crys.Growth* **72**, 102 (1985).
- ¹⁸ J.E. Jensen, P.D. Brewer, G.L. Olson, L.W. Tutt, and J.J. Zinck, "Excimer Laser-Assisted Metalorganic Vapor Phase Epitaxy of CdTe and HgTe on (100)GaAs," *J.Vac.Sci.Tech.A* **6**, 2808 (1988).
- ¹⁹ Y. Rytz-Froidevaux, R.P. Salathe, H.H. Gilgen, and H.P. Weber, "Cadmium Deposition on Transparent Substrates by Laser Induced Dissociation of DM Cd at Visible Wavelengths," *Appl.Phys.A* **27**, 133 (1982).

- ²⁰ C.J. Chen and R.M. Osgood, "A Spectroscopic Study of the Excited States of Dimethylzinc, Dimethylcadmium, and Dimethylmercury," *J.Chem.Phys.* **81**, 327 (1984).
- ²¹ Y. Fujita, S. Fujii, and T. Iuchi, "Ultraviolet Spectra of II-VI Organometallic Compounds and their Application to *in situ* Measurements of the Photolysis in a Metalorganic Chemical Vapor Deposition Reactor," *J.Vac.Sci.Tech.A* **7**, 276 (1989).
- ²² T. Ibuki, A. Hiraya, and K. Shobatake, "Photoexcitation of DM(Zn, Cd, Hg) Compounds in the 106-270 nm Region," *J.Chem.Phys.* **92**, 2797 (1990).
- ²³ R. Solanki and G.J. Collins, "Laser Induced Deposition of Zinc Oxide," *Appl.Phys.Lett.* **42**, 662 (1983).
- ²⁴ H.W. Thompson and J.W. Linnett, "The Absorption Spectra of Polyatomic Molecules Containing Methyl and Ethyl Radicals-III," *Pr.Roy.Soc.Lond.A* **156**, 108 (1936).
- ²⁵ H.W. Thompson, "The Absorption Spectra of Some Polyatomic Molecules Containing Methyl and Ethyl Radicals," *Pr.Roy.Soc.Lond.A* **150**, 603 (1935).
- ²⁶ D.R.J. Boyd, H.W. Thompson, and R.L. Williams, "Internal Rotation in Zinc Dimethyl and Mercury Dimethyl," *Disc.Far.Soc.* **9**, 154 (1950).

- ²⁷ P.J. Young, R.K. Gosavi, J. Connor, O.P. Strausz, and H.E. Gunning, "Ultraviolet Absorption Spectra of MMCd, MMZn, and MMTe," *J.Chem.Phys.* **58**, 5280 (1973).
- ²⁸ R.L. Jackson, "Vibrational Energy of the Monoalkyl Zinc Product Formed in the Photodissociation of Dimethyl Zinc, Diethyl Zinc, and Dipropyl Zinc," *J.Chem.Phys.* **96**, 5938 (1992).
- ²⁹ R.L. Jackson, "Observation of MMZn as a Stable Product in the KrF Laser Photodissociation of DMZn," *J.Chem.Phys.* **92**, 807 (1990).
- ³⁰ C. Jonah, P. Chandra, and R. Bersohn, "Anisotropic Photodissociation of Cadmium Dimethyl," *J.Chem.Phys.* **55**, 1903 (1971).
- ³¹ P. Bender, "II. Optical Excitation of Cadmium Hydride and Zinc Hydride Bands," *Phys.Rev.* **36**, 1543 (1930).
- ³² H. Habeeb, D.J. LeRoy, and E.W. Steacie, "Zinc Photosensitized Reactions of Ethylene," *J.Chem.Phys.* **10**, 261 (1942).
- ³³ K.P. Giapis, K.F. Jensen, J.E. Potts, and S.J. Pachuta, "Investigation of Carbon Incorporation in ZnSe: Effects on Morphology, Electrical, and Photoluminescence Properties," *J.Electr.Mater.* **19**, 453 (1990).

- ³⁴ M.A. Rueter and J.M. Vohs, "Reaction Pathways and Intermediates in the Decomposition of Dimethyl Zinc on GaAs(100)," *Surf.Science* **268**, 217 (1992).
- ³⁵ G.S. Higashi and L.J. Rothberg, "Investigation of the Surface Photochemical Basis for Metal Film Nucleation in Laser Chemical Vapor Deposition," *Appl.Phys.Lett.* **47**, 1288 (1985).
- ³⁶ G.S. Higashi and L.J. Rothberg, "Surface Photochemical Phenomena in Laser Chemical Vapor Deposition," *J.Vac.Sci.Tech.B* **3**, 1460 (1985).
- ³⁷ Y. Zhang and M. Stuke, "Laser Multiphoton Ionization Spectrum of MMAI Radicals Formed by UV Excimer Laser Photolysis of Gaseous TMA at 248 nm and 193 nm," *Jap.J.Appl.Phys.* **27**, L1349 (1988).
- ³⁸ V.M. Donnelly, M. Geva, J. Long, and R.F. Karlicek, "Excimer Laser Induced Deposition of InP and Indium-oxide Films," *Appl.Phys.Lett.* **44**, 951 (1984).
- ³⁹ R. Larciprete and E. Borsella, "Laser Multiphoton Mass Spectroscopy of Zinc Dialkyls," *Chem.Phys.Lett.* **147**, 161 (1988).
- ⁴⁰ E.S.J. Robles, A.M. Ellis, and T.A. Miller, "Laser-Induced Fluorescence Spectra of the Cold Radicals, MMZn and MMCd, and their Inert-Gas Complexes, (He, Ne, Ar, Kr, Xe) - MMCd," *Chem.Phys.Lett.* **178**, 185 (1991).

- ⁴¹ C.E. Moore, Atomic Energy Levels. (National Bureau of Standards, 1971), NSRDS-NBS 35, p. 124.
- ⁴² G. Herzberg, Molecular Spectra and Molecular Structure III. Electronic Spectra of Polyatomic Molecules. (New York: Van Nostrand Co., 1966), p. 514
- ⁴³ A.D. Walsh, "The Electronic Orbitals, Shapes, and Spectra of Polyatomic Molecules. Part I. AH₂ Molecules," *J.Chem.Soc.* **1953**, 2260 (1953).
- ⁴⁴ R.T. Pack, "Simple Theory of Diffuse Vibrational Structure in Continuous UV Spectra of Polyatomic Molecules. I. Collinear Photodissociation of Symmetric Triatomics," *J.Chem.Phys.* **65**, 4765 (1976).
- ⁴⁵ A.M. Baake, "A Molecular Study of DMHd, DMCd, DMZn, and the Deuterated Compounds," *J.Mol.Spectr.* **41**, 1 (1972).
- ⁴⁶ I.A. Levine, Molecular Spectroscopy. (New York: John Wiley & Sons, Inc., 1975), p. 460
- ⁴⁷ G.M. Bancroft, D.K. Creber, and H. Basch, "Valence and Core Electron Energies from ab initio Calculations and Photoelectron Spectra: Electric Field Gradients in Gas Phase Cd Compounds," *J.Chem.Phys.* **67**, 4891 (1977).

⁴⁸ P. Laporte, N. Damany, and H. Damany, "Pulsed-Laser-Generated Rare-Gas Plasma as a Light Source in the Vacuum Ultraviolet," *Optics Letters* **12**, 987 (1987).

⁴⁹ T.P. Hughes, Plasmas and Laser Light. (London: Adam-Hilger, 1975), p. 30

⁵⁰ S. Kubodera, P.J. Wisoff, and R. Sauerbrey, "Absorption Spectra of Alkali Halide Molecules in the Vacuum Ultraviolet," *J.Chem.Phys.* **92**, 5867 (1990).

⁵¹ P.S. Millar, T. Peterson, G. Warwar, P.J. Wisoff, and R. Sauerbrey, "Neutral and Ionic Excimer Molecules Produced by Reactive Kinetics in a Laser-Produced Plasma," *Optics Letters* **14**, 171 (1989).

⁵² C.E. Max, "Physics of the Coronal Plasma in Laser Fusion Targets", in Laser-Plasma Interaction, ed. R. Balian and J. C. Adam (New York: North-Holland, 1982), p. 304.

⁵³ S. Kubodera, Studies of Ionic Alkali Halide Excimer Molecules Excited by Laser-Produced Plasmas. (Ph.D., Rice University, 1991)

⁵⁴ G. Herzberg, "The Bakerian Lecture. The Spectra and Structure of Free Methyl and Free Methylene," *Pr.Roy.Soc.Lond.A* **262**, 291 (1961).

⁵⁵ R.D. Anderson and H.A. Taylor, "The Photolysis of Cadmium Dimethyl," *J.Phys.Chem.* **56**, 498 (1952).

⁵⁶ A.M. Bass and A.H. Laufer, "The Methyl Radical Combination Rate Constant as Determined by Kinetic Spectroscopy," *Int.J.Chem.Kin.* **5**, 1053 (1973).

⁵⁷ W. Tsang and R.F. Hampson, "Chemical Kinetic Data Base for Combustion Chemistry. Part I. Methane and Related Compounds," *J.Phys.Chem.Ref.Data* **15**, 1087 (1986).

⁵⁸ J.I. Steinfeld, Chemical Kinetics and Dynamics. (Englewood Cliffs, N.J.: Prentice Hall, 1989), p. 8

⁵⁹ A. Callear and H.E. van den Berg, "Relaxation of Excited Methyl Radicals Produced in the Flash Photolysis of Dimethyl Mercury," *Chem.Phys.Lett.* **5**, 23 (1970).

⁶⁰ A. Corney, Atomic and Laser Spectroscopy. (Oxford: Clarendon Press, 1988), p. 300

⁶¹ A.P. Thorne, Spectrophysics. (New York: John Wiley and Sons, 1974), p. 308

⁶² C.H. Corliss and W.R. Bozman, Experimental Transition Probabilities for Spectral Lines of Seventy Elements. (National Bureau of Standards, 1962), Monograph 53, p. 540.

⁶³ W.R. Hindmarsh and J.M. Farr, Collisional Broadening of Spectral Lines by Neutral Atoms. (New York: Pergamon Press, 1972), p. 195

⁶⁴ P.W. Milonni and J.H. Eberly, Lasers. (New York: John Wiley & Sons, Inc., 1988), p. 99

⁶⁵ R. Sauerbrey, F. Emmert, and H. Langhoff, "Fluorescence and Absorption in Electron Beam Excited Argon," *J.Phys.B: At.Mol.Phys.* **17**, 2057 (1984).

⁶⁶ R.H. Barnes, C.E. Moeller, J.F. Kircher, and C.M. Verber, "Dye-Laser Excited CH Flame Fluorescence," *Appl. Optics* **12**, 2531 (1973).

⁶⁷ M. Clerc and M. Schmidt, "Nanosecond Kinetic Study of the Rotational Temperature Decay of the CH(A→X) Emission Produced by Pulse Radiolysis of CH₄ and C₂H₂," *Far.Disc.Chem.Soc.* **53**, 217 (1972).

⁶⁸ A.P. Baronavski and J.R. McDonald, "Multiphoton Vacuum Ultraviolet Laser Dissociation of CH₃Br - Analysis of Chemiluminescent Products," *Chem.Phys.Lett.* **56**, 369 (1978).

⁶⁹ M. Suto, C. Ye, and L.C. Lee, "Quantitative Absorption and Fluorescence Spectroscopy of DMCd in Vacuum Ultraviolet," *J.Chem.Phys.* **89**, 160 (1988).

⁷⁰ J.T. Verdeyen, Laser Electronics. (Englewood Cliffs, NJ: Prentice Hall, 1989), p. 173, 244

⁷¹ R.L. Jackson, "Metal-Alkyl Bond Dissociation Energies for DMZn, DEZn, DMCd, and DMHg," *Chem.Phys.Lett.* **163**, 315 (1989).

⁷² S.J. Jeans, An Introduction to the Kinetic Theory of Gases. (New York: Cambridge University Press, 1962), p. 153

⁷³ L. Pauling, General Chemistry. (New York: Dover Publications, Inc., 1970), p. 151

⁷⁴ C.J. Chen, "Kinetic Theory of Laser Photochemical Deposition," *J.Vac.Sci.Tech.A* **5**, 3386 (1987).

⁷⁵ J. Berkowitz, Photoabsorption, Photoionization, and Photoelectron Spectroscopy. (New York: Academic Press, 1979), p. 139

⁷⁶ Sz. Fujita, S. Maruo, H. Ishio, P. Murawala, and Sg. Fujita, "Surface Photochemical Reactions for Alkyl Group Elimination from Precursors in OMVPE," *J.Crys.Growth* **107**, 644 (1991).

- ⁷⁷ Sz. Fujita, S. Hirata, and Sg. Fujita, "Observation of Photoinduced Alkyl Group Elimination from Precursors in Organometallic Vapor-Phase Epitaxy of Zn-Based II-VI Semiconductors," *Jap.J.Appl.Phys.* **30**, L507 (1991).
- ⁷⁸ C.F. Yu, F. Youngs, K. Tsukiyama, R. Bersohn, and J. Preses, "Photodissociation Dynamics of Cadmium and Zinc Dimethyl," *J.Chem.Phys.* **85**, 1382 (1986).
- ⁷⁹ W.H. Breckenridge and J.H. Wang, "Initial Internal Energy Distributions of ZnH (ZnD) Produced in the Reaction of Zn(4-3P1) with H₂, D₂, and HD," *Chem.Phys.Lett.* **123**, 17 (1986).
- ⁸⁰ W. Kedzierski, J. Supronowicz, J.B. Atkinson, and L. Krause, "Laser-induced Fluorescence and Excitation Spectra of the ZnH Molecule," *Can.J.Phys.* **68**, 526 (1990).
- ⁸¹ G. Herzberg, Molecular Spectra and Molecular Structure I. Spectra of Diatomic Molecules. (Malabar, Fl.: Krieger Publishing Co., 1989), p. 579
- ⁸² R.L. Jackson and G.W. Tyndall, "Photodissociation of the Metal Carbonyls and Metal Dialkyls," *Chemtronics* **4**, 127 (1989).
- ⁸³ W. Braun, J.R. McNesby, and A.M. Bass, "Flash Photolysis of Methane in the Vacuum Ultraviolet. II. Absolute Rate Constants for Reactions of CH with Methane, Hydrogen, and Nitrogen," *J.Chem.Phys.* **46**, 2071 (1967).

⁸⁴ R.E. Continetti, B.A. Balko, and Y.T. Lee, "Symmetric Stretch Excitation of CH₃ in the 193.3 nm Photolysis of CH₃I," *J.Chem.Phys.* **89**, 3383 (1988).

⁸⁵ G.V. Marr, Photoionization Processes in Gases. (New York: Academic Press, 1967), p. 119

⁸⁶ H.S. Gutowsky, "The Infrared Spectrum of Dimethylcadmium," *J.Am.Chem.Soc.* **71**, 3194 (1949).

⁸⁷ H.S. Gutowsky, "The Infra-Red and Raman Spectra of Dimethyl Mercury and Dimethyl Zinc," *J.Chem.Phys.* **17**, 128 (1949).

⁸⁸ S.L. Baughcum and S.R. Leone, "Laser Photodissociation of DMHg: Infrared Emission Studies of Vibrational and Rotational Excitation in the CH₃ Fragments," *Chem.Phys.Lett.* **89**, 183 (1982).

⁸⁹ J.O. Chu, G.W. Flynn, C.J. Chen, and R.M. Osgood, "Infrared Emission Studies of Vibrational Excitation in CH₃ Fragments Produced from the ArF and KrF Laser Photolysis of DMCd and DMZn," *Chem.Phys.Lett.* **119**, 206 (1985).

⁹⁰ D.A. Parkes, D.M. Paul, and C.P. Quinn, "Study of the Spectra and Recombination Kinetics of Alkyl Radicals by Molecular Spectrometry," *J.Chem.Soc.Far.Tr. I* **72**, 1935 (1976).

- ⁹¹ C. Ye, M. Suto, and L.C. Lee, "CH(A,B- \rightarrow X) Fluorescence from Vacuum Ultraviolet Excitation of CH₃," *J.Chem.Phys.* **89**, 2797 (1988).
- ⁹² M.R. Levy and J.P. Simons, "Vacuum Ultraviolet Photodissociation of Alkyl Iodides," *J.Chem.Soc.Far.Tr. II* **71**, 561 (1975).
- ⁹³ G.A. Hebner, K.P. Killeen, and R.M. Biefeld, "*In Situ* Measurement of the Metalorganic and Hydride Partial Pressures in a MOCVD Reactor using Ultraviolet Absorption Spectroscopy," *J.Crys.Growth* **98**, 293 (1989).

Appendix A: DMZn Specifications

Exclusive Sales Agent

TEXAS ALKYLs, INC.

Akzo Chemicals Inc.
300 South Riverside Plaza
Chicago, Illinois 60606
(800) 828-7929

Semiconductor Grade Metalorganic
Analysis Report

DIMETHYLZINC
Lot Number 6EZ109
Analytical Code Number DMZ-8718

Metallic Composition^a

<u>Metal</u>	<u>Detection Limits (ug/g)</u>	<u>Concentration Found (ug/g)</u>
Al	0.1	N.D. ^c
Cd	0.1	N.D. ^c
Cu	0.05	N.D. ^c
Fe	0.05	N.D. ^c
Ge	0.1	N.D. ^c
Mg	0.03	N.D. ^c
Na	0.1	N.D. ^c
Ni	0.05	N.D. ^c
Pb	0.10	N.D. ^c
Si	0.2	5.0
Total Trace Metals:		5.0
Zinc ^b :	99.99950 %	

^a Determined by inductively coupled plasma emission spectroscopy.

^b Determined by difference.

^c Not detected at limit of sensitivity.

Wavelength	Wavenumbers	Atom/Molecule	Transition	Prob. (gA)	O.S. (gI)	Reference
1109.1	90163	Zn II	4(1S)(0)-4(1P)(1) ?	0.305		CRC 1982
2025.51	49354	Zn II	4(2S)(0.5)-4(2P)(1.5)	2.1	1.3	NBS 1962
2025.5				6.6		CRC 1982
2061.91	48481	Zn II	4(2S)(0.5)-4(2P)(0.5)	9.2	5.8	NBS 1962
2064.2	48445	Zn II	4(2S)(0.5)-4(2D)(1.5)	9.2		CRC 1982
2099.9	47621	Zn II	4(2S)(0.5)-4(2D)(2.5)	8.4		CRC 1982
2102.2	47569	Zn II	4(2P)(1.5)-4(2D)(1.5)	0.93		CRC 1982
2138.56	46745	Zn I	4(1S)(0)-4(1P)(1)	19	1.3	NBS 1962
2138.6				21.27		CRC 1982
2671	37439	Zn(CH3)	B <- X			Young ('73)
2739	36510	Zn(CH3)	B <- X			Young ('73)
2756.45	32268	Zn I	4(3P)(0)-5(3D)(1)	0.69	0.079	NBS 1962
2770.86	36080	Zn I	4(3P)(1)-5(3D)(2)	1.2	0.14	NBS 1962
2800.87	35693	Zn I	4(3P)(2)-5(3d)(3)	1.8	0.21	NBS 1962
3072.06	35542	Zn I	4(3P)(2)-6(2S)(1)	2	0.29	NBS 1962
3075.9	32502	Zn I	4(1S)(1)-4(3P)(1)	0.013	0.0018	NBS 1962
3075.9				0.00099		CRC 1982
3282.33	30458	Zn I	4(3P)(0)-4(3D)(1)	4	0.64	NBS 1962
3282.3				2.7		CRC 1982
3302.59	30271	Zn I	4(3P)(1)-4(3D)(2)	18	2.9	NBS 1962
3302.6				2		CRC 1982
3302.94	30268	Zn I	4(3P)(1)-4(3D)(1)	5.6	0.91	NBS 1962
3302.9				0.67		CRC 1982
3345.02	29887	Zn I	4(3P)(2)-4(3D)(3)	28	4.7	NBS 1962
3345				2.38		CRC 1982
3345.57	29882	Zn I	4(3P)(2)-4(3D)(2)	6.1	1	NBS 1962
3345.6				0.4		CRC 1982
3345.93	29879	Zn I	4(3P)(2)-4(3D)(1)	1.2	0.2	NBS 1962
3345.9				0.027		CRC 1982
4126.3	24235	Zn(CH3)	A <- X			Young ('73)
4127.6	24227	Zn(CH3)	A <- X			Young ('73)
4127.6	24227	Zn(CH3)	A <- X			Yu ('86)
4173.3	23962	Zn(CH3)	A <- X			Jackson ('90)
4174.3	23956	Zn(CH3)	A <- X			Young ('73)
4175.6	23949	Zn(CH3)	A <- X			Young ('73)
4175.6	23949	Zn(CH3)	A <- X			Yu ('86)
4630		ZnH				Bender 1930
4656		ZnH				Bender 1930
4680.14	21361	Zn I	4(3P)(0)-5(3S)(1)	5.8	1.9	NBS 1962
4722.16	21171	Zn I	4(3P)(1)-5(3S)(1)	15	4.9	NBS 1962
4720		ZnH				Bender 1930
4746		ZnH				Bender 1930
4810.53	20782	Zn I	4(3P)(2)-5(3S)(1)	2.1	7.2	NBS 1962
4911.6	20360	Zn II	4(2D)(1.5)-4(2F)(2.5)	2.4		CRC 1982
6362.35	15713	Zn I	4(1P)(1)-4(1D)(1)	4.5	2.8	NBS 1962
6362.3				0.79		CRC 1982

Appendix B: Computer Programs

B1. Code to determine the density of molecule in the absorption cell

```

CLS
PRINT " ": PRINT " ": PRINT " ": PRINT " ":
PRINT " Calculation of the Partial Pressure and Number of Molecules of DMZn"
PRINT " "
PRINT " by"
PRINT " "
PRINT " Joseph Elias"
FOR T = 1 TO 10000
NEXT T

10 /
QBUB = 0: QBYP = 0: QPUR = 0: PABC = 0: Q1 = 0: Q2 = 0: Q3 = 0
QDMZ = 0: QTOT = 0: PDMZ = 0: NDMZ = 0: NTOT = 0
TEMP = 100
CLS
PRINT " ": PRINT " ": PRINT " ":
PRINT " The default temperature of the DMZn bubbler is -5 C = 268 K"
PRINT " "
PRINT " Input the name of the experiment": INPUT NAMES
PRINT " "
PRINT " Input the setting of the BUBBLER Mass Flow Controller": INPUT Q1
QBUB = Q1 * 10

PRINT " "
PRINT " "
PRINT " Input the setting of the BYPASS Mass Flow Controller": INPUT Q2
QBYP = Q2 * 100

PRINT " "
PRINT " "
PRINT " Input the setting of the PURGE Mass Flow Controller": INPUT Q3
QPUR = Q3 * 100

PRINT " "
PRINT " "
PRINT " Input the pressure in the absorption cell in torr ": INPUT PABC
PRINT " "

CLS
QDMZ = QBUB * (95.7) / (760 - 95.7)
QTOT = QBYP + QBUB + QDMZ + QPUR
PDMZ = QDMZ * PABC / QTOT
NDMZ = 9.661E+18 * PDMZ / TEMP
NTOT = 9.661E+18 * PABC / TEMP

PRINT " "
PRINT " These settings were entered for experimental record ": PRINT NAMES
PRINT " "
PRINT " The setting on the BUBBLER MFC was : ": PRINT Q1: PRINT " or"
PRINT " : PRINT QBUB: "scm"
PRINT " "
PRINT " The setting on the BYPASS MFC was : ": PRINT Q2: PRINT " or"
PRINT " : PRINT QBYP: "scm"
PRINT " "
PRINT " The setting on the PURGE MFC was : ": PRINT Q3: PRINT " or"
PRINT " : PRINT QPUR: "scm"
PRINT " "
PRINT " The pressure in the absorption cell was : ": PRINT PABC: PRINT "to"
PRINT " "
PRINT " The total flow rate was : ": PRINT QTOT: PRINT "sc"
PRINT " "
PRINT " "
PRINT " The PARTIAL pressure of DMZn is : ": PRINT PDMZ: PRINT "to"
PRINT " "
PRINT " "
PRINT " The TOTAL number of molecules is : ": PRINT NTOT: PRINT "cm"
PRINT " "
PRINT " "
PRINT " The number of molecules of DMZn is : ": PRINT NDMZ: PRINT "cm"
PRINT " "
PRINT " "
PRINT " Run again (y/n) ": INPUT AGAIN
IF AGAIN = "Y" OR AGAIN = "y" THEN 10
END

```

B2. Code to simulate saturation effects in a three level molecular system

```
% Population of levels

% initializing variables
clear
c1=0;          c=0;          tot3=0;
tot1=0;        tot2=0;        avslope2=0;
avslope1=0;    avslope3=0;

% n1 is the population of the first level - DMZn
% n2 is the population of the second level - CH3*
% n3 is the population of the third level - CH*

n1=1e15;
n2=0;
n3=0;

% h is Planck's constant
% f is the frequency of the ArF laser beam

h=6.626e-34;
f=1.55e15;

% input upper state lifetimes
% t1=input(' time constant for level 1 (in usecs) ?');
t1=1000;
tau1=t1*1e-6;
t2=input(' time constant for level 2 (in usecs) ?');
tau2=t2*1e-6;
t3=input(' time constant for level 3 (in usecs) ?');
tau3=t3*1e-6;

% input cross sections for species
% s1=input(' cross section for level 1 (in A^2) ?');
s1=0.15;
sigma12=s1*1e-16;
s2=input(' cross section for level 2 (in A^2) ?');
sigma23=s2*1e-16;

% t is the time of the excitation pulse
% e is the ArF energy density
% phflux is the intensity / energy per photon

%
% intensity loop in mJ/cm2
%

for e=1:100
    phflux=(e/1000) / (h*f*2e-8);

    c1=c1+1;

    % initialize the levels again
    n1=1e15;
    n2=0;
    n3=0;

    % integrate over the pulse time of the ArF
    for pulse = 0:0.25:20
        c=c+1;

        dn1dt= -sigma12*(n1)*phflux
        dn2dt= sigma12*(n1)*phflux-sigma23*(n2)*phflux-(n2/tau2);
        dn3dt= sigma23*(n2)*phflux-(n3/tau3);

    % integrate over the delta t step

    n1= n1 + dn1dt*0.25e-9;
        if n1<=0;
            n1=0;
        end
    n2= n2 + dn2dt*0.25e-9;
        if n2<=0;
            n2=0;
        end
    n3= n3 + dn3dt*0.25e-9;
        if n3<=0;
            n3=0;
        end
    end
end
```

```

l1(c)=n1;
l2(c)=n2;
l3(c)=n3;

end
% end of pulse time loop

t=(0:0.25:20);
%plot(t,l1)
%pause
%plot(t,l2)
%pause
plot(t,l3)
%pause
c=0;

% populations for each energy step
pop1(c1)=n1;
pop2(c1)=n2;
pop3(c1)=n3;

peak3(c1)=max(l3);

% log of intensities for each energy
if n1==0;
    int1(c1)=0;
else
    int1(c1)=log(n1/tau1)/2.303;
end
if n2==0;
    int2(c1)=0;
else
    int2(c1)=log(n2/tau2)/2.303;
end
if n3==0;
    int3(c1)=0;
else
    int3(c1)=log(n3/tau3)/2.303;
end

% log of photon flux, energy density
flux(c1)=log(phflux)/2.303;

% calculate the slope for the first 50 points
if c1>1, e<50;
    slope1(c1-1)=(int1(c1)-int1(c1-1)) / (flux(c1)-flux(c1-1));
end
if c1>1, e<50;
    slope2(c1-1)=(int2(c1)-int2(c1-1)) / (flux(c1)-flux(c1-1));
end
if c1>1, e<50;
    slope3(c1-1)=(int3(c1)-int3(c1-1)) / (flux(c1)-flux(c1-1));
end

end
% end of energy density loop

% average the first 5 slopes
for a=1:5
    tot1=tot1+slope1(a);
    tot2=tot2+slope2(a);
    tot3=tot3+slope3(a);
end
avslope1=tot1/5;
avslope2=tot2/5;
avslope3=tot3/5;

% log graphs of populations in levels (1, 2, 3) vs. energy density
en=(1:100);

%loglog(en,pop1)
%title(['initial slope level1 is ',num2str(avslope1)])
%pause
%loglog(en,pop2)
%title(['initial slope level2 is ',num2str(avslope1)])
%pause

loglog(en,peak3)
axis([1 100 1e11 1e16]);

title('Population of Level #3 vs. Energy Density')
xlabel(['Energy Density (mJ/cm2)'])
ylabel(['Population (cm-3)'])
text(.70,.90,['Initial slope is ',num2str(avslope3)],'sc')
text(.05,.90,['Lifetimes (secs): ',num2str(tau2)],'sc')
text(.05,.85,['t2 = ',num2str(tau2)],'sc')
text(.05,.80,['t3 = ',num2str(tau3)],'sc')
text(.35,.90,['Cross Sections (A^2) : ',num2str(sigma12)],'sc')
text(.35,.85,['sigma12 = ',num2str(sigma12)],'sc')
text(.35,.80,['sigma23 = ',num2str(sigma23)],'sc')

```

B3. Code to determine the diffusion of the photoproducts to the substrate

```
% Calculating the diffusion rate for
% different values of temperature,
% mean free path, and density of H2, Zn, and CH3

% initialize variables
clear
n=0;
nztime=0;

mol1=input('What is molecule #1 ?','s');
%mol2=input('What is molecule #2 ?','s');
mol2='H2';

temp=input('What is the temperature [K] ?');
%temp=673;

press1=input(['What is the pressure [torr] of the ',mol1,' ?']);
%press1=1;
n1=9.66e18*press1/temp;

d1=input(['What is the diameter [Å] of the ',mol1,' ?']);
%d1=3.8;
d1=d1*1e-8;

m1=input(['What is the mass [amu] of the ',mol1,' ?']);
%m1=15;
vth1=157.9*sqrt(temp/m1)*100;

press2=input(['What is the pressure [torr] of the ',mol2,' ?']);
%press2=100;
n2=9.66e18*press2/temp;

d2=input(['What is the diameter [Å] of the ',mol2,' ?']);
%d2=0.74;
d2=d2*1e-8;

m2=input(['What is the mass [amu] of the ',mol2,' ?']);
%m2=2;
vth2=157.9*sqrt(temp/m2)*100;

w=input('What is the gaussian spot size [cm] of the ArF ?');
%w=1.25;
spot=w;
w0=w;

endt=input('How long do you want to look [ms] ?');
deltat=input('What is step size of t [ms] ?');
deltaz=input('What is step size of z [cm] ?');

% estimation of mean free path assuming m1>>m2
%mfpl=0.7071 / ( (d1*1e-8)^2 * n1 * pi );
%mfpp=0.7071 / ( (d2*1e-8)^2 * n2 * pi );

% complete expression of mean free path in mixture of two gases
mfpl=(1.414*pi*n1*d1^2 + sqrt(1+(m1/m2))*pi*n2*(d1/2 + d2/2)^2)^(-1);
mfpp=(1.414*pi*n2*d2^2 + sqrt(1+(m2/m1))*pi*n1*(d1/2 + d2/2)^2)^(-1);

% distance z in cm from the center of the Gaussian
z=(0.01:deltaz:0.5);
```

```

% determine whether molecule recombines, and determine concentration
ans=input(['Does the ',mol1,' decay as second order function ?'],'s');
if ans=='y'
    nrecomb=(nl/(nl*8.8e-14*1 + 1));
    n=(nrecomb/w)*w0 * exp(-(z/w).^2);
else
    n=(nl      /w)*w0 * exp(-(z/w).^2);
end

% plot initial Gaussian distribution of molecules
plot(z,n)
pause

nz=n;
cnt=0;

%
% Time loop in ms
%
for time=0.1:deltat:endt
    cnt=cnt+1;

    % diffusion coefficient in [cm2 / ms]
    dl2=(nz*mf2*vt2 + n2*mf1*vt1) / (3 * (nz+n2) *1e3 );

    % Complete expression of the diffusion equation
    %dndz2=2* (2*z.^2-w^2)/(w^4) .*nz;
    %cndt=dl2*dndz2;
    %nz=nz + cndt*deltat;

    % Recombination of methyl radicals follows second order decay
    % 2*k*1e-3 = 8.8e-14, where k=4.4 e-11 (molecules)-1(cm)3(sec)-1
    if ans=='y'
        nrecomb=(nl/(nl*8.8e-14*time + 1));
        nz=(nrecomb*w0)/w * exp(-(z/w).^2);
    else
        nz=(nl      *w0)/w * exp(-(z/w).^2);
    end

    % Gaussian parameter which is the 1/e point of the distribution
    w=w + deltat*2*dl2/w;

    %nz at t = 100 us
    if cnt*deltat==0.1
        nztime=nz;
    end

    %nz at t=500 us
    if (cnt*deltat)==0.4
        nztime=[nztime;nz];
    end

    %nz at t=1ms
    if (cnt*deltat)==0.9
        nztime=[nztime;nz];
    end

    %nz at t=5ms
    if (cnt*deltat)==4.9
        nztime=[nztime;nz];
    end
end

```



```

    %nz at t=10ms
    if (cnt*deltat)==9.9
        nztime=(nztime;nz);
    end

% End of the time loop
end

% Plotting of N(z) for discrete times in one graph

% Semilog plot of concentration

semilogy( z, nztime )

title(['Concentration of ',moll,' vs. Distance (up to ', num2str(endt),' ms)'])
xlabel('Distance (cm)')
ylabel('Concentration (cm-3)')

text(.13,.85,'M1 =','sc')
text(.20,.85,num2str(m1),'sc')
text(.13,.80,'M2 =','sc')
text(.20,.80,num2str(m2),'sc')

text(.29,.85,'P1 =','sc')
text(.36,.85,num2str(press1),'sc')
text(.29,.80,'P2 =','sc')
text(.36,.80,num2str(press2),'sc')

text(.45,.85,'temp =','sc')
text(.54,.85,num2str(temp),'sc')
text(.45,.80,'spot size =','sc')
text(.58,.80,num2str(spot),'sc')

text(.65,.85,'molecule #1 is ','sc')
text(.82,.85,mol1,'sc')
text(.65,.80,'molecule #2 is ','sc')
text(.82,.80,mol2,'sc')
pause

```